Output-Only Experimental Modal Testing of Large Residential Structures and Acoustic Cavities Using Sonic Booms

Joseph M. Corcoran

Thesis submitted to the faculty of the Virginia Polytechnic Institute and State University in partial fulfillment of the requirements for the degree of

Master of Science
In
Mechanical Engineering

Ricardo A. Burdisso
Georg Reichard
Daniel J. Inman

February 9, 2010
Blacksburg, Virginia

Keywords: Modal testing, Natural Excitation Technique (NExT), sonic boom, residential structure, acoustic cavity.

Output-Only Experimental Modal Testing of Large Residential Structures and Acoustic Cavities Using Sonic Booms

Joseph M. Corcoran

ABSTRACT

In this thesis, an output-only experimental modal testing and analysis technique known as the Natural Excitation Technique (NExT) is examined for use with large residential structures and interior cavities. The technique which assumes a random, stationary input causing the response data is reviewed and extended for the first time to include the assumption of an impulse input. This technique is examined with respect to the experimental modal analysis of single and two room residential structures. Each structure is first tested using conventional modal testing methods. Then, NExT is applied using each structure's response to a simulated sonic boom, an impulsive input. The results of these analyses along with the results obtained from a finite element model are compared. Then, the interior cavities enclosed by the residential structures are examined using NExT. Therefore, this thesis also demonstrates the successful use of NExT on acoustic systems for the first time. Three configurations of the interconnected cavities enclosed by the two room structure are considered to study physical phenomena. Both interior pressure response to random, stationary inputs and the sonic boom response are used with NExT to determine modal properties. The results of these analyses are compared to a theoretical analysis. Advantages to using NExT with both the response to a random, stationary input and an impulsive input are demonstrated for structural and acoustic systems.

Acknowledgments

First and foremost, I would like to thank my advisor, Dr. Ricardo A. Burdisso, not only for the support and advice he gives his students, but also for his care, concern, and respect for them outside of the university environment. I extend my gratitude to Drs. Georg Reichard and Dan Inman for their service on my academic committee and to Dr. Reichard also for his building construction advice, assistance, and even physical labor in support of the NASA sonic boom project. Special thanks goes to my fellow student team members, Ryan Haac and Marcel Remillieux, for their dedicated, hard work in all aspects of the NASA project which kept it going and for their friendship which made the project enjoyable to work on.

The financial support from the NASA Langley Research Center provided the means to accomplish the work presented in this thesis. I would like to thank the technical monitor for the sonic boom project, Mr. Jacob Klos, for his help and advice concerning the sonic boom experiments.

My gratitude goes out to the faculty and teachers of the Mechanical Engineering department at Virginia Tech for imparting their knowledge in class which enables the quality research performed by the graduate students they teach. Finally, I would like to thank the staff of the Mechanical Engineering department at Virginia Tech, especially Ms. Gail Coe, for the endless unseen help and support they provide.

All photographs by the author, Joseph M. Corcoran, 2010, unless noted otherwise.

Table of Contents

List of Figures

List of Tables

1 Introduction

In this introduction, motivation for the work done in this thesis will be given. This will be followed by a review of literature related to the topic of this thesis. Then, the objectives of the thesis will be discussed. Finally, an overview of the thesis organization will be discussed.

1.1 Motivation

Commercial supersonic flight debuted in 1969 with the maiden voyage of the Concorde shown in Figure 1.1. The supersonic jet seated 100 people and flew across the Atlantic Ocean in just under three hours. One inherent problem of supersonic flight is the noise produced by large pressure waves colliding with one another when travelling faster than the speed of sound, called a sonic boom. It is this noise, which can even cause windows, doors, and furniture at ground level to rattle, along with other environmental concerns which caused the FAA to restrict the Concorde to transoceanic flights (Pawlowski, 2009).

Figure 1.1: The Concorde, a 100-seat supersonic jet whose maiden voyage in 1969 across the Atlantic Ocean opened supersonic flight to the public (Pawlowski, 2009) [fair use].

Since the Concorde's grounding in 2000 due to a fatal accident and a decline in the airline industry, interest in commercial supersonic flight has not declined. Over the past several years, several aerospace companies including Lockheed Martin and Supersonic Aerospace International (SAI) have undertaken the task of designing a Quiet Supersonic Transport (QSST) capable of transporting about a dozen passengers across the US in only two hours shown in Figure 1.2. The

QSST is projected to hit the market by 2014 and SAI plans to have a fleet 300 to 400 strong in the next 20 years (Hagerman, 2007). These smaller supersonic jets could be succeeded by larger ones capable of transporting around 75 passengers in 2025 with even larger airliners by 2030 (Pawlowski, 2009).

Thanks to its fine-tuned aerodynamic design, such as the small wings towards the front of the aircraft and the swept-V tail shown in Figure 1.2, the sonic booms generated by the QSST are predicted to be one hundredth the strength of a typical Concorde, meeting the noise regulations set forth by the FAA which took effect in 2006 (Hagerman, 2007).

Figure 1.2: Quiet Supersonic Transport in development by Lockheed Martin and Supersonic Aerospace Institute (Hagerman, 2007) [fair use].

In order to lift the ban on overland supersonic flights, the FAA requires proof based on subjective testing that the weak sonic booms will not disturb anyone nearby at ground level, particularly in areas of residence. One method of carrying out these tests would be to generate a sonic boom from a supersonic jet for a focus group. However, this approach is expensive, relatively dangerous due to the complex maneuver required, and suffers from limited flexibility with the capability of generating one type of sonic boom (Klos and Buehrle, 2007; Klos, 2008). Another sonic boom generation method consists of using a linear distribution of detonating cord (Hawkins and Hicks, 1966). Again, this method is again limited in the type of booms that can be generated and expensive due to material and transportation costs and detonation experts (Haac et al., 2009). Using large speakers to generate sonic booms fails due to insufficient low frequency output. A numerical model to predict the transmission of sonic booms into structures would be a cheap, efficient, and flexible method to carry out the subjective testing required by the FAA.

After experiencing the limitations of using a supersonic jet to generate a real sonic boom to collect vibro-acoustic response data from actual residential structures (Klos and Buehrle, 2007; Klos, 2008), NASA has funded projects whose ultimate goal is to determine and validate a model for the prediction of the transmission of a weak sonic boom from the aircraft into a typical residential structure. This model can then be used to generate digital sound clips representative of the actual sonic boom which can be used in the subjective testing necessary to lift the ban on overland supersonic flights.

The approach taken by the Virginia Tech team sponsored by NASA was to first design and code a numerical model to predict the transmission of a sonic boom through a building due to the pressure loading caused by the boom. This model is based on developing the interior acoustic response from the modal response of the structure and interior acoustic cavities (Remillieux et al., 2009). Then, the task became to build and test a simple, rectangular test structure with typical residential construction. Sonic booms were simulated with detonating cord and the vibro-acoustic response of the structure was recorded to provide experimental validation of the numerical model with a simple residential structure (Haac et al., 2009). Next, additions were made to the simple structure including another room, attics, large windows, and a door connecting the two interior cavities to increase the complexity of the structure. The response of this more complex structure to simulated sonic booms was measured to validate the numerical model's robustness (Haac et al., 2009).

Obviously, a key to this numerical modeling approach is the method of accurately obtaining structural and acoustic modal properties from the structure's construction and geometry so the model can be extended to other residential structures. This method must then be validated by experimentally measuring structural and acoustic modal properties using new and conventional techniques and comparing them to the modal properties determined from the numerical model (Corcoran et al., 2009).

Determining modal properties experimentally can be quite challenging, especially for large structures. Often, output-only experimental modal analysis techniques are used for cases in which traditional excitation devices such as shakers or impact hammers do not input enough energy to excite the entire system (Peeters and de Roeck, 1999; Brincker et al., 2001; Peeters and de Roeck, 2001; Shen et al., 2003). Usually these techniques are used when coupled with

measured response due to ambient excitation coming from wind, vehicles, or seismic vibrations assuming that this excitation is random and stationary.

This thesis examines the use of output-only experimental modal testing and analysis techniques with the use of the structural and acoustic response to impulsive excitations for cases in which ambient excitation is insufficient in exciting modes of the structure or acoustic cavity. Specifically, the derivation of the Natural Excitation Technique (NExT) has been extended to include the use of the response to an impulse. NExT is applied to the sonic boom response of two large residential structures and validated by comparison with conventional experimental modal test results and finite element results. NExT is also applied for the first time to acoustic cavities in this thesis. Specifically, it is applied to the cavities enclosed by the residential structures using the interior pressure response to white noise played through a speaker and sonic booms transmitted into the structure. Assuming this technique provides useful modal results, it can even be applied to the sonic boom response of the real residential structures and cavities tested by Klos and Buehrle (2007) and Klos (2008). This would be useful to provide extensive validation of the numerical model developed by Virginia Tech applied to a real residential structure.

1.2 Literature Review

Presented in this section is a review of literature pertaining to the topic of this report split into two sections. First, a review of literature published about residential structure vibration is given. Then, published work on output-only experimental modal testing and analysis is examined.

1.2.1 Residential Structure Vibration

Most research on the vibration of residential structures has been limited to very ideal built-up plate and beam systems with simple geometry. In their paper, Dickinson and Warburton (1967) studied the vibration of an elastic, homogeneous, isotropic box consisting of rectangular plates of uniform thickness. Under the assumptions that the transverse displacement is much smaller than the wavelength of flexural vibrations, membrane stresses can be neglected, each corner has zero deflection, and only symmetric and anti-symmetric modes can exist, they obtain analytical series solutions to both closed and open boxes, an open box being a box with one of the six plates removed. It is demonstrated experimentally that the natural frequencies and mode shapes of the boxes are well-predicted, with a few exceptions that can be predicted using other techniques such as the fundamental acoustic modes in the closed box.

In an effort to analyze the vibration of more complex box-type structures, Popplewell (1971) applied the finite element technique to the boxes analyzed by Dickinson and Warburton (1967) and extended the model to include structural discontinuities. Adding the assumption that the corners of the box were not allowed to twist in one of the models presented, it was shown that overall agreement in natural frequencies and mode shapes was good between the finite element model developed and the results published by Dickinson and Warburton (1967). Finite elements with three unknowns per node, transverse displacement and two rotations, and with four unknowns per node, transverse displacement, two rotations, and twist, were analyzed. Popplewell (1971) showed that the element that included twist gave much more accurate results than the element with only three unknowns per node. Popplewell (1971) also briefly demonstrated the flexibility of the finite element method in analyzing complex structures by introducing structural discontinuities in the form of rectangular holes in the closed box and studying the effect on the lowest natural frequencies.

However, many assumptions of these analyses are clearly violated in a complex structure, such as the large residential structures which are the topic of this thesis. Homogeneity cannot be assumed since the structure is built of many different materials. The wood used in construction cannot be considered isotropic with differing material properties parallel and perpendicular to the fibers. Typically, only the base of a residential structure is supported, so the corners of the roof are free to move, violating another assumption. Finally, symmetry in mode shapes is probably violated due to the wall construction differences between a plain wall and a wall with a window or a door. Due to the violation of these assumptions, these simple, idealized models are insufficient to predict the vibration of a structure built with orthotropic or anisotropic components like walls with studs, geometry more complex than a simple box, and other substructures built in, such as windows or doors. For these reasons, the vibration of the individual components of residential structures has been researched.

Wahba (1990a) studied the vibration of a plaster-wood wall like those used in residential structures using a series solution. The research included the construction of a sample plaster-wood wall along with the measurement of material properties associated with each component of the wall: plaster, plywood, and wooden joists or studs. It was found that the plaster was an isotropic material while the plywood and studs were orthotropic with differing properties in the dominant direction of the wood fibers than the direction perpendicular to the wood fibers. The

theoretical analysis adopted Mindler- or Reissner-type plate theory in which both transverse-shear deformation and rotary inertia are taken into account, important when the modal wavelength is of the same order as the thickness of the wall. The equations of motion are then formed from the Lagrange equations, assuming a series solution for the displacement fields, and solved using the normal mode method for the natural frequencies and mode shapes of the structure. It was found that more half-wavelengths existed in the direction perpendicular to the studs in the lower modes, due to their stiffening effect. The static response of the wall due to a 100 N/m^2 load on the plywood surface was studied using the theoretical formulation and it was found that only the first two modes contributed significantly to the response. From the static response, it was also concluded that the displacement and normal in-plane strain in the direction perpendicular to the studs are close to zero at the plaster surface and maximum at the plywood surface while the displacement and normal in-plane strain in the direction parallel to the studs are of the same order of magnitude on both surfaces. Also, the maximum lateral displacement and normal in-plane stresses occur at the center of the wall and the shear stresses were very small when compared with in-plane stresses. The natural frequencies of the first few modes were also determined experimentally using the resonance test and found to be in good agreement with the frequencies predicted theoretically. Modal damping ratios were assigned based on experimental data.

Wahba (1990b) confirmed this analytical technique by modeling the plaster-wood wall with finite elements. The wall was built up of 8-noded parabolic quadrilateral elements with five degrees of freedom per node, namely, two in-plane displacements, the two corresponding rotations, and one transverse displacement. Thus, the elements are consistent with higher-order plate theory such as Mindler- or Reissner-type theory used previously in which transverse-shear deformation and rotary inertia are accounted for. The results obtained from this finite element model using a consistent mass approach confirmed the series solution studied previously. It was determined that, while the finite-element method requires more degrees of freedom than the series solution to obtain accurate results, the finite-element method is a better-suited approximate way of dealing with complex geometry or boundary conditions. To reduce the computational cost, Wahba (1990b) used a lumped-mass approach for the finite element model which resulted in good agreement with the series solution.

A numerical model to predict the vibro-acoustic responses of simplified residential structures at low frequencies due to sonic boom exposure has been presented by Remillieux et al. (2010a). The model uses a modal-decomposition approach to compute the dynamics of the fluid-structure system in the time domain. The structural displacement is expressed as the summation over the *in vacuo* modes of vibration computed by a finite element model. A new shell element which incorporates an analytical method to compute equivalent orthotropic plate properties of residential structure components is utilized by the finite element model. The acoustic modes of the interior cavity are computed analytically for rectangular geometries assuming rigid boundaries. This model is validated experimentally by comparison of measured and predicted vibro-acoustic responses of two simple residential structures to a simulated sonic boom and the comparison of measured modal properties with properties computed from the finite element model in a companion paper (Remillieux et al., 2010b).

The use of double-panel windows is very common in residential construction and can be a primary path for sound transmission into a structure. Thus, Xin et al. (2008) studied the vibro-acoustic characteristics of a double-panel partition with an enclosed air cavity mounted in an infinite rigid acoustic baffle analytically. The analytical model was developed using Fourier series expansions for the panel displacements and for the acoustic velocity potential in the air cavity, taking into account the interaction between the fluid in the cavity and the two panels. The solution for each panel and the cavity is obtained using the Galerkin method; good agreement was achieved between this analytical model and published experimental data. Various parameters of the model are then investigated. Akin to the mass law for single-panel partitions, an increase in the thickness of the panels enhances the sound insulation of the system, particularly for low frequencies. Increasing the thickness of the enclosed cavity lowers the frequency of the acoustic resonance in the cavity. Thus, it is possible to design a system which has good sound insulation over a wide frequency range between this acoustic resonance and the panel resonances. Angle of incident sound was also studied. It was shown that incident sound waves with a large incident angle of elevation transmit easier than those with smaller angles of elevation while the incident azimuth angle has negligible effect on the sound transmission through the system (Xin et al., 2008).

1.2.2 Output-Only Experimental Modal Analysis

It is frequently inconvenient and often impossible to conduct a conventional modal test in which an input device such as a shaker or impact hammer can be used to excite a structure into vibration and measure its response at many locations on the structure. This is particularly the case when the structures of interest are large, e.g. buildings, bridges, space structures, large mechanical structures, etc., and shakers or impact hammers may not provide enough force to excite all of the structural modes. Also, the input force is difficult to accurately measure if a speaker provides excitation of the modes of an acoustic cavity to be extracted. This is especially true if interest is in very low frequencies such as sonic boom applications where the typical speaker has little to no input. Output-only modal testing and analysis techniques provide methods for extracting modal properties from systems in which only the response is measured and provides a simple remedy for these issues. These methods known as output-only modal analysis, operational modal analysis, or response-only modal analysis, are based off of a new technique developed by James et al. (1993) called the Natural Excitation Technique (NExT).

In NExT, the measured vibration or pressure responses are cross-correlated with a selected reference response signal. Assuming that the input force is random and stationary, it can be shown that these cross-correlations, referred to as NExT impulse response functions (IRFs), contain the same modal properties as the IRFs of the system. Time domain modal parameter extraction methods, such as the single reference Least Squares Complex Exponential (LSCE) method (Mohanty and Rixen, 2004a), can then be applied to the NExT IRFs. Another option is to calculate simple Discrete Fourier Transforms to convert NExT IRFs to NExT frequency response functions (FRFs), or cross-correlations to cross spectral density functions, and apply a frequency domain modal parameter extraction method such as the Global Singular Value Decomposition (Global SVD) method (Ewins, 2000). The technique was applied to an operating wind turbine demonstrating good agreement in the modal properties obtained with NExT compared to the modal properties obtained from a conventional modal test (James et al., 1993).

Many experimental modal analysis techniques have been examined and some created for use with NExT accompanied with experimental validation (Peeters and Roech, 1999; Brincker et al., 2001; Peeters and de Roeck, 2001; Shen et al., 2003). Other experimental modal analysis techniques have been modified for use with NExT when a strong, known harmonic component is

included in the random, stationary response (Mohanty and Rixen, 2004a; Mohanty and Rixen, 2004b; Mohanty and Rixen, 2006).

Peeters and Roech (1999) showed that system identification algorithms, specifically realization algorithms, that were developed for impulse responses can be extended to output covariances with the ambient input unknown. This idea was then extended to include only the output covariances with a few reference sensors. Then, they replace output covariances with data-driven stochastic subspace algorithms to lighten the computational load. This technique is validated experimentally for a large steel mast excited by wind. A review of the extension of many experimental modal analysis techniques was later written by Peeters and Roech (2000). First, several models and types of measurement data of vibrating structures were reviewed including the classical physical structural model, state-space models, and frequency domain models. Then, frequency domain experimental techniques were reviewed with respect to output-only data including the peak picking method, the complex mode indicator function method, and maximum likelihood identification. Following, time domain techniques such as the instrumental variable method and the stochastic subspace identification methods were reviewed. Each of these methods was reviewed and compared with a finite element model of the large steel mast.

A new frequency domain technique for output-only modal analysis was discussed by Brincker et al. (2001). An extension of the simple peak picking technique for experimental modal analysis was demonstrated to provide experimental modal properties when applied to output-only autospectrums assuming stationary white noise. Then, a SVD was applied to the output autospectrums and it was demonstrated that even closely spaced modes could be identified through peak picking of the singular values plotted against frequency. This technique was applied with success to the simulation of a simple two storey building where it was shown that dominant frequency components in the unknown input could be extracted in addition to the modal properties.

Shen et al. (2003) investigated the use of NExT with more sophisticated frequency domain techniques applied to the auto and cross spectral density functions. Specifically, the frequency domain poly reference modal identification scheme was demonstrated to extract modal properties from the spectral density functions theoretically. Then, the conventional and output-only techniques were compared for validation by experimentally testing a small airplane model.

Mohanty and Rixen (2004a) extended the single reference LSCE method to include the presence of known, strong, harmonic components in addition to the random, stationary input assumed in NExT. The method was applied successfully experimentally to a pinned beam excited with white noise superimposed with several strong harmonic components. The modal properties of the beam were extracted accurately even when the known, harmonic components were close in frequency to the natural frequencies of the modes. Mohanty and Rixen (2004b) then extended the Ibrahim time domain method similarly to include known, harmonic components. The success of this extended method was demonstrated experimentally for a simply supported plate. Finally, Mohanty and Rixen (2006) extended the eigensystem realization algorithm to include known, harmonic components in addition to random noise. Similarly, the extended method was validated experimentally for a pinned beam.

1.3 Thesis Objectives

The overall goal of this thesis is to examine the use of NExT for experimental modal analysis of structural and acoustic systems using the response to different types of inputs. First, the theoretical derivation of the technique is discussed demonstrating the need for the assumption of a random, stationary input to allow for the experimental modal analysis of output-only systems. Then, a new extension of NExT is given to allow for the assumption of an impulsive input rather than a random, stationary input. The rest of the thesis demonstrates the use of NExT for experimental modal analysis with both a random, stationary input and an impulsive input to both structural and acoustic subsystems.

This is accomplished through the experimental modal testing and analysis of two simple residential structures and their interior acoustic cavities. The structures are analyzed first with conventional impact hammer modal testing. This is followed by experimental modal analysis of the structures using NExT and the response to a simulated sonic boom. The modal results of these analyses are compared along with the results from a finite element model to compare the use of NExT with impulsive inputs to more conventional analysis techniques.

Then, experimental modal testing and analysis using NExT is performed on the interior acoustic cavities contained by the single and two room structures. Therefore, this thesis also demonstrates for the first time that NExT can be applied to the response of acoustic systems for the experimental modal analysis of acoustic cavities. First, the cavities of the structures are analyzed theoretically to predict natural frequencies of the acoustic modes. Then, NExT is used

with the interior pressure response to stationary, random inputs to extract modal properties of the cavities, adhering to the assumptions inherent in the original derivation of NExT. NExT is then used with the interior pressure response to a sonic boom to determine modal properties of the cavities. The results of the three analyses are compared.

1.4 Thesis Organization

This thesis is organized in several chapters. An overview of the experimental modal analysis techniques used is given in Chapter 2. This begins with a summary of the derivation and application of NExT followed by the simple extension of NExT to include the assumption of an impulse input instead of a random, stationary input assumed in the original derivation. Then, two commonly used experimental modal analysis methods for the extraction of modal properties are discussed. These are the Global SVD and single reference LSCE methods.

Chapter 3 includes the modal testing and analysis of the structural subsystems of the single and two room residential structures. This chapter is organized as shown in Figure 1.3(a). It is divided into two major sections analyzing the single room structure in one and the two room structure in the other. The modal testing and analysis procedure remains essentially the same for each structure. First, a conventional modal test is undertaken. Then, experimental modal analysis using NExT with the sonic boom response is discussed. The chapter ends with a comparison of the results of these techniques with the results calculated from a finite element model.

The modal testing and analysis of the acoustic cavities contained in the single and two room structures is discussed in Chapter 4 which is organized as shown in Figure 1.3(b). Again, the analysis of the different cavities is parallel for the single and two room structures which are divided into two major sections of the chapter. Each section begins with a theoretical analysis to determine the natural frequencies of acoustic modes. Then, an experimental modal analysis of the cavities using a stationary, random input is given followed by an analysis using NExT and the response to a sonic boom. Three different configurations of the interconnected cavities of the two room structure are considered in the chapter. The thesis ends with conclusions drawn in Chapter 5.

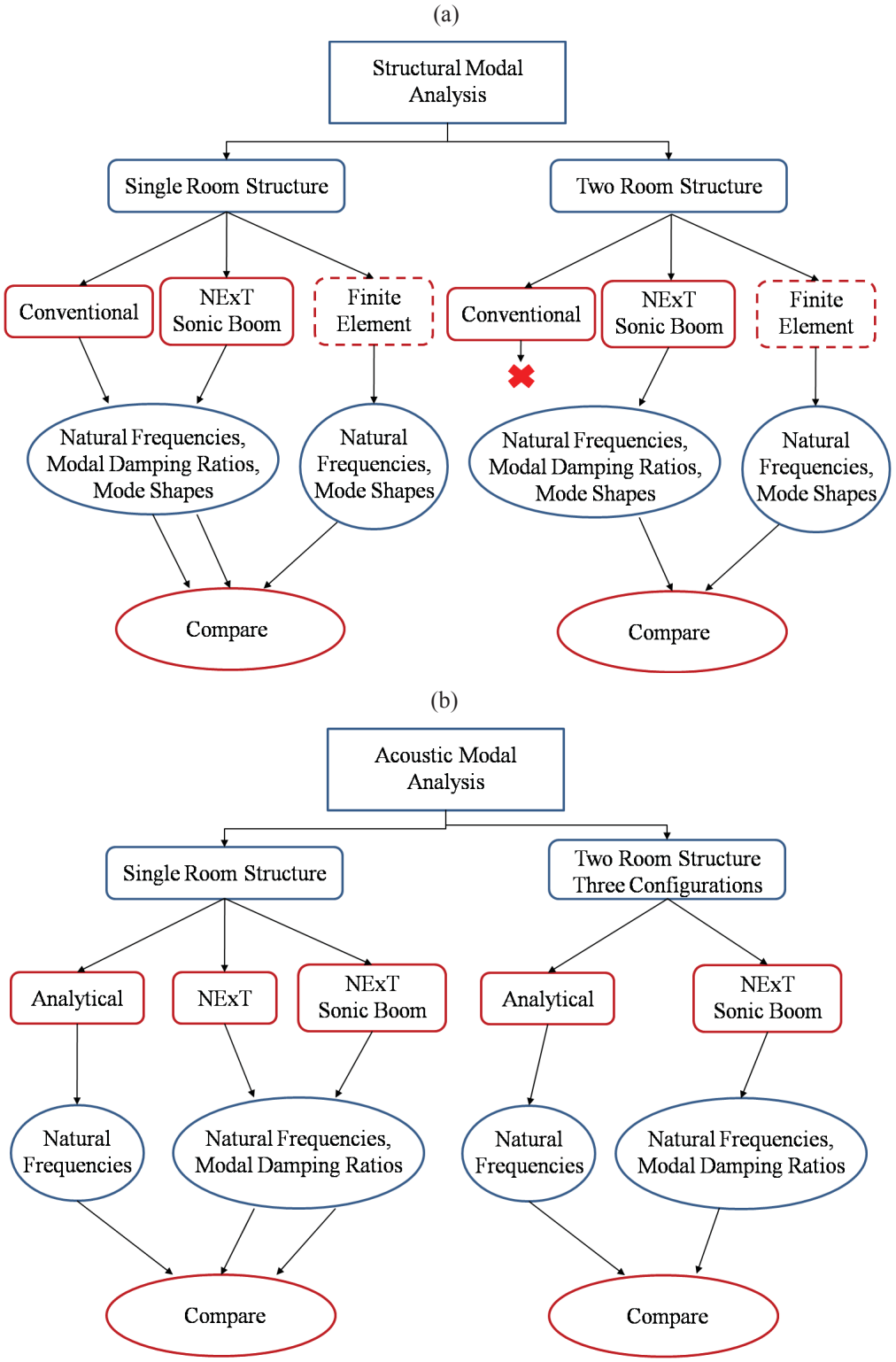

Figure 1.3: Organization of thesis to provide comparisons of the use of NExT with sonic boom response to other techniques for experimental modal analysis of (a) structural modes and (b) acoustic modes of the single room structure and cavity and the two room structure and cavities. Finite element analyses not presented in this thesis.

2 *Experimental Modal Analysis Methods*

Descriptions of the experimental modal analysis methods used in this report are presented in this chapter. First, NExT, which is used to obtain curves with the same eigenproperties as IRFs from response data without measurement of the input force as long as the input is random and stationary, is described. This technique is then extended to include the use of the response to an impulse excitation. Then, the Global SVD method used to extract structural modes is described. This method is a mathematical procedure in the frequency domain which simultaneously fits curves described by the sum of modes to an experimentally obtained data set of FRFs at many response locations with a common excitation point. Finally, the single reference LSCE method used to extract acoustic eigenproperties in the NExT analyses is described. This method is similar to the Global SVD method in that it simultaneously fits curves to experimental modal data sets at many response locations with a common excitation point. However, the procedure is carried out in the time domain where the curves described by the sum of decaying exponential modes are fitted to IRFs.

The experimental modal analysis techniques described in this section relate as shown in Figure 2.1. As shown in the figure, the LSCE and Global SVD methods are numerical procedures used to calculate modal properties from measured data. They can be used whether the data comes from conventional modal tests or from output-only tests. NExT is a technique which provides curves for which these methods can be used so modal properties can be extracted.

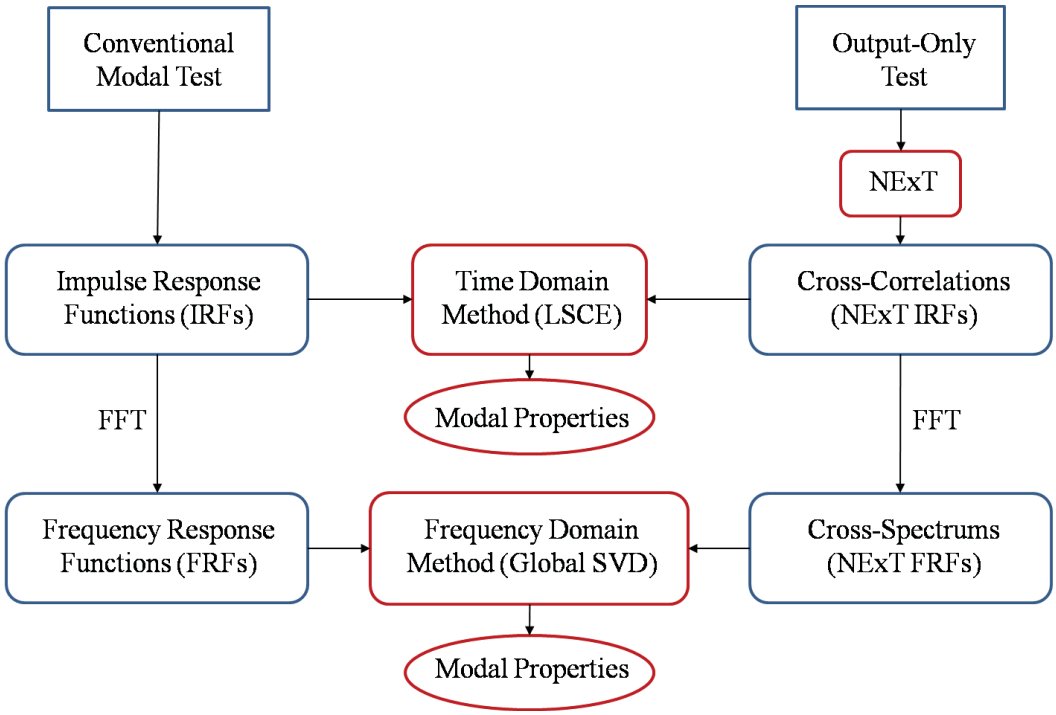

Figure 2.1: Diagram showing relation between experimental modal analysis methods and techniques.

2.1 Natural Excitation Technique (NExT)

Frequently, it is inconvenient and often near-impossible to set up and conduct a full-scale modal test with an excitation device where the force input to the system can be measured, especially on large structures. NExT, also known as output-only modal analysis or operational modal analysis, is a common remedy to this issue. The structure is instrumented with sensors to measure its response under operating conditions. NExT is then used to generate a set of curves containing the same eigenproperties as the IRFs, referred to as NExT IRFs, from the structure using response-only data. Modal parameters can then be extracted from the NExT IRFs using any time-domain modal analysis method or the IRFs can be transformed into the frequency domain via Fourier transform and modal parameters can be extracted using frequency-domain techniques (James et al., 1993).

The key result behind NExT is that, if the unknown input is assumed to be random and stationary, the cross-correlation between the response at point j and the response at point k is the sum of decaying sinusoids containing the same information as the IRF at point j due to excitation at point k (James et al., 1993). This result is obtained starting with the standard matrix form of the equations of motion for any proportionally damped, linear structure,

$$[M]\{\ddot{x}(t)\}+[C]\{\dot{x}(t)\}+[K]\{x(t)\}=\{f(t)\}, \tag{2.1}$$

where $[M]$ is the mass matrix, $[C]$ is the proportional damping matrix, $[K]$ is the stiffness matrix, $\{f(t)\}$ is a general vector of forces, and $\{x(t)\}$ is the vector of displacements. Equation (2.1) can be transformed into modal coordinates using

$$\{x(t)\}=[\Phi]\{q(t)\}=\sum_{r=1}^{N}\{\phi_r\}q_r(t) \tag{2.2}$$

where $[\Phi]$ is the modal matrix, $\{q(t)\}$ is a vector of modal coordinates, $\{\phi_r\}$ is the r^{th} mode shape, and N is the total number of modes included in the response. Substituting eq. (2.2) into (2.1) and premultiplying by $[\Phi]^T$ diagonalizes the mass, damping, and stiffness matrices (assuming real normal modes) and gives a set of scalar equations in modal coordinates:

$$\ddot{q}_r(t)+2\zeta_r\omega_n^r\dot{q}_r(t)+\omega_n^{r^2}q_r(t)=\frac{1}{m_r}\{\phi_r\}^T\{f(t)\} \tag{2.3}$$

where ω_n^r is the r^{th} natural frequency, ζ_r is the r^{th} modal damping ratio, and m_r is the r^{th} modal mass. The solution to eq. (2.3) assuming zero initial conditions is the convolution integral:

$$q_r(t)=\int_{-\infty}^{t}\{\phi_r\}^T\{f(\tau)\}g_r(t-\tau)d\tau \tag{2.4}$$

where

$$g_r(t)=\frac{1}{m_r\omega_d^r}e^{-\zeta_r\omega_n^r t}\sin(\omega_d^r t) \tag{2.5}$$

and ω_d^r is the r^{th} damped natural frequency and τ is a time shift. Substituting eq. (2.4) into (2.2) gives the solution in physical coordinates as

$$\{x(t)\}=\sum_{r=1}^{N}\{\phi_r\}\int_{-\infty}^{t}\{\phi_r\}^T\{f(\tau)\}g_r(t-\tau)d\tau\,. \tag{2.6}$$

Considering only the i^{th} point's response due to an input at point k, $x_{ik}(t)$, eq. (2.6) can be rewritten as

$$x_{ik}(t) = \sum_{r=1}^{N} \phi_{ir}\phi_{kr} \int_{-\infty}^{t} f_k(\tau) g_r(t-\tau) d\tau \tag{2.7}$$

where ϕ_{ir} and ϕ_{kr} are the i^{th} and k^{th} components of the mode shape vector, respectively, and $f_k(\tau)$ is the k^{th} component of the general forcing vector, $\{f(\tau)\}$, where the force is applied. If the forcing function, $f_k(\tau)$, is the Dirac delta function with no time shift, the integral in eq. (2.7) collapses and the equation becomes

$$x_{ik}(t) = \sum_{r=1}^{N} \frac{\phi_{ir}\phi_{kr}}{m_r \omega_d^r} e^{-\zeta_r \omega_n^r t} \sin(\omega_d^r t), \tag{2.8}$$

which is the formula for the IRF of point *i* due to excitation at point *k*.

Next, the cross-correlation between the response at two arbitrary points, *i* and *j*, due to an input at point *k* is formed. Since the only random variable is the forcing function, the cross-correlation, $R_{ijk}(T)$, is

$$R_{ijk}(T) = \sum_{r=1}^{N}\sum_{s=1}^{N} \phi_{ir}\phi_{kr}\phi_{js}\phi_{ks} \int_{-\infty}^{t}\int_{-\infty}^{t+T} g_r(t+T-\sigma) g_s(t-\tau) E[f_k(\sigma) f_k(\tau)] d\sigma d\tau \tag{2.9}$$

where *E* is the expected value operator. Assuming a stationary random input, the autocorrelation of the input force, $R_{ff}^k(\tau-\sigma)$, becomes

$$R_{ff}^k(\tau-\sigma) = E[f_k(\sigma) f_k(\tau)] = \alpha_k \delta(\tau-\sigma) \tag{2.10}$$

where α_k is a constant given by $\alpha_k = \int_{-\infty}^{\infty} f_k^2(\tau) d\tau$.

Substituting eq. (2.10) into (2.9) and carrying out the interior integral gives

$$R_{ijk}(T) = \sum_{r=1}^{N}\sum_{s=1}^{N} \alpha_k \phi_{ir}\phi_{kr}\phi_{js}\phi_{ks} \int_{-\infty}^{t} g_r(t+T-\tau) g_s(t-\tau) d\tau . \tag{2.11}$$

Letting $\lambda = t-\tau$ and making a change in the variable of integration gives

$$R_{ijk}(T) = \sum_{r=1}^{N}\sum_{s=1}^{N} \alpha_k \phi_{ir}\phi_{kr}\phi_{js}\phi_{ks} \int_{0}^{\infty} g_r(\lambda+T) g_s(\lambda) d\lambda . \tag{2.12}$$

Using eq. (2.5) and the trig identity for the sine of a sum allows for the separation of terms in λ and terms in T under the integral giving

$$g_r(\lambda+T) = e^{-\zeta_r\omega_n^r T}\cos(\omega_d^r T)\frac{e^{-\zeta_r\omega_n^r\lambda}\sin(\omega_d^r\lambda)}{m_r\omega_d^r} + e^{-\zeta_r\omega_n^r T}\sin(\omega_d^r T)\frac{e^{-\zeta_r\omega_n^r\lambda}\cos(\omega_d^r\lambda)}{m_r\omega_d^r}. \qquad (2.13)$$

Now, all terms in T can be factored out of the integral with respect to λ and the inner summation on s. Equation (2.12) becomes

$$R_{ijk}(T) = \sum_{r=1}^{N}\left[e^{-\zeta_r\omega_n^r T}\cos(\omega_d^r T)G_{ijk}^r + e^{-\zeta_r\omega_n^r T}\sin(\omega_d^r T)H_{ijk}^r\right]. \qquad (2.14)$$

where G_{ijk}^r and H_{ijk}^r are constants completely dependent on the modal parameters given by

$$\begin{Bmatrix} G_{ijk}^r \\ H_{ijk}^r \end{Bmatrix} = \sum_{s=1}^{N}\frac{\alpha_k\phi_{ir}\phi_{kr}\phi_{js}\phi_{ks}}{m_r\omega_d^r m_s\omega_d^s}\int_0^\infty e^{\left(-\zeta_r\omega_n^r-\zeta_s\omega_n^s\right)\lambda}\sin(\omega_d^s\lambda)\begin{Bmatrix}\sin(\omega_d^r\lambda)\\ \cos(\omega_d^r\lambda)\end{Bmatrix}d\lambda. \qquad (2.15)$$

Equation (2.15) can be simplified by evaluating the integral which gives

$$G_{ijk}^r = \sum_{s=1}^{N}\frac{\alpha_k\phi_{ir}\phi_{kr}\phi_{js}\phi_{ks}}{m_r m_s\omega_d^r}\left(\frac{I_{rs}}{J_{rs}^2+I_{rs}^2}\right) \qquad (2.16)$$

and

$$H_{ijk}^r = \sum_{s=1}^{N}\frac{\alpha_k\phi_{ir}\phi_{kr}\phi_{js}\phi_{ks}}{m_r m_s\omega_d^r}\left(\frac{J_{rs}}{J_{rs}^2+I_{rs}^2}\right) \qquad (2.17)$$

where

$$J_{rs} = \left(\omega_d^{s^2}-\omega_d^{r^2}\right)+\left(\zeta_r\omega_n^r+\zeta_s\omega_n^s\right)^2, \qquad (2.18)$$

$$I_{rs} = 2\omega_d^r\left(\zeta_r\omega_n^r+\zeta_s\omega_n^s\right). \qquad (2.19)$$

Defining a quantity, γ_{rs}, by

$$\gamma_{rs} = \tan^{-1}\left(I_{rs}/J_{rs}\right) \qquad (2.20)$$

and using eq. (2.20) in eqs. (2.16) and (2.17) gives

$$G_{ijk}^{r} = \frac{\phi_{ir}}{m_r \omega_d^r} \sum_{s=1}^{N} \beta_{jk}^{rs} \sqrt{J_{rs}^2 + I_{rs}^2} \sin(\gamma_{rs}) \tag{2.21}$$

and

$$H_{ijk}^{r} = \frac{\phi_{ir}}{m_r \omega_d^r} \sum_{s=1}^{N} \beta_{jk}^{rs} \sqrt{J_{rs}^2 + I_{rs}^2} \cos(\gamma_{rs}) \tag{2.22}$$

where

$$\beta_{jk}^{rs} = \frac{\alpha_k \phi_{kr} \phi_{js} \phi_{ks}}{m_s} . \tag{2.23}$$

Substituting eqs. (2.21) and (2.22) into eq. (2.14) and summing over all input locations, *k*, to find the cross-correlation due to all inputs gives

$$R_{ij}(T) = \sum_{r=1}^{N} \frac{\phi_{ir}}{m_r \omega_d^r} e^{-\zeta_r \omega_n^r T} \sum_{s=1}^{N} \sum_{k=1}^{N} \beta_{jk}^{rs} \left(J_{rs}^2 + I_{rs}^2 \right)^{-1/2} \sin\left(\omega_d^r T + \gamma_{rs} \right). \tag{2.24}$$

The inner two summations of eq. (2.24) are simply constants multiplied by a sine function with variable phase but fixed frequency. Therefore, (2.24) can be rewritten as

$$R_{ij}(T) = \sum_{r=1}^{N} \frac{\phi_{ir} C_{jr}}{m_r \omega_d^r} e^{-\zeta_r \omega_n^r T} \sin(\omega_d^r T + \theta_{jr}) \tag{2.25}$$

where

$$C_{jr} = \sqrt{\left(\sum_{s=1}^{N} \sum_{k=1}^{N} \beta_{jk}^{rs} \left(J_{rs}^2 + I_{rs}^2 \right)^{-1/2} \sin(\gamma_{rs}) \right)^2 + \left(\sum_{s=1}^{N} \sum_{k=1}^{N} \beta_{jk}^{rs} \left(J_{rs}^2 + I_{rs}^2 \right)^{-1/2} \cos(\gamma_{rs}) \right)^2} \tag{2.26}$$

is simply a constant multiplier and

$$\tan(\theta_{jr}) = \frac{\sum_{s=1}^{N} \sum_{k=1}^{N} \beta_{jk}^{rs} \left(J_{rs}^2 + I_{rs}^2 \right)^{-1/2} \cos(\gamma_{rs})}{\sum_{s=1}^{N} \sum_{k=1}^{N} \beta_{jk}^{rs} \left(J_{rs}^2 + I_{rs}^2 \right)^{-1/2} \sin(\gamma_{rs})} \tag{2.27}$$

where θ_{jr} is a constant phase angle. Comparing eq. (2.25) with (2.8), it can be seen that the cross-correlation function is a sum of decaying sinusoids with the same eigenvalues as the impulse response function of the original system (James et al., 1993).

2.2 Extension of Natural Excitation Technique (NExT)

A new extension of NExT using an impulse force as input has been developed for the work in this thesis and is presented in this section. Since an impulsive sonic boom is used in this thesis as the input force to both structural and acoustic systems, this is a useful exercise to prove the validity of using the response to a sonic boom with NExT. The derivation is the same as in the previous section up to eq. (2.9) which is repeated here for convenience:

$$R_{ijk}(T) = \sum_{r=1}^{N}\sum_{s=1}^{N}\phi_{ir}\phi_{kr}\phi_{js}\phi_{ks}\int_{-\infty}^{t}\int_{-\infty}^{t+T} g_r(t+T-\sigma)g_s(t-\tau)R_{ff}^{k}(\tau-\sigma)d\sigma d\tau\,. \tag{2.28}$$

If the input force is an impulse of infinitesimal duration and finite amplitude, the autocorrelation of the input force, becomes

$$R_{ff}^{k}(\tau-\sigma) = \alpha'_k\,\delta(\tau-\sigma)\,. \tag{2.29}$$

where α'_k is the square of the amplitude of the impulse input. Comparing eqs. (2.29) and (2.10), it can be seen that the same result is derived. Thus, the autocorrelation of an infinitesimal impulse is exactly the same as the autocorrelation of a stationary, random input and the derivation of NExT carries out in the same manner as described in the previous section. The only difference in the derivation presented using an impulse input rather than a random, stationary input is the calculation of the value of α'_k which is the square of the amplitude of the impulse, different from α_k defined by $\alpha_k = \int_{-\infty}^{\infty} f_k^2(\tau)d\tau$.

In practice, an ideal infinitesimal impulse input is impossible to attain; all impulsive excitations will have some finite duration such as the sonic boom used in this thesis. The result of using a non-ideal impulse is that the cross-correlations of the responses measured are now convolved with the autocorrelation of the finite duration impulse input force, R_{ff}^{k}, as demonstrated by eq. (2.28). This, in turn, limits the frequency range of analysis because the magnitude of the spectrum of R_{ff}^{k}, or the power spectral density of the input, now rolls off as

frequency is increased instead of remaining constant over the entire frequency range as in the case of stationary, random noise or an infinitesimal impulse.

How quickly this roll off occurs depends on how long the impulsive input remains correlated with itself called the correlation duration, T_C. The duration of the correlation is roughly equal to twice the duration of the finite impulse, T_I, or

$$T_C \approx 2T_I . \tag{2.30}$$

For a mode to be identified using this technique, its modal period, T_N, must be longer than the correlation duration, T_C, or

$$T_N > T_C . \tag{2.31}$$

Otherwise the amplitude of the mode will be suppressed by its multiplication with the spectrum of R_{ff}^k which has a small magnitude beyond the frequency corresponding to the correlation duration,

$$f_C = \frac{1}{T_C} . \tag{2.32}$$

Thus, the largest natural frequency, $f_N = 1/T_N$, which will not be suppressed when using NExT with an impulsive input is given by

$$f_N < f_C . \tag{2.33}$$

Therefore, the shorter the impulse, the shorter the correlation duration and the larger the frequency range of analysis can extend using NExT with an impulsive input.

2.3 Global Singular Value Decomposition (Global SVD) Method

The Global SVD method is explained in detail in this section (Ewins, 2000). This method is well-suited for the analysis of the global modal data sets which contain many FRFs and have high modal density, even at low frequencies. This is because 1) it is a global method capable of fitting many curves to many different FRFs simultaneously and 2) it is a multi-degree of freedom method which can extract closely spaced and even coupled modes (Ewins, 2000).

The method requires measuring the FRFs between a single excitation point and M response locations on the structure. To calculate the required inputs for the Global SVD method, all

measured accelerance FRFs, $H_a(\omega)$, (acceleration over force) are integrated twice to get mobility, $H_v(\omega)$, (velocity over force) and receptance, $H_d(\omega)$, (displacement over force) FRFs. In the frequency domain, they are simply related as

$$H_v(\omega) = \frac{H_a(\omega)}{i\omega} \qquad H_d(\omega) = -\frac{H_a(\omega)}{\omega^2} \tag{2.34}$$

where ω is the frequency in rad/s and i is the imaginary unit.

The measured receptance and mobility FRFs are arranged in matrix forms with each row corresponding to a different response point and each column corresponding to a different excitation point. For the Global SVD method, only one excitation point is considered, so the receptance is a frequency dependent vector. Assuming proportional damping, the receptance vector $\{H_d(\omega)\}$ can be expressed as

$$\{H_d(\omega)\}_{Mx1} = [\Phi]_{MxN} \left[\left(i\omega - s_r\right)\right]^{-1}_{NxN} \{\phi_k\}_{Nx1} + \{R(\omega)\}_{Mx1} \tag{2.35}$$

where $[\Phi]$ is the mode shape matrix, $\left[\left(i\omega - s_r\right)\right]$ is a frequency dependant diagonal matrix, s_r is the r^{th} eigenvalue, $\{\phi_k\}$ is the column of the modal matrix associated with the k^{th} degree of freedom at the point of excitation, $\{R(\omega)\}$ is a vector containing terms to account for residual modes outside the frequency range of interest, M is the number of measured response points (degrees of freedom), N is the number of modes in the frequency range, and r indicates the mode number (Ewins, 2000).

Denoting

$$\{g(\omega)\}_{Nx1} = \left[\left(i\omega - s_r\right)\right]^{-1}_{NxN} \{\phi_k\}_{Nx1} \tag{2.36}$$

and replacing this into eq. (2.35) leads to

$$\{H_d(\omega)\}_{Mx1} = [\Phi]_{MxN} \{g(\omega)\}_{Nx1} + \{R(\omega)\}_{Mx1} \tag{2.37}$$

The mobility vector which is obtained by differentiating eq. (2.37) with respect to time, is then

$$\{H_v(\omega)\}_{Mx1} = [\Phi]_{MxN} [s_r]_{NxN} \{g(\omega)\}_{Nx1} + \{R(\omega)\}_{Mx1}. \tag{2.38}$$

where $[s_r]$ is a diagonal matrix of eigenvalues. To lessen the contribution of residual modes to the modes being extracted, frequency response difference vectors, $\{\Delta H_d(\omega)\}$ and $\{\Delta H_v(\omega)\}$, are defined by

$$\{\Delta H_{d,v}(\omega)\} = \{H_{d,v}(\omega_l)\} - \{H_{d,v}(\omega_{l+c})\}, \tag{2.39}$$

where the subscript l is an integer indicating the l^{th} frequency and c is some small integer constant dependent upon the frequency resolution and modal density (Ewins, 2000). Then, eqs. (2.37) and (2.38) can be approximated as

$$\begin{aligned} \{\Delta H_d(\omega)\} &\approx [\Phi]\{\Delta g(\omega)\} \\ \{\Delta H_v(\omega)\} &\approx [\Phi][s_r]\{\Delta g(\omega)\} \end{aligned}. \tag{2.40}$$

Now, frequencies up to l=L are considered and eq. (2.40) becomes

$$\begin{aligned} [\Delta H_d]_{MxL} &= [\Phi]_{MxN}[\Delta g]_{NxL} \\ [\Delta H_v]_{MxL} &= [\Phi]_{MxN}[s_r]_{NxN}[\Delta g]_{NxL} \end{aligned}. \tag{2.41}$$

Eliminating $[\Delta g]$, eq. (2.41) can be rewritten as

$$[\Phi^+][\Delta H_v] = [s_r][\Phi^+][\Delta H_d] \tag{2.42}$$

where the $^+$ superscript denotes a generalized or pseudo-inverse which is used because the modal matrix is not necessarily square and a true inverse may not exist. Considering one eigenvalue at a time, the $[s_r]$ matrix becomes a scalar and $[\Phi^+]$ becomes a vector and eq. (2.42) becomes

$$\{z_r\}^T_{1xM}[\Delta H_v]_{MxL} = s_r\{z_r\}^T_{1xM}[\Delta H_d]_{MxL} \tag{2.43}$$

where $[z] = [\Phi^+]^T$ and $\{z_r\}$ is one column of this matrix pertaining to the r^{th} mode.

Taking the transpose and rearranging, eq. (2.43) becomes

$$\left([\Delta H_v]^T_{LxM} - s_r[\Delta H_d]^T_{LxM}\right)\{z_r\}_{Mx1} = \{0\}_{Lx1}. \tag{2.44}$$

Next, applying a SVD on $[\Delta H_d]^T$ gives

$$\left[\Delta H_d\right]^T{}_{LxM} = \left[P\right]_{LxL}\left[\sigma\right]_{LxM}\left[Q\right]^T{}_{MxM}. \tag{2.45}$$

The generalized inverse of $\left[\Delta H_d\right]^T$ can be reconstructed from the first N' modes of the SVD if $\sigma_{N'}$ is much smaller than the first singular value:

$$\left(\left[\Delta H_d\right]^T\right)^+{}_{MxL} = \left[Q\right]_{MxN'}\left[\sigma^{-1}\right]_{N'xN'}\left[P\right]^T{}_{N'xL}. \tag{2.46}$$

Premultiplying eq. (2.44) by $\left(\left[\Delta H_d\right]^T\right)^+$ gives the eigenvalue problem

$$\left\{\left(\left[\Delta H_d{}^T\right]\right)^+{}_{MxL}\left[\Delta H_v\right]^T{}_{LxM} - \left[I\right]_{MxM}s_r\right\}\left\{z_r\right\}_{Mx1} = \left\{0\right\}_{Mx1}. \tag{2.47}$$

Solving this eigenvalue problem gives N' non-zero eigenvalues which relate to the eigenproperties according to the assumed proportional damping model by

$$s_r = -\omega_n^r\zeta_r + i\omega_n^r\sqrt{1-\zeta_r{}^2} \tag{2.48}$$

where ω_n^r is the r^{th} natural frequency and ζ_r is the r^{th} modal damping ratio (assumed to be less than critical, e.g. $\zeta_r < 1$). A matrix of modal constants, A, related to the mode shapes are determined by solving

$$\begin{Bmatrix} H_{d,jk}(\omega_1) \\ H_{d,jk}(\omega_2) \\ \cdots \\ H_{d,jk}(\omega_L) \end{Bmatrix}_{Lx1} = \begin{bmatrix} (i\omega_1 - s_1)^{-1} & (i\omega_1 - s_2)^{-1} & \cdots & (i\omega_1 - s_{N'})^{-1} \\ (i\omega_2 - s_1)^{-1} & (i\omega_2 - s_2)^{-1} & \ddots & \vdots \\ \vdots & \ddots & \ddots & \vdots \\ (i\omega_L - s_1)^{-1} & \cdots & \cdots & (i\omega_L - s_{N'})^{-1} \end{bmatrix}_{LxN'} \begin{Bmatrix} {}_1A_{jk} \\ {}_2A_{jk} \\ \vdots \\ {}_{N'}A_{jk} \end{Bmatrix}_{N'x1} \tag{2.49}$$

in a least-squares sense for each measured degree of freedom, j, where ${}_rA_{jk}$ is the r^{th} modal constant for the j^{th} degree of freedom with the k^{th} degree of freedom being excited defined by a multiplication of the r^{th} mode shape values at point j and point k:

$${}_rA_{jk} = \phi_{jr}\phi_{kr}. \tag{2.50}$$

A drivepoint FRF is the FRF whose response point coincides with the point of excitation. If this FRF is measured, then the entire mode shape matrix can be obtained using

$$\phi_{kr} = \sqrt{{}_r A_{kk}} \tag{2.51}$$

to obtain the mode shape element, ϕ_{kr}, for each mode at the point of excitation. The other elements of the modal matrix, ϕ_{jr}, can be obtained with (Ewins, 2000)

$$\phi_{jr} = \frac{{}_r A_{jk}}{\phi_{kr}}. \tag{2.52}$$

If these modes are assumed to be real and normal, the modal matrix can be simplified to a matrix of real numbers. Each element's amplitude is defined by the magnitude of ϕ_{jr} and its phase is simplified to either completely in phase or out of phase by assigning a positive magnitude for phase angles of ϕ_{jr} between positive and negative 90^o and a negative magnitude for phase angles outside this range.

In order to determine how well the Global SVD method performed, FRFs can be regenerated from the eigenproperties extracted and compared to the measured FRFs. If the drivepoint FRF measurement was made, then the FRFs can be regenerated using eq. (2.35). If no drivepoint FRF was measured, the FRFs can be regenerated using

$$\left[H_d(\omega)\right]_{MxL} = \left[A\right]_{MxN'}\left[\left(i\omega - s_r\right)^{-1}\right]_{N'xL} + \left[R(\omega)\right]_{MxL} \tag{2.53}$$

where $\left[\left(i\omega - s_r\right)^{-1}\right]$ is the matrix defined in eq. (2.49). In either case, residual terms, $\left[R(\omega)\right]$, must be included to account for out of range modes which effect the FRF in the frequency range of interest. These residual modes can be accounted for by two terms: mass-like behavior for low-frequency residual modes and a stiffness effect for high-frequency residual modes (Ewins, 2000). For a single FRF, this can be expressed as

$$H_{d,jk}(\omega) \approx -\frac{1}{\omega^2 M_{jk}} + \sum_{r=N_1}^{N_2}\left(\frac{{}_r A_{jk}}{i\omega - s_r}\right) + \frac{1}{K_{jk}} \tag{2.54}$$

where M_{jk} is a constant associated with the residual mass mode and K_{jk} is a constant associated with the residual stiffness mode. The two constants M_{jk} and K_{jk} can be determined by comparing individual measured FRFs and their corresponding regenerated FRFs at one point at the low end of the frequency range and one point at the high end of the frequency range (Ewins, 2000). Once these terms are added to the regenerated FRF, quantitative and qualitative comparisons between the measured and regenerated FRFs can be made to determine the success of the curve-fitting procedure.

2.4 Least Squares Complex Exponential (LSCE) Method

This section presents the mathematical details behind the single-reference Least Squares Complex Exponential (LSCE) method for modal analysis as discussed by Mohanty and Rixen (2004a). LSCE is a time-domain curve-fitting procedure used to extract eigenproperties from the IRFs, $h(t)$, of a system. The discrete response, $h_{jk}(l\Delta t)$, at point j due to an impulse at point k can be written as the sum of decaying exponentials and their complex conjugates, denoted with an asterisk, as in

$$h_{jk}(l\Delta t) = \sum_{r=1}^{N} \phi_{jr} e^{s_r l\Delta t} \phi_{kr} + \sum_{r=1}^{N} \phi_{jr}^{*} e^{s_r^{*} l\Delta t} \phi_{kr}^{*} \tag{2.55}$$

where l is an integer number starting at zero, Δt is a constant discrete time step, r is the mode index, N is the total number of modes included in the response, and ϕ is the scaled mode shape constant. The eigenvalue, s_r, is defined by

$$s_r = \omega_n^r \zeta_r + i\omega_n^r \sqrt{1-\zeta_r^{\,2}} \tag{2.56}$$

where ω_n^r is the r^{th} natural frequency and ζ_r is the r^{th} damping ratio. Equation (2.55) can be rewritten more conveniently by

$$h_{jk}(l\Delta t) = \sum_{r=1}^{2N} {}_{r}A'_{jk}\, e^{s_r l\Delta t} \tag{2.57}$$

where ${}_{r}A'_{jk}$ is now the combination of the scaled mode shape constants and

$$\begin{matrix} {}_{r+N}A'_{jk} = {}_{r}A'^{*}_{jk} \\ s_{r+N} = s_r^* \end{matrix}. \tag{2.58}$$

Since the eigenvalues appear in complex conjugate form in eq. (2.57), there must exist a polynomial of order 2*N*, known as Prony's equation, of which $e^{s_r \Delta t}$ are the roots. This equation is defined by

$$\beta_0 + \beta_1 V_r^1 + \beta_2 V_r^2 + ... + \beta_{2N-1} V_r^{2N-1} + V_r^{2N} = 0 \tag{2.59}$$

where β are constant coefficients and

$$V_r = e^{s_r \Delta t}. \tag{2.60}$$

The coefficients, β, can be determined by multiplying the impulse response at time $l\Delta t$ by the coefficient β_l and summing the values from *l*=0 to 2*N* demonstrated by

$$\sum_{l=0}^{2N} \beta_l h_{jk}(l\Delta t) = \sum_{l=0}^{2N} \left(\beta_l \sum_{r=1}^{2N} {}_{r}A'_{jk} V_r^l \right) = \sum_{r=1}^{2N} \left({}_{r}A'_{jk} \sum_{l=0}^{2N} \beta_l V_r^l \right) = 0. \tag{2.61}$$

Now, to obtain the necessary number of equations to solve for the coefficients, eq. (2.61) is written at least 2*N* times beginning at consecutively increasing time samples, *l*:

$$\beta_0 h_l + \beta_1 h_{l+1} + ... + \beta_{2N-1} h_{l+2N-1} = -h_{l+2N},\ l = 0,1,...,L. \tag{2.62}$$

Here, the notation is simplified by $h_l = h_{jk}(l\Delta t)$ and $L > 2N-1$ to obtain an overdetermined system of equations which can be solved in a least-squares sense for β. In matrix form, eq. (2.62) is written

$$[h]_{Lx2N} \{\beta\}_{2Nx1} = -\{h'\}_{Lx1}. \tag{2.63}$$

To determine the coefficients in an average sense for *P* IRFs with a common reference point, *k*, eq. (2.63) can be written *P* times,

$$\begin{bmatrix} [h]_1 \\ [h]_2 \\ \vdots \\ [h]_p \end{bmatrix}_{PLx2N} \{\beta\}_{2Nx1} = -\begin{Bmatrix} \{h'\}_1 \\ \{h'\}_2 \\ \vdots \\ \{h'\}_p \end{Bmatrix}_{PLx1}, \tag{2.64}$$

since the eigenvalues, and thus, the coefficients will not change for a linear system by altering only the point of response. Solving eq. (2.64) in a least-squares sense results in the values for β. As demonstrated previously, the roots of these coefficients are V_r from which the eigenvalues, s_r, can be obtained from the solution to eq. (2.60). The modal properties can then be calculated by solving eq. (2.56).

A vector of unscaled modal constants, $\{A'_{jk}\}$, can then be recovered for each response point, *j*, using

$$\{A'_{jk}\}_{2Nx1} = [V_{jk}]^{-1}_{2Nx2N} \{h_{jk}(l\Delta t)\}_{2Nx1} \tag{2.65}$$

where the vector, $\{h_{jk}(l\Delta t)\}$, is the first column of each matrix, $[h]_p$ in eq. (2.64) and the coefficient matrix, $[V_{jk}]$, is defined by (Ewins, 2000)

$$[V_{jk}]_{2Nx2N} = \begin{bmatrix} V_1^0 & V_2^0 & \cdots & V_{2N}^0 \\ V_1^1 & V_2^1 & \ddots & V_{2N}^1 \\ \vdots & \ddots & \ddots & \vdots \\ V_1^{2N-1} & V_2^{2N-1} & \cdots & V_{2N}^{2N-1} \end{bmatrix}. \tag{2.66}$$

If a drivepoint IRF is measured, scaled mode shapes, ϕ, can be determined by first noting that

$$\phi_{kr} = \sqrt{{}_r A'_{kk}}\ . \tag{2.67}$$

The other elements of the modal matrix can then be found by

$$\phi_{jr} = \frac{{}_r A'_{jk}}{\phi_{kr}}. \tag{2.68}$$

For analysis of the performance of the curve-fitting procedure described, IRFs can be regenerated from the extracted eigenvalues using eq. (2.55) or (2.57) and error between measured and regenerated IRFs can be calculated.

3 *Structural Experimental Modal Analysis*

In this chapter, experimental modal analysis of the structural subsystems will be discussed. First, the single room structure will be examined followed by the two room structure. For each structure, a conventional modal test is first undertaken. This is followed by experimental modal analysis using NExT and the response to a sonic boom. Then, a comparison of the results of these techniques along with results obtained from a finite element model will be discussed.

3.1 Single Room Structure Modal Analysis

In this section, the structural modal testing and analysis of the single room structure shown in Figure 3.1 will be presented. First, conventional modal testing and analysis will be discussed followed by output-only modal testing and analysis using NExT. Then, a comparison between these analyses and a finite element analysis will be given to provide a validation of using sonic boom response with NExT to obtain modal properties.

(a) (b)

Figure 3.1: (a) Front and (b) back sides of the completely assembled and instrumented single room structure .

Overall, the structure is 4.9 x 2.8 x 3.0 m and was built using standard residential construction techniques and materials consisting of lumber, oriented strand board (OSB), drywall, and insulation. The dimensions of the room were measured to be 4.6 x 2.6 x 2.5 m. Additional features of the structure include two double-pane glass windows and a hollow core masonite door. The six sides of the structure are referred to as the wall with windows, wall with door, long plain wall, short plain wall, roof, and floor. For a detailed description of the single room structure, refer to Haac et al. (2009).

3.1.1 Conventional Modal Testing

In this section, conventional modal testing in which both the input force and structural response are measured of the single room structure is discussed. It begins with an overview of the instrumentation and experimental setup followed by a description of the tests performed. Then, the procedure used to analyze the data collected is presented. The section concludes with the structural modal properties obtained as a result of the conventional modal analysis.

3.1.1.1 Experimental Setup

These structural tests were performed as part of a separate project (Ravetta et al., 2009) and will be briefly described in this section. The data was then transferred to Virginia Tech for the analysis presented later. In the conventional modal tests, accelerometers measured the response of the systems and impact hammers provided input. To this end, an array of accelerometers was used to measure the response to impulsive inputs using impact hammers. Three types of accelerometers were used in the conventional modal tests. Fifteen PCB model 330A accelerometers shown in Figure 3.2 were mounted to the interior surfaces of the structure. Ten of these accelerometers were mounted to the centers and a corner of each surface of the test structure except for the floor. Two were mounted to the interior surfaces of each window, one in the center and one in a corner. The last accelerometer was mounted to the center of the door of the structure (Ravetta et al., 2009). These accelerometers are shown mounted in Figure 3.3. In addition to the PCB 330A accelerometers, three PCB 338B34 accelerometers and one PCB 353B18 were also used to measure the vibration response of the structure. These accelerometers are also shown in Figure 3.2. The accelerometers were mounted on the inside panel of one of the window, and near the center of the wall with windows, ceiling, and both short side walls on the inside as shown in Figure 3.3. All wall accelerometers were mounted on studs of the structure (Ravetta et al., 2009).

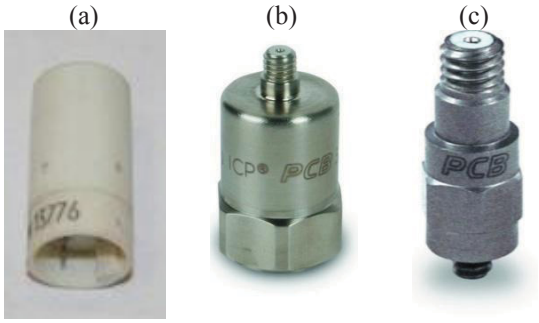

Figure 3.2: Pictures of (a) PCB 330A accelerometer, (b) PCB 338B34 accelerometer, and (c) PCB 353B18 accelerometer used in the conventional impact hammer modal testing.

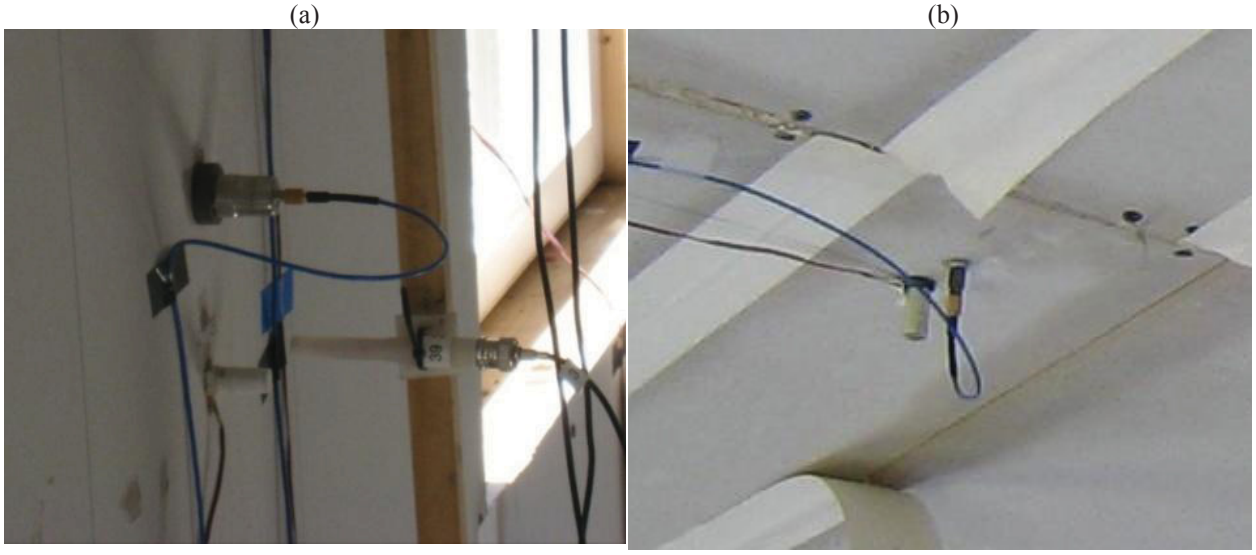

Figure 3.3: (a) PCB 330A and PCB 338B34 accelerometers and (b) PCB 330A and PCB 353B18 accelerometers mounted to single room structure for modal testing.

Two different sized impact hammers were used to excite the structure. A large B&K Modal Sledge Hammer (Type 8208), shown in Figure 3.4, was used when impacting the exterior surfaces of the walls of the structure themselves. The hammer has a three pound head and was fitted with the hardest impact tip in all tests. A small PCB Impact Hammer (086C03), shown in Figure 3.4, was used to excite the windows and doors (Ravetta et al., 2009).

Figure 3.4: Large Brüel and Kjær Modal Sledge Hammer (Type 8208) used to provide impulsive excitation of the test structure's walls and and small PCB Impact Hammer (086C03) used to provide impulsive excitation to the windows and doors of the test structure.

A 128-channel data acquisition system was used to acquire signals from the accelerometers and microphones in the conventional modal tests. The acquisition system was kept on two racks along with the signal conditioning equipment in the center of the room. In the tests, each exterior surface of the structure was divided into a non-uniform grid of excitation points, shown in Figure 3.5. There were 19 points on the wall with windows, 11 points on the wall with the door, 16 points on the long plain wall, 12 points on the short plain wall, and 17 points on the roof of the structure. All of these points were located on studs to input energy effectively into the structure. The exterior surfaces of the windows and door were divided into separate, uniform grids consisting of 9 points per window and 15 points on the door. There were a total of 108 excitation points on the structure (Ravetta et al., 2009).

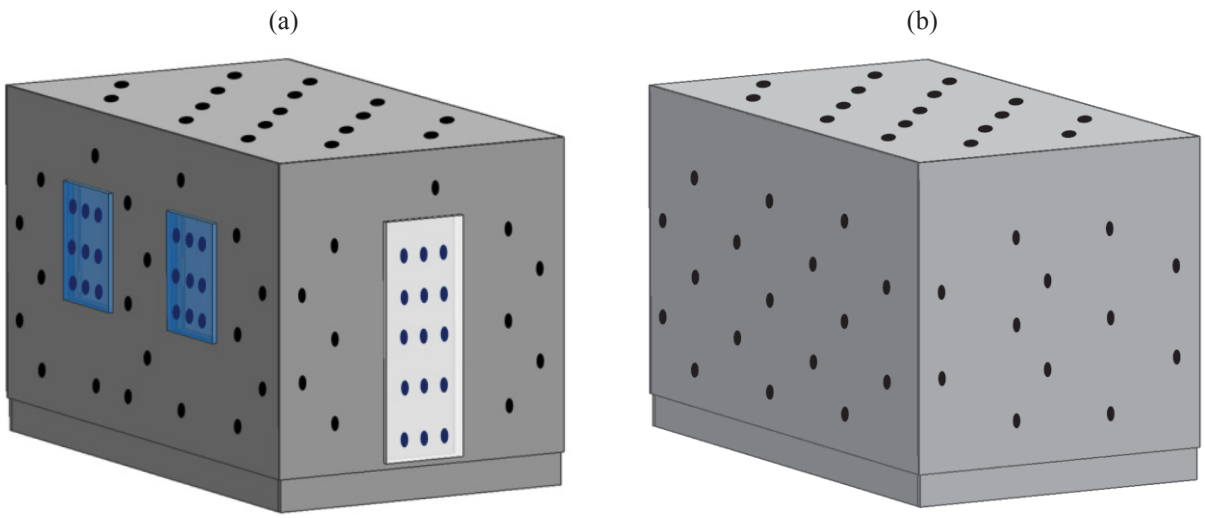

Figure 3.5: Drawing showing approximate locations of all the positions hammered on (a) the front of the single room structure and (b) the back in the conventional modal testing. Black dots indicate positions where the larger impact hammer was used and blue dots indicate the use of the smaller impact hammer.

3.1.1.2 Analysis and Results

The procedure used to analyze the data collected from the conventional modal test will be discussed in this section followed by the results of the analysis. A diagram of the basic analysis procedure is shown in Figure 3.6. From the frequency response functions (FRFs) and coherence measured in the modal test, a mode indicator function is calculated to estimate the number of modes in the frequency range. The Global SVD method is applied assuming this number of modes and square error between measured and regenerated FRFs is computed. The number of modes is increased and the Global SVD method is repeated until twice the original number of modes is reached. The correct number of modes in the frequency range is determined from the least square error in real and imaginary parts. Then, the Global SVD method is repeated for this number of modes using slightly perturbed frequency ranges to separate physical modes from computational. Modal Assurance Criterion (MAC) values are calculated between the original analysis and perturbed analyses. Modes with high MAC values are said to be the physical modes of the structure.

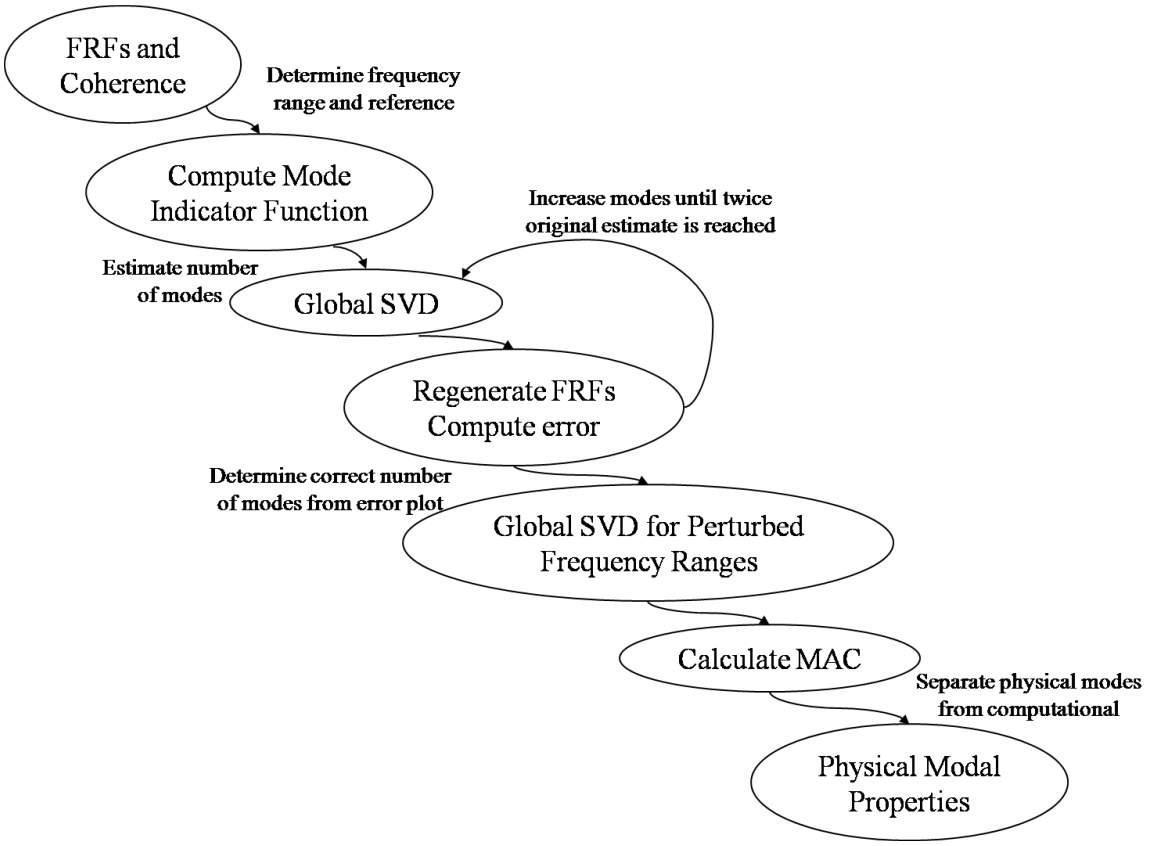

Figure 3.6: Diagram demonstrating the approach used to determine the physical modal properties of the single room structure from the conventional modal test.

The structural response, measured using 15 PCB 330A accelerometers and 4 high-quality PCB accelerometers discussed previously, and the input force, measured by the impact hammers discussed previously, was sampled at about 51.2 kHz. The data was then downsampled to 6400 Hz. Average frequency response functions (FRFs) were then computed between five hits of each excitation and response position for a total of 1,944 transfer functions. In general, the coherence of the average transfer functions was good in the frequency range from about 7 to 100 Hz as shown in the typical sample coherence plot in Figure 3.7 (Ravetta et al., 2009). This average coherence plot was obtained by an accelerometer close to the center of the wall with windows due to excitation on the wall near that point on the exterior surface. A Poisson exponential window with α equal to 3 was used for the averaging process and applied to the accelerometer response to reduce leakage in the resulting FRF (Ravetta et al., 2009). The average FRFs were corrected for the exponential window use by simply dividing by 0.64 (Harris, 1978). The exponential window also adds artificial damping to the response which was corrected using a

simple technique applied directly to the modal damping ratios once extracted (Taber et al., 1985).

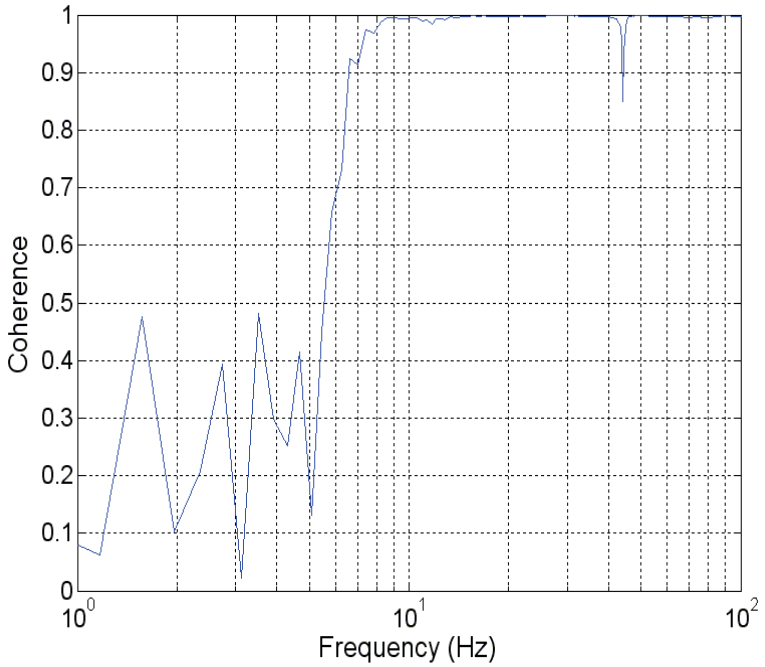

Figure 3.7: Typical sample average coherence plot measured by an accelerometer close to the center of the wall with windows due to excitation on the wall near that point on the exterior surface

The impact hammer test FRFs were analyzed as described next. First, one of the nineteen accelerometers was selected as a reference for analysis. The choice was made based on visual inspection of a simple mode indicator function obtained by summing up all the transfer functions measured by a single accelerometer. This method removes random variations in the frequency and damping characteristics of the structure which may shift depending on the individual FRF. However, the constant multiplier of each mode is now a very complicated combination of mode shape elements (Ewins, 2000), rendering this technique unsuitable for modal analysis but effective in determining which accelerometer to use as a reference since all the information obtained by that sensor is represented in a single function. The reference accelerometer selected for analysis was located slightly off-center on the wall with windows. The associated simple mode indicator function is shown in Figure 3.8. All of the FRFs measured with this accelerometer from the grid of impulse excitation points described previously were then stored in a matrix with the rows corresponding to different excitation points and the columns corresponding to different frequencies.

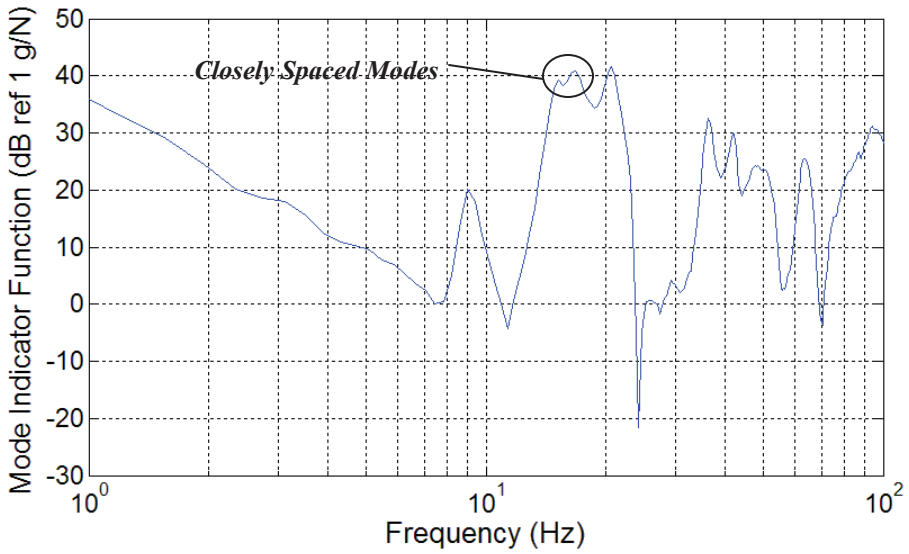

Figure 3.8: Simple mode indicator function for the reference accelerometer used in modal analysis located slightly off-center on the wall with windows.

Next, the structure was assumed to satisfy reciprocity. The principle of reciprocity states that, for any linear elastic structure, the response measured at point 'A' due to an excitation force at point 'B' is equal to the response measured at point 'B' due to the same excitation force at point 'A' (Pierce, 1989). Thus, the response at the single reference points due to impulsive forces located on the grid of excitation points becomes the response at each point of the grid of excitation points due to an impulsive force at the location of the reference accelerometer. The accelerance FRFs measured by the reference accelerometer were then integrated with respect to time. Since the mode indicator function in Figure 3.8 demonstrates closely spaced resonances starting around 15 Hz and 109 total FRFs were to be analyzed, the Global SVD method was chosen for experimental modal analysis. This is a multiple degree of freedom curve-fitting procedure capable of extracting closely spaced modes from FRFs obtained from many response points with the same excitation point (Ewins, 2000).

The curve-fitting procedure was carried out over the frequency range from 5 to 100 Hz, where the measured FRFs demonstrated good coherence. More difficult to determine was the correct number of modes to be extracted. First, an initial estimate of the number of modes in the frequency range of interest by counting the number of peaks in the simple mode indicator function plotted in Figure 3.8. This number, 13, was assumed to be the minimum number of modes required to accurately represent the FRFs measured from the structure. The Global SVD

method was carried out over the frequency range using this minimum number of modes and the eigenproperties were extracted.

Since no drivepoint FRF was measured, FRFs were regenerated and the residual terms were calculated and added to the regenerated FRFs as discussed in the description of the Global SVD method in section 2.3. The total square error in real and imaginary parts was then calculated for each FRF and averaged. The assumed number of modes was then increased, consecutively, to twice the number of modes originally assumed. A general rule of thumb is to include 1.5 to 2 times the number of physical modes present in a system to successfully model that system numerically (Ewins, 2000). At each assumed number of modes, the eigenproperties were extracted, FRFs were regenerated, and average square error in real and imaginary parts was calculated.

Based on the square error, 22 modes were used as the correct number of modes in the frequency range of interest (Corcoran et al., 2009). To determine the overall success of the curve-fit procedure, the measured FRFs were regenerated from the extracted eigenproperties. The regenerated FRFs were summed linearly to regenerate the simple mode indicator discussed previously. The measured and regenerated mode indicator functions are plotted in Figure 3.9. Overall, the curve-fit procedure did a fairly good job over the entire frequency range with some discrepancies towards the edges of the range. However, an antiresonance near 25 Hz caused an approximate 360 degree jump in phase which is captured in the measured mode indicator function but missed by the regenerated function. Since this is a jump of one full cycle, the response will be unaffected by the absence of this jump in the regenerated FRFs.

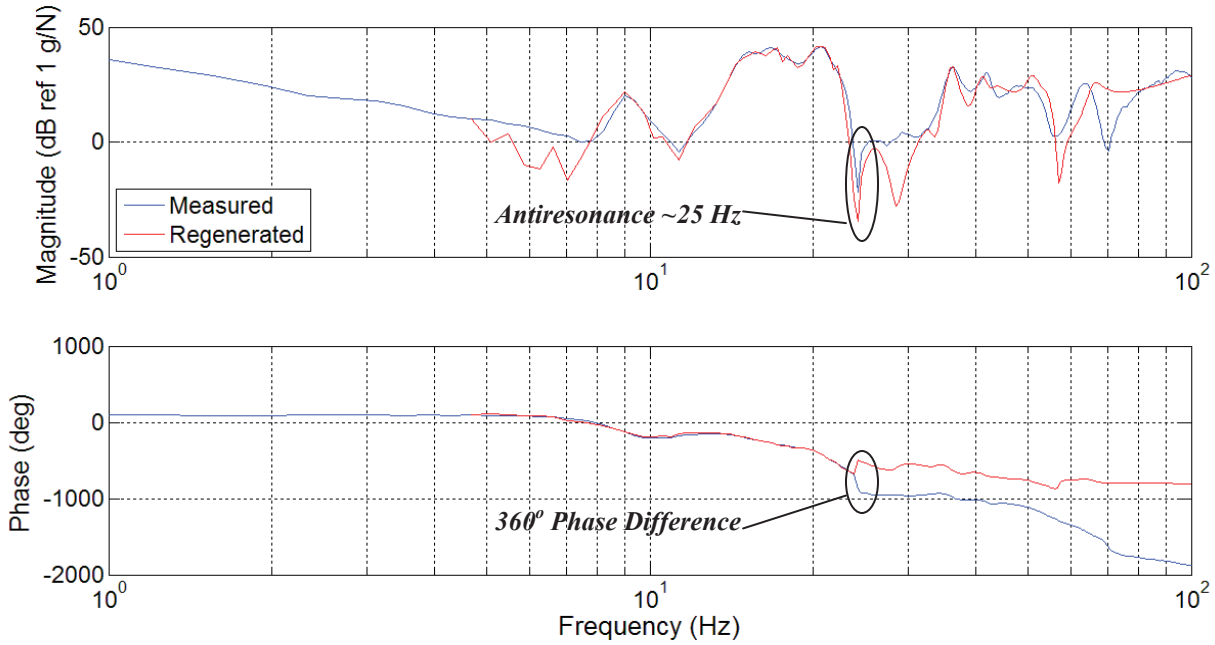

Figure 3.9: Comparison between measured and regenerated simple mode indicator functions.

Not all of the extracted modes were genuine, physical modes; some computational modes exist due to noise or other irregularities in the measured data. The procedure used for identifying these computational modes which involves calculating MAC values between the original analysis and analyses using perturbed frequency ranges is discussed by Corcoran et al. (2009). The modal parameters for the genuine, physical modes are listed in Table 3.1 and the mode shapes can be found in Figure 3.10 and Figure 3.11. The damping ratios listed were corrected for the damping added by the exponential window using the simple expression (Taber et al., 1985)

$$\zeta_r = \zeta_r' - \frac{\alpha f_s}{N \omega_n^r} \tag{3.1}$$

where ζ_r is the r^{th} corrected modal damping ratio, ζ_r' is the r^{th} extracted modal damping ratio, ω_n^r is the r^{th} natural frequency, f_s is the sampling frequency, N is the number of data points in the window, and α is the coefficient of the exponential window used (3.0 in this case). The mode shapes were calculated by assuming real, normal modes and simplifying the modal constants to real numbers either in or out of phase as discussed in the description of the Global SVD method. They were then amplified for plotting.

Table 3.1: Modal parameters of the physical modes of the single room structure.

Mode	*Natural Frequency (Hz)*	*Damping Ratio (%)*
1	8.84	0.35
2	14.47	1.94
3	17.20	0.03
4	20.28	3.19
5	21.60	0.10
6	43.08	2.47
7	50.96	2.14
8	65.82	2.95

Three dimensional (3D) views of the mode shapes are given in Figure 3.10. In Figure 3.11, three two dimensional (2D) views of the physical global mode shapes are given. In the first column is the front view facing the wall with windows. In the second is a side view facing the wall with the door and the last column contains a top view looking down on the roof of the structure. In each plot, the undeformed structure is plotted as a red box with separate boxes for the two windows and door and the mode shape is plotted as a blue mesh. The mode shape grid was obtained by cubic interpolation between measured points on the structure. There was no extrapolation or interpolation between surfaces of the structure.

From Table 3.1, Figure 3.10, and Figure 3.11, it is clear that the conventional modal testing was not a complete success. It can be seen in the mode indicator function plotted in Figure 3.8 that there are more resonances in the frequency range beyond the last mode extracted at about 66 Hz. The Global SVD method failed to extract physical modes in this range probably due to the high modal density demonstrated in Figure 3.8. It can also be seen from Figure 3.8 that there are some resonances in the mode indicator function which were not extracted as physical modes with the Global SVD method, e.g. the resonances around 25, 29, 37, and 48 Hz.

From Figure 3.10 and Figure 3.11, it can be seen that the mode shapes of the physical modes that were extracted at lower frequencies are not very clear. There are many irregularities in the deformed shapes of the structure which make it difficult to interpret how the structure physically vibrates in its modes. This is probably due to the real, normal mode assumption made to simplify the complex modes of the structure. However, some information useful to the numerical model can be obtained from the conventional modal test. The natural frequencies of the physical modes

do correspond to resonances in the mode indicator function indicating that they are accurate. The mode shapes in Figure 3.10 and Figure 3.11 provide information as to where the primary motion is for each mode. Also, the modal damping ratios of the physical modes which can only be determined experimentally range from 0.03 to 3.2 % in the frequency range with an average of about 1.7 %, a median of about 2.0 %, and demonstrate an increasing trend as frequency increases.

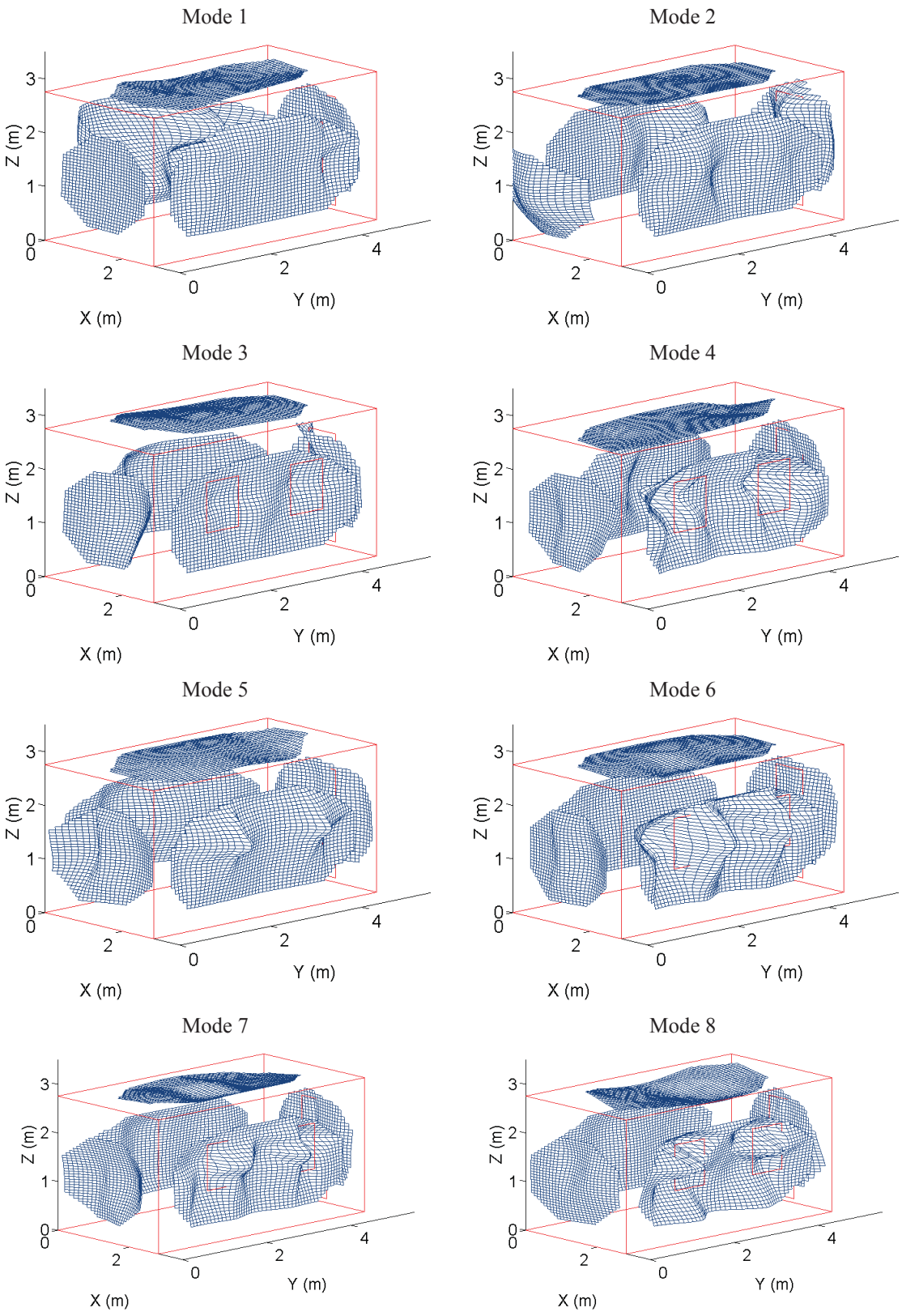

Figure 3.10: Three dimensional (3D) views of physical mode shapes of the single room structure obtained in the conventional experimental modal analysis.

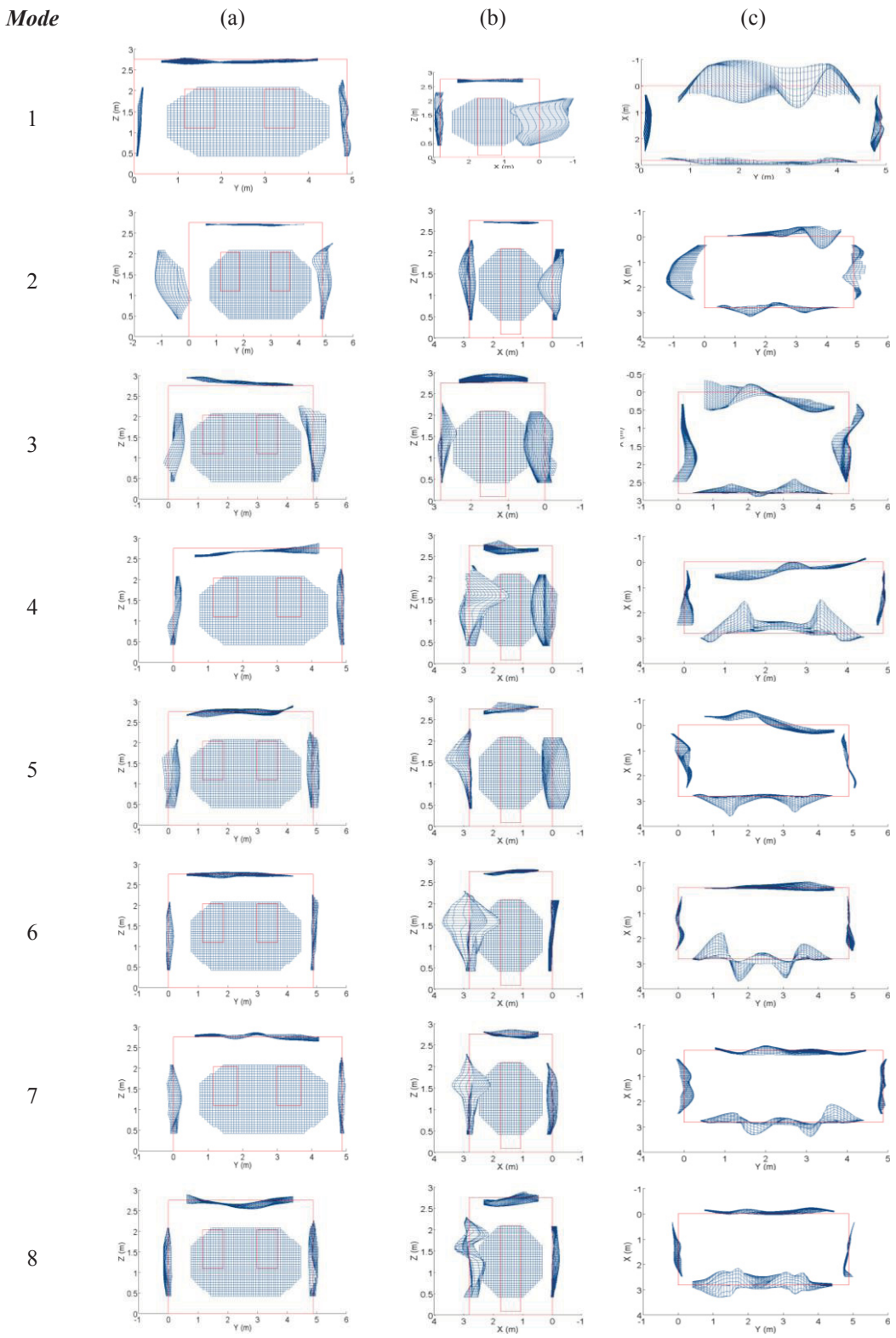

Figure 3.11: Physical mode shapes of the single room structure obtained in conventional experimental modal testing plotted (a) facing the wall with windows, (b) facing the wall with door, and (c) looking down on the ceiling.

3.1.2 NExT Modal Analysis

Presented in this section is a discussion of the experimental modal testing and analysis of the single room structure using NExT and the structural response to a simulated sonic boom measured by Haac et al. (2009). First, the instrumentation and experimental setup used will be briefly discussed with a description of the tests. Then, the procedure used to analyze the collected data will be given followed by the results of the output-only analysis. For full details regarding the instrumentation, setups, and procedure of the simulated sonic boom testing, refer to Haac et al. (2009).

A diagram of the approach used to determine the physical modal properties from the response to a sonic boom is shown in Figure 3.12. Cross-correlations between each acceleration response and a reference response are computed. The FFTs of these cross-correlations are calculated and summed to get the mode indicator function. This function is calculated for various reference responses and used to determine the best reference to use. The Global SVD method is applied assuming some initial estimate of the number of modes from the mode indicator function. NExT FRFs are regenerated and the square error between measured and regenerated FRFs is calculated. The Global SVD method is repeated for consecutively increasing numbers of modes until about twice the initial estimate is reached computing square error in each analysis. The correct number of modes is found from the least square error and the analysis is repeated using this number for perturbed frequency ranges. MAC values are computed between the modes of the original analysis and the modes of the perturbed analyses to determine the physical modes of the structure.

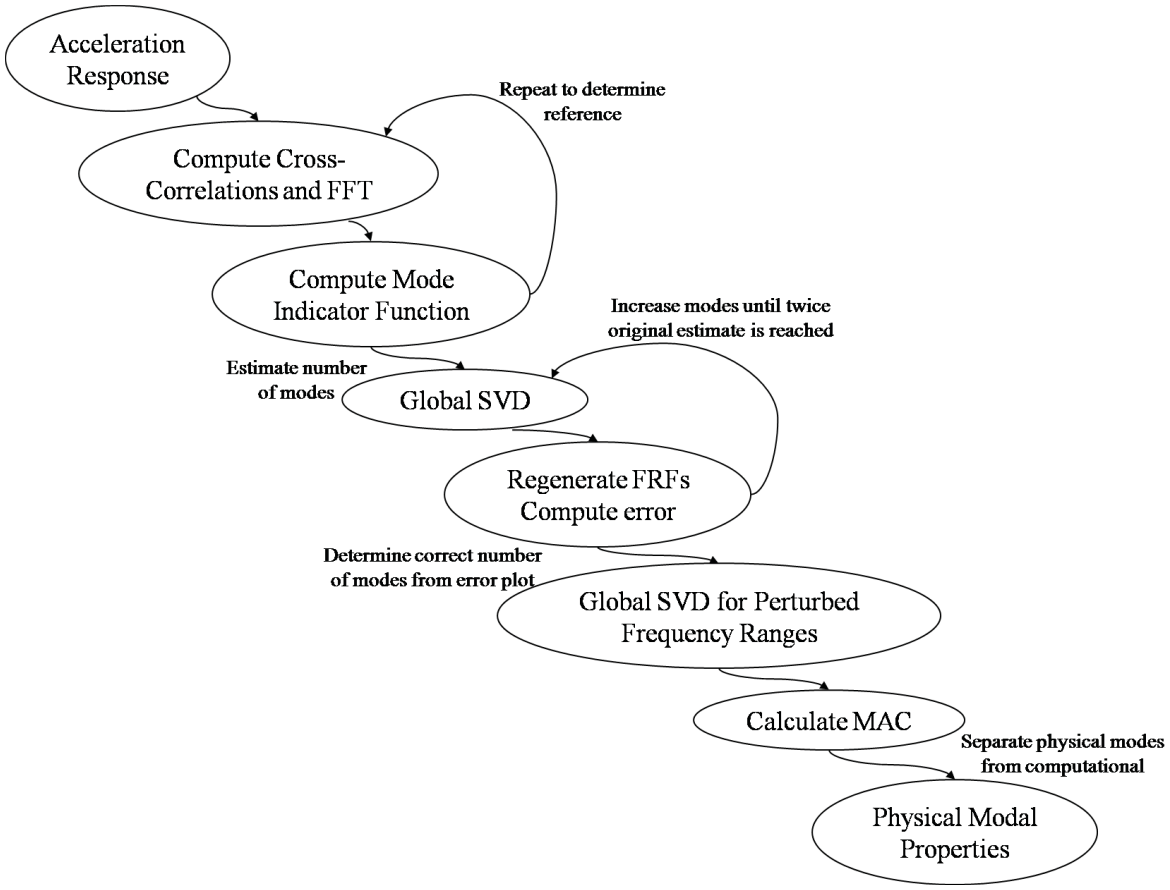

Figure 3.12: Diagram demonstrating the approach used to determine the physical modal properties of the single room structure with NExT from the sonic boom response.

The accelerometers used in these tests were the PCB 330A sensors discussed previously. 150 of these accelerometers were mounted inside and out of the test structure (Haac et al., 2009). To simulate a sonic boom, a linear distribution of detonating cord as suggested by Hawkins and Hicks (1966) was ignited as shown in Figure 3.13. The detonating cord was strung up between two poles about 11 m off the ground and 91 m away from the front of the single room structure (Haac et al., 2009).

Figure 3.13: Picture of linear charge being detonated to simulate a sonic boom propogating towards the single room structure.

The pressure loading recorded at one point on the exterior of the window wall of the structure is shown in Figure 3.14. This is the actual impulsive input which is not usually measured when using NExT. The autocorrelation and the magnitude of the autospectrum of this input are also shown in Figure 3.14. From the plots, it can be seen that the duration of the sonic boom, T_I, is about 90 ms, while the correlation duration, T_C, is about 180 ms. Therefore, it is expected that the magnitude of the impulsive input's autospectrum will begin to decay around the frequency, f_C, which is calculated to be about 6 Hz. However, the autospectrum demonstrates this decay to begin around 9 Hz. Since the cross-spectrums used in the NExT analysis will be multiplied by the autospectrum of the input as demonstrated in section 2.2, suppression of modes beyond about 9 Hz is expected.

(a)

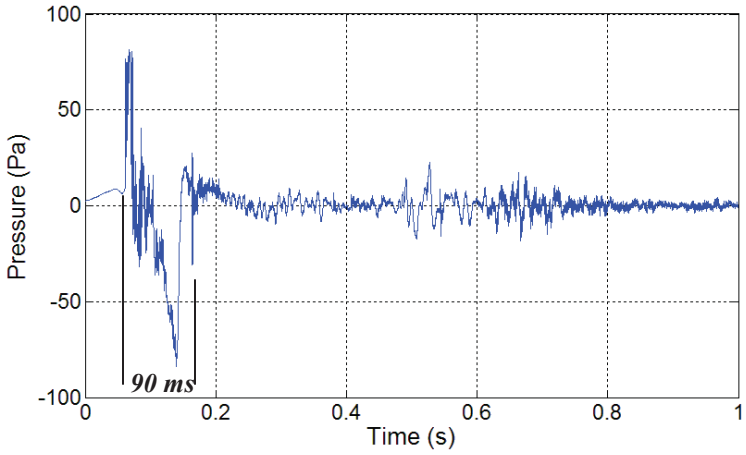

(b)

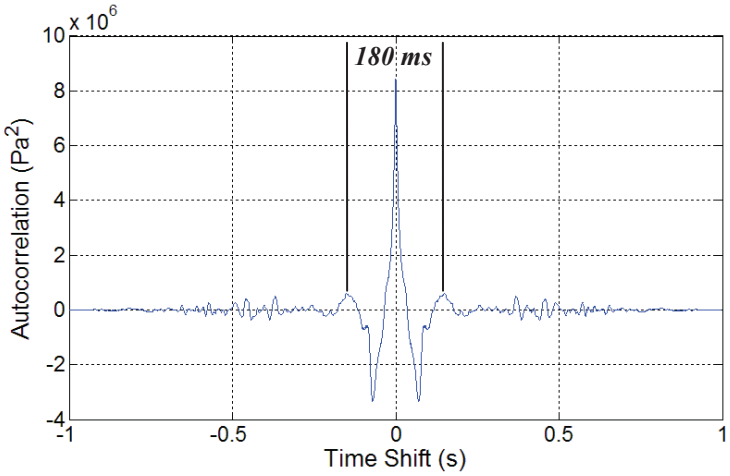

(c)

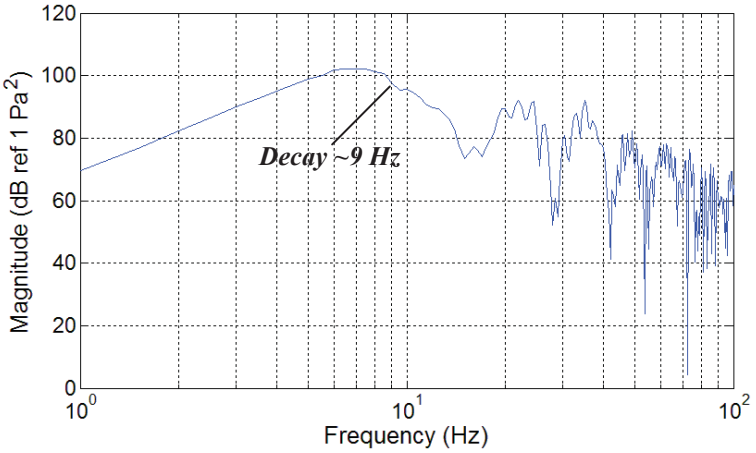

Figure 3.14: Plots of (a) input sonic boom, (b) autocorrelation of input, and (c) autospectrum of input.

To truly examine the differences between conventional modal analysis and output-only modal analysis, an attempt was made to stay as consistent as possible with the conventional modal analysis procedure in the following process. First, the accelerometer data corrected for DC offset was downsampled from about 51.2 kHz to 6400 Hz. Then, a reference accelerometer was selected and cross-correlations were calculated between all structural response signals and this reference signal. The reference accelerometer used in this analysis was on the window wall, the accelerometer closest to the reference accelerometer used in the conventional modal analysis procedure discussed previously.

The second halves starting from zero time difference of these cross-correlations contain the sum of decaying sinusoids with the same modal properties as the IRFs of the response positions due to an impulse at the reference response position demonstrated in the derivation of NExT discussed previously. These cross-correlation functions will be referred to as NExT IRFs of the structure. To analyze these NExT IRFs using the same technique as in the conventional modal analysis, they were converted to NExT FRFs simply by calculating the Fast Fourier Transform (FFT) of each NExT IRF. The simple mode indicator function, calculated as discussed previously, for this set of NExT FRFs is shown in Figure 3.15 from 1 to 100 Hz.

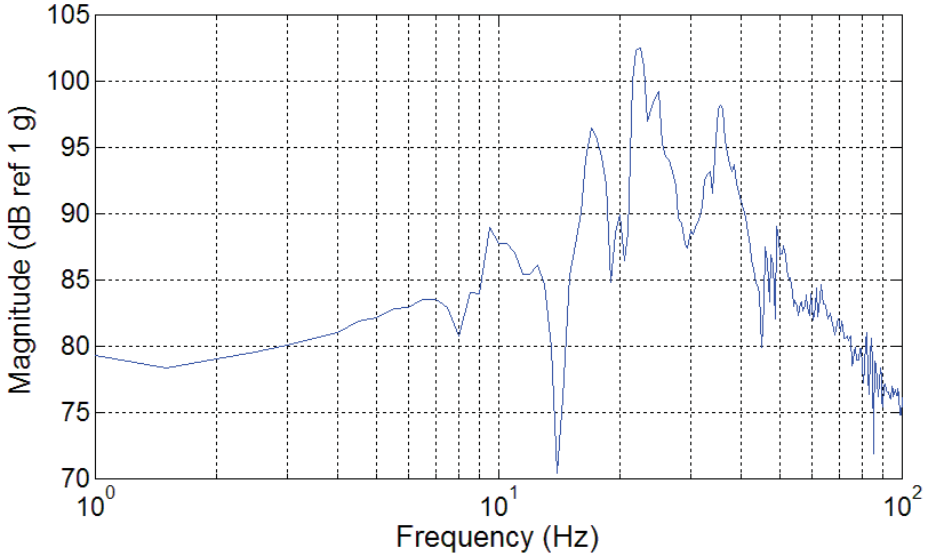

Figure 3.15: Simple mode indicator function obtained using NExT and the structural response to a simulated sonic boom with an accelerometer near the center of the wall with windows as the reference.

Comparing this mode indicator function with the one calculated in conventional modal analysis, shown in Figure 3.8, it can be seen that NExT FRFs are less smooth than the FRFs

obtained conventionally. Therefore, it is expected that a curve-fitting procedure will not be able to extract eigenproperties as easily. Still, the low-frequency resonances from about 10 to 40 Hz appear to be fairly clean and well-separated, so the Global SVD curve-fitting procedure was used again to extract the eigenproperties of the structure. The analysis from this point remains much the same as the conventional experimental modal analysis.

Based on the square error between measured and regenerated NExT FRFs, 20 modes were assumed in the frequency range (Corcoran et al., 2009). To check the results of the curve-fitting procedure, the regenerated FRFs were summed to form a regenerated mode indicator function and this was plotted against the measured mode indicator function in Figure 3.16.

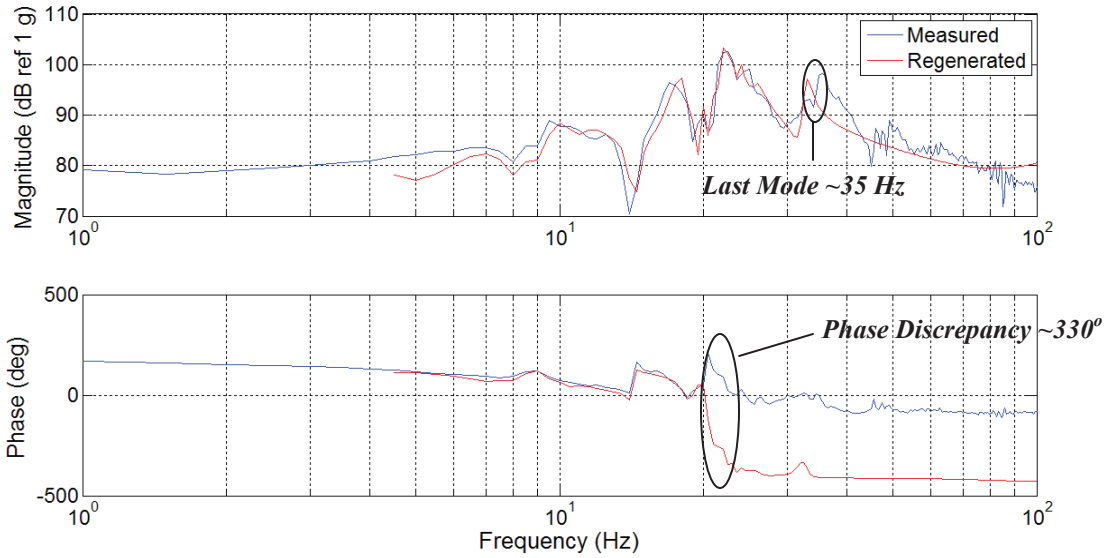

Figure 3.16: Comparison between magnitude and phase of measured and regenerated mode indicator functions.

It is evident from this plot that the curve-fitting procedure performs well in general over the frequency range. However, it appears that after about 35 Hz, no further modes are identified as the magnitude of the regenerated indicator function simply slopes downward without resonance. There is also a discrepancy in phase at about 20 Hz when the measured mode indicator function jumps upward but the regenerated function jumps down. The difference in phase from this point forward is about 330 degrees. Again, many fictitious, computational modes were extracted along with the genuine computational modes of the single room structure.

After identifying and removing the computational modes (Corcoran et al., 2009), the eigenproperties of the genuine physical modes extracted for the single room structure are given in Table 3.2. Three dimensional (3D) views of the physical mode shapes are plotted in Figure

3.17 and three 2D views of the same mode shapes are plotted in Figure 3.18. The front view faces the wall with windows, the side view faces the wall with the door, and the top view looks down at the structure ceiling. In each view, the front face is removed to see inside and the undeformed structure is plotted as a red outline.

Table 3.2: Modal properties of single room structure physical modes extracted using the Global SVD method in conjunction with NExT on structural response data to a simulated sonic boom over the 5 to 100 Hz frequency range.

Mode	***Natural Frequency (Hz)***	***Damping Ratio (%)***
1	7.62	6.82
2	9.09	1.85
3	18.03	3.51
4	20.23	1.28
5	22.21	1.12

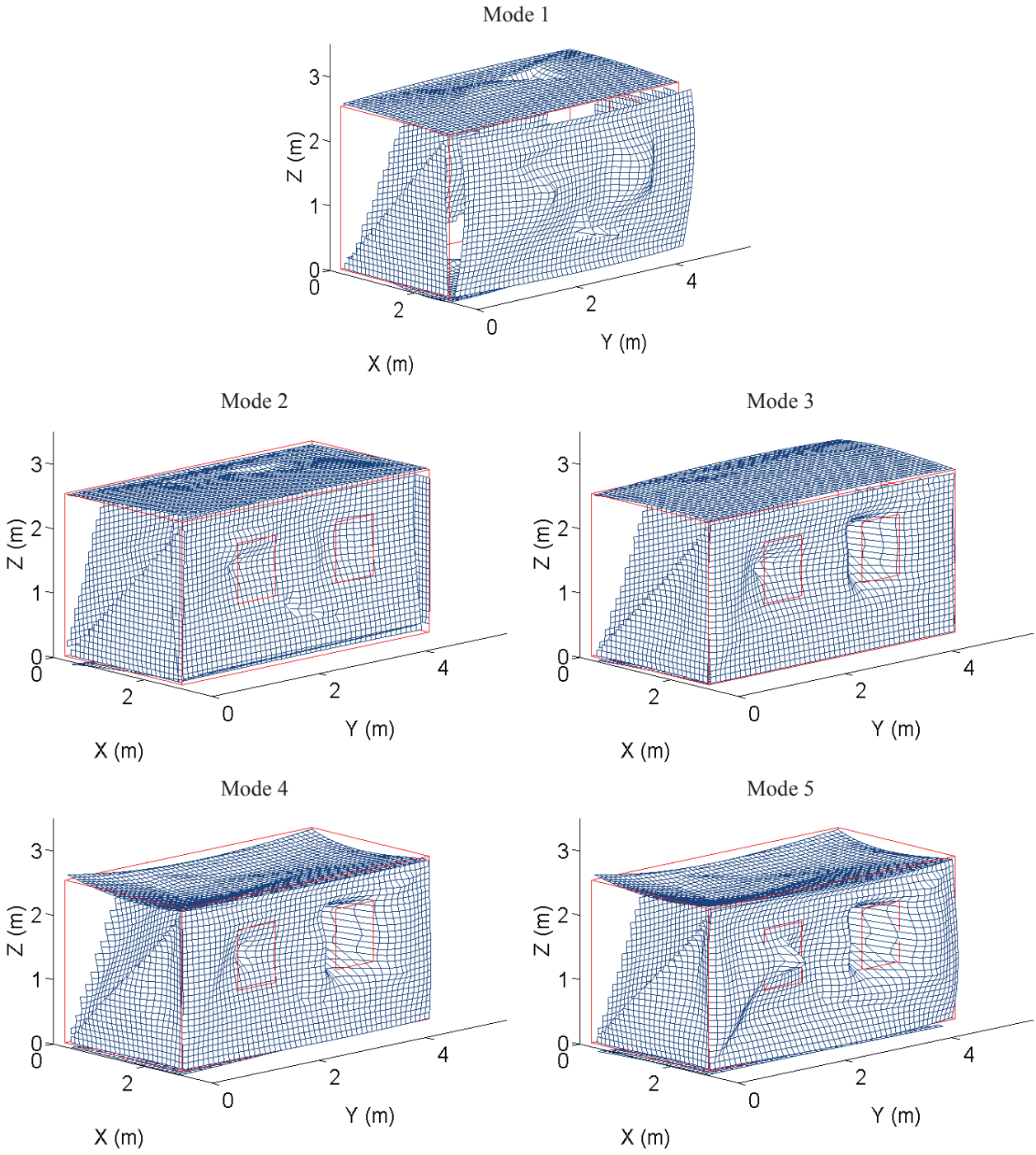

Figure 3.17: Three dimensional (3D) views of physical mode shapes of the single room structure obtained using NExT and the response to a simulated sonic boom.

\

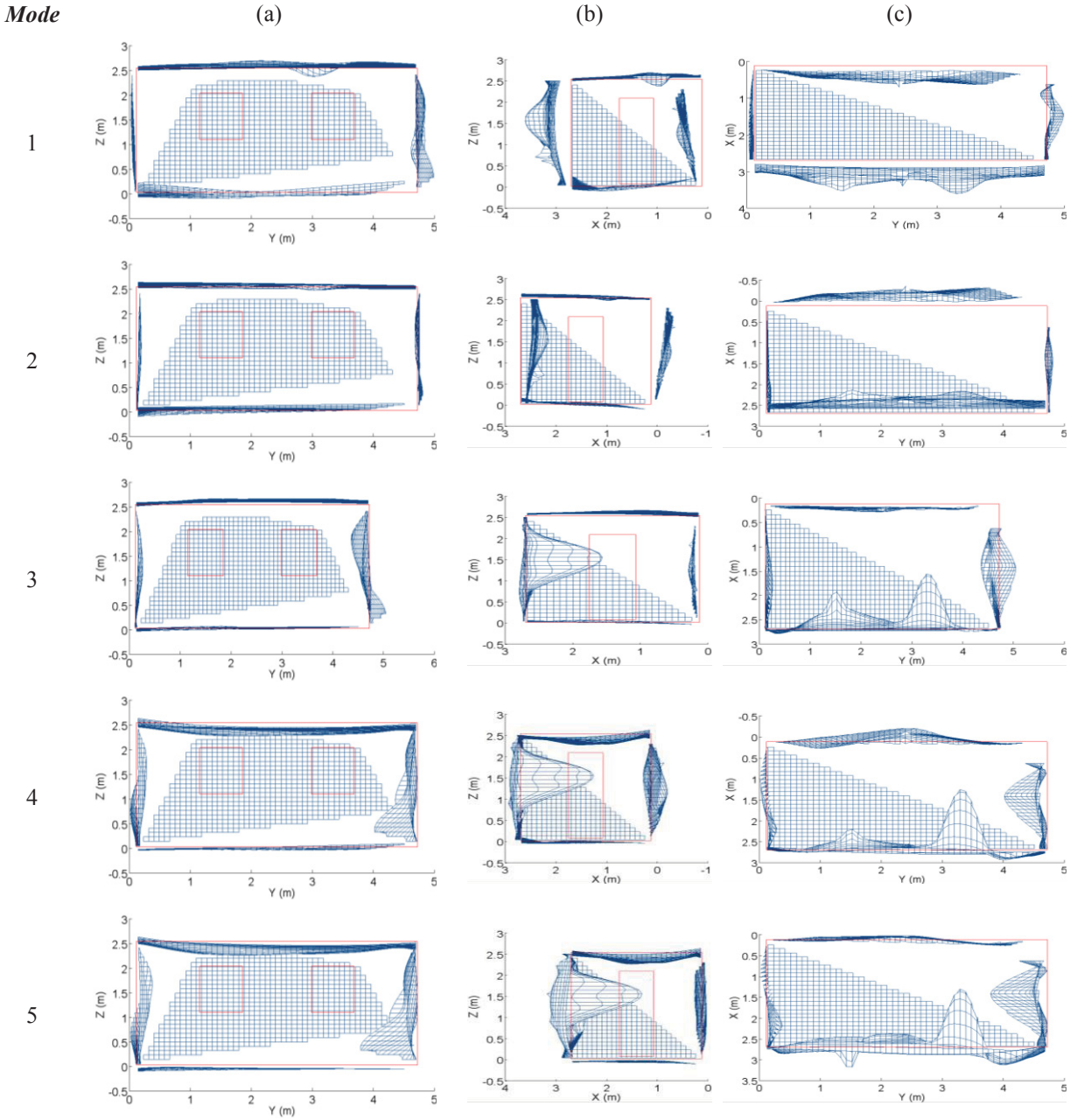

Figure 3.18: Physical mode shapes of the structure extracted using NExT and the Global SVD method on structural response data to a simulated sonic boom plotted facing (a) the wall with windows, (b) the wall with the door, and (c) the ceiling.

The downsides to the NExT analysis are demonstrated in the mode indicator function in Figure 3.15 and the natural frequencies in Table 3.2. Although the chosen frequency range extended to 100 Hz, only physical modes up to 22 Hz were extracted. The reason is clearly seen by examining the mode indicator function in Figure 3.15. The NExT FRFs are not smooth curves which makes extracting modes with a curve-fitting procedure difficult. This is probably caused

by the fact that the sonic boom input is not a perfect impulse but an impulsive input with a finite duration of about 90 ms. Therefore, its autocorrelation is convolved with the response cross-correlations calculated for use with NExT as demonstrated in the extension of NExT in section 2.2. It follows that the cross-spectrums, or NExT FRFs, actually used in the Global SVD method are multiplied by the autospectrum of the input which is shown in Figure 3.14. Therefore, the modes beyond a frequency of about 9 Hz will be suppressed by the decay of the autospectrum of the input sonic boom. This lowers the accuracy by which their modal properties can be extracted or even causes their resonances to be suppressed far enough that they become indistinguishable from random peaks caused by inaccuracies in measured response data.

However, one advantage of this analysis is the clarity in the mode shapes plotted in Figure 3.17 and Figure 3.18. It is easy to physically interpret the motion of the structure from the plots of the deformed structure. For example, the first two modes have a very similar shape which is basically a simple leaning of the structure. In fact, the first mode is probably not a physical mode of the single room structure which is enforced by several facts. First, its natural frequency is very close to the fundamental frequency of the simulated sonic boom related to the boom duration. Second, comparing the shape of this mode with the shape of the 9.09 Hz mode, also extracted using the NExT analysis, it can be seen that they are almost identical if the phase is reversed. Finally, it can be seen that the damping ratio of the mode is abnormally high compared to the other structural modes. Since the sonic boom input was impulsive in nature which violates the random, stationary input assumption of NExT and does not exactly match a perfect impulse as discussed in the extension of NExT, this mode is probably a component of the input which is damped out fairly quickly leaving the structure to vibrate freely.

The third, fourth, and fifth modes have similar shapes which consist primarily of motion from the windows of the structure. The differences in the third and fourth modes come from the motion of the ceiling, the wall with the door, and the long plain wall. In the third mode, the long plain wall moves in the opposite direction of the windows which causes the ceiling to be pushed upwards. In the fourth mode, the long plain wall moves in the same direction as the windows and the ceiling pushes downwards. The fifth mode is nearly identical to the fourth except that the windows move in opposite directions. Damping ratios of these modes range from 1.1 to 6.8 % with an average of 2.9 %, a median of 1.9 %, and a trend that decreases as frequency increases.

3.1.3 Comparison of Modal Analysis Methods

Presented in this section is a comparison of the structural modal analysis results obtained with three different techniques: 1) conventional modal testing and analysis techniques, 2) NExT modal analysis using structural response data to a simulated sonic boom, and 3) numerical modal analysis using a finite element model (Remillieux et al., 2009). The results of the finite element model are used to help interpret the results obtained from experimental methods. For instance, it is clear from the finite element model results that modal density is very high even at low frequencies for such a complex structure. The experimental results were not used as an input or to tune the finite element model. Modal results from the three analyses are compared to examine the use of NExT with the structural response to a sonic boom to extract modal properties of the single room structure.

The natural frequencies and mode shapes of the single room structure calculated from a finite element model (Remillieux et al., 2009) are compared to the natural frequencies and mode shapes measured experimentally in Figure 3.19. In the figure, modes are matched in rows by inspection of similar natural frequencies and mode shape characteristics. Only the first few modes up to a natural frequency of about 25 Hz are considered and the first mode extracted in the NExT analysis is removed due to the likelihood of it being a component of the sonic boom excitation and not a physical structural mode as discussed previously.

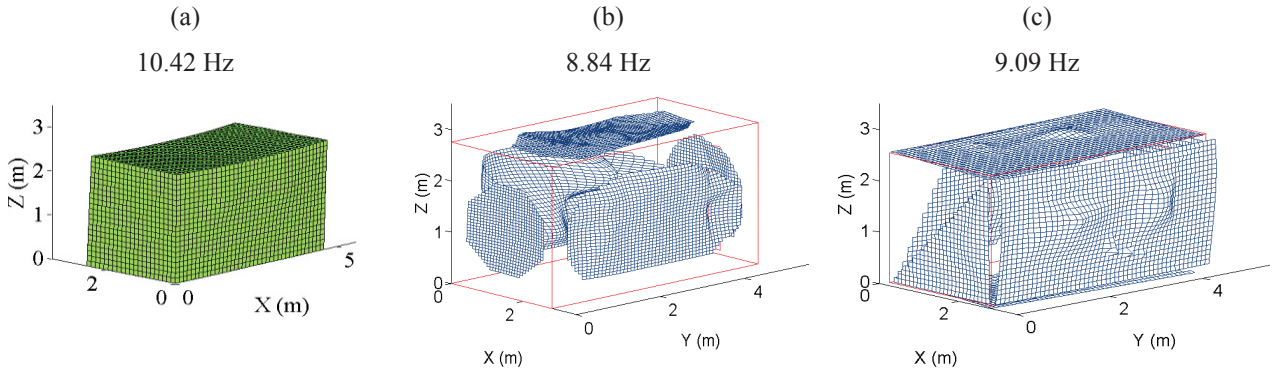

Figure 3.19: Comparison of natural frequencies and mode shapes of the single room structure calculated (a) from a finite element model (Remillieux et al., 2009), (b) in the conventional modal analysis, and (c) in the NExT experimental modal analysis.

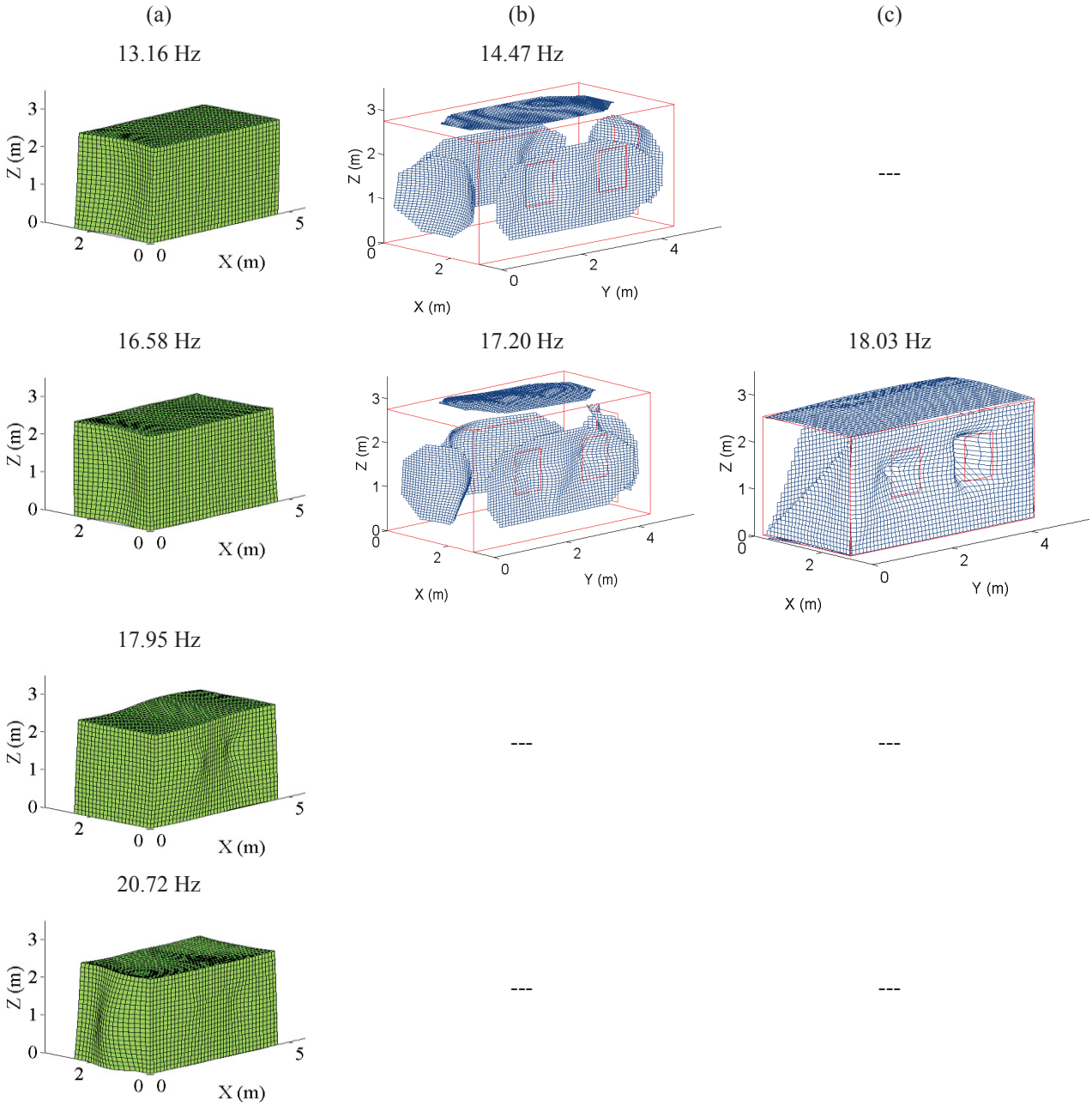

Figure 3.19: Comparison of natural frequencies and mode shapes of the single room structure calculated (a) from a finite element model (Remillieux et al., 2009), (b) in the conventional modal analysis, and (c) in the NExT experimental modal analysis, cont.

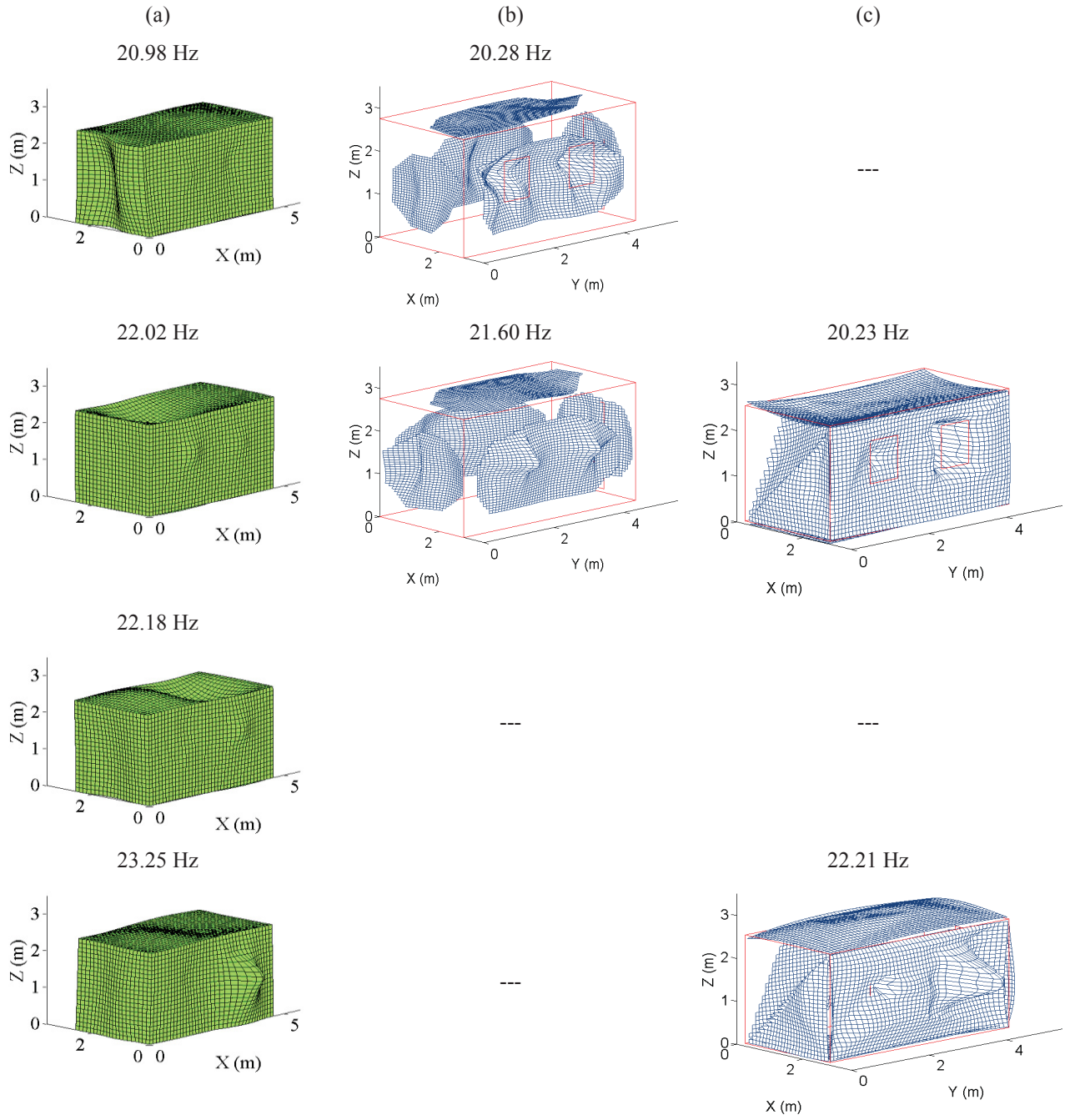

Figure 3.19: Comparison of natural frequencies and mode shapes of the single room structure calculated (a) from a finite element model (Remillieux et al., 2009), (b) in the conventional modal analysis, and (c) in the NExT experimental modal analysis, cont.

Aside from the fact that the finite element model extracts more modes than were measured experimentally, it can be seen that fairly good agreement is obtained between the finite element results and the experimental results for some modes. The fundamental mode extracted in all three analyses has a consistent natural frequency of around 9 or 10 Hz. Its mode shape consists of a

leaning of the wall with windows and the long plain wall which is clearly seen by the finite element result and the shape extracted in the NExT analysis. While this is not as clear in the shape from the conventional modal test, the motion is primarily from the long plain wall.

The second mode with a natural frequency of about 13 to 14.5 Hz demonstrates the structure leaning in the other direction with the short plain wall and the door wall bowing out. This is clearly seen in the finite element results and the conventional test results. However, this mode is missed by the NExT analysis probably due to the lack of excitation of this mode by the simulated sonic boom which propagated parallel to these surfaces. The third mode with a frequency of about 16.5 to 18 Hz consists of motion from these same two walls but now they move out of phase. This result is captured in all analyses; however, the experimental results now demonstrate motion from the windows of the structure which is not captured in the finite element results. The next two modes are again missed by the experimental modal tests.

The next mode of around 20 or 21 Hz demonstrates two half wavelengths horizontally from the side plain wall with the windows moving inward from both the finite element and conventional results. Then, a mode occurs in all three analyses around 22 Hz in which the ceiling moves along with the windows. A mode extracted in the finite element analysis around 22 Hz which consists of two half wavelengths in the ceiling is missed by the experimental results. The last mode pictured which has a natural frequency of around 22 or 23 Hz shows the windows moving out of phase with each other with additional motion from the ceiling. This was captured by both the finite element model and the NExT modal analysis. Overall, agreement was very good in the modal results obtained with the three different analyses. Therefore, using NExT to extract modal properties experimentally from the structural sonic boom response has produced reasonable results.

3.2 Two Room Structure Modal Analysis

Presented in this section will be the details behind the structural experimental modal testing and analysis performed on the two room structure shown in Figure 3.20. First, extraction of structural eigenproperties using conventional modal testing and analysis will be discussed. Then, the experimental modal analysis with NExT used to extract structural eigenproperties will be presented. Finally, a comparison between the results of the two techniques and modal results from a finite element model of the structure (Remillieux et al., 2009) will be given.

(a) (b)

Figure 3.20: Pictures of the two room structure showing (a) the original structure and (b) the addition structure.

The two room structure consists of the original, single room structure, an addition to this structure forming the second room, and a slanted roof over each structure forming two attics. Although part of the same structure, the two different parts of the two room structure will be referred to as the original structure and the addition structure. The walls of the original structure will be referred to as the window wall, the exterior door wall, the interior door wall, the long plain wall, the ceiling, and the floor. The walls of the addition structure will be referred to as the window wall, the door wall, the short plain wall, the long plain wall, the ceiling, and the floor.

The structure has an overall size of about 7.5 x 4.3 x 3.8 m. It is made of a wooden frame consisting of dimensioned lumber, a sheathing of OSB, drywall mounted to the interior of the frame with insulation filling the gaps in between, and a shingled roof. Additionally, there are two doors, two windows, and a large window pane wall. No foundation for the structure exists; it rests on twelve level cinderblocks. Further details regarding the geometry and construction of the two room structure are discussed by Haac et al. (2009).

3.2.1 Conventional Modal Analysis

Before conducting a detailed, extensive, conventional experimental modal test on the two room structure, preliminary conventional modal tests as were run to determine natural frequencies and damping ratios of the low frequency modes of the structure (Corcoran et al., 2009). Because only natural frequencies and damping ratios of the structural modes were of interest at this point, a single accelerometer was used to collect structural response data to impulses provided by impact hammers at a few points over the structure. This is because, for any

linear, elastic structure, all FRFs that are measured at any point on that structure will contain the same eigenvalues relating to natural frequency and damping ratio. Only the mode shape constant will change depending on where the FRF was measured which was not of interest at this point. The conventional tests will be briefly described here. For full details, refer to Corcoran et al. (2009).

The sensor used to measure the response of the structure was a PCB accelerometer model 353B15 discussed previously. It was attached using wax and a mount to the interior surface of the two room structure and it was moved depending on where the input force to the structure was located. To provide excitation to the structure, the two impact hammers used in the previous conventional modal tests were used. The FRFs were measured directly using an HP Agilent Dynamic Signal Analyzer (35665A) shown in Figure 3.21 (Corcoran et al., 2009).

Figure 3.21: HP Agilent Dynamic Signal Analyzer used to measure FRFs in impact hammer modal testing of two room structure placed on instrumentation racks with other equipment in center of original structure room.

The accelerometer was positioned at several points on the interior surface of the two room structure on studs. The structure was then excited with the large modal sledge hammer at a few points on studs for each accelerometer position including a point as close as possible to the accelerometer without risking damage to the sensor (Corcoran et al., 2009). To obtain the best coherence possible between response and input signals, all hammer points were on the interior surface of the structure and the structure was struck as hard as possible without causing damage to the structure.

The measurement range of the signal analyzer was set from 0 to 400 Hz using 800 spectral lines giving a frequency resolution of about 0.5 Hz. A force window of 60 ms width was applied

to the impulse signal from the hammer and an exponential window of 80 ms decay was applied to the response signal from the accelerometer. The FFTs of these windowed signals were divided to obtain individual FRFs at each point. Ten individual FRFs were obtained at each point and averaged to calculate the average FRFs.

Typical FRFs obtained from the modal testing of the two room structure are shown in Figure 3.22. The drivepoint FRF measured by a hit close to the accelerometer position on the long plain wall of the original structure with the associated coherence is shown in Figure 3.22(a) and the FRF measured on the long plain wall of the original structure due to an input on the window wall of the original structure is shown in Figure 3.22(b) with its coherence. It can be seen that when good coherence is maintained the magnitude of the FRF is smooth indicating that none of the modes in this frequency range are captured at this point as shown in Figure 3.22(a). This could be due to the point lying on the node of every mode in this range or that the impulse used to excite the structure into vibration was not enough to excite the modes at these low frequencies. When the modes in the frequency range are captured, the coherence drops significantly as shown in Figure 3.22(b). This indicates that, by the time the structural wave travels across the structure, the signals are uncorrelated and that the response is likely caused by something other than the input. Neither of these types of typical FRF are suitable for extracting modal properties, so conventional modal analysis techniques such as Global SVD could not be employed.

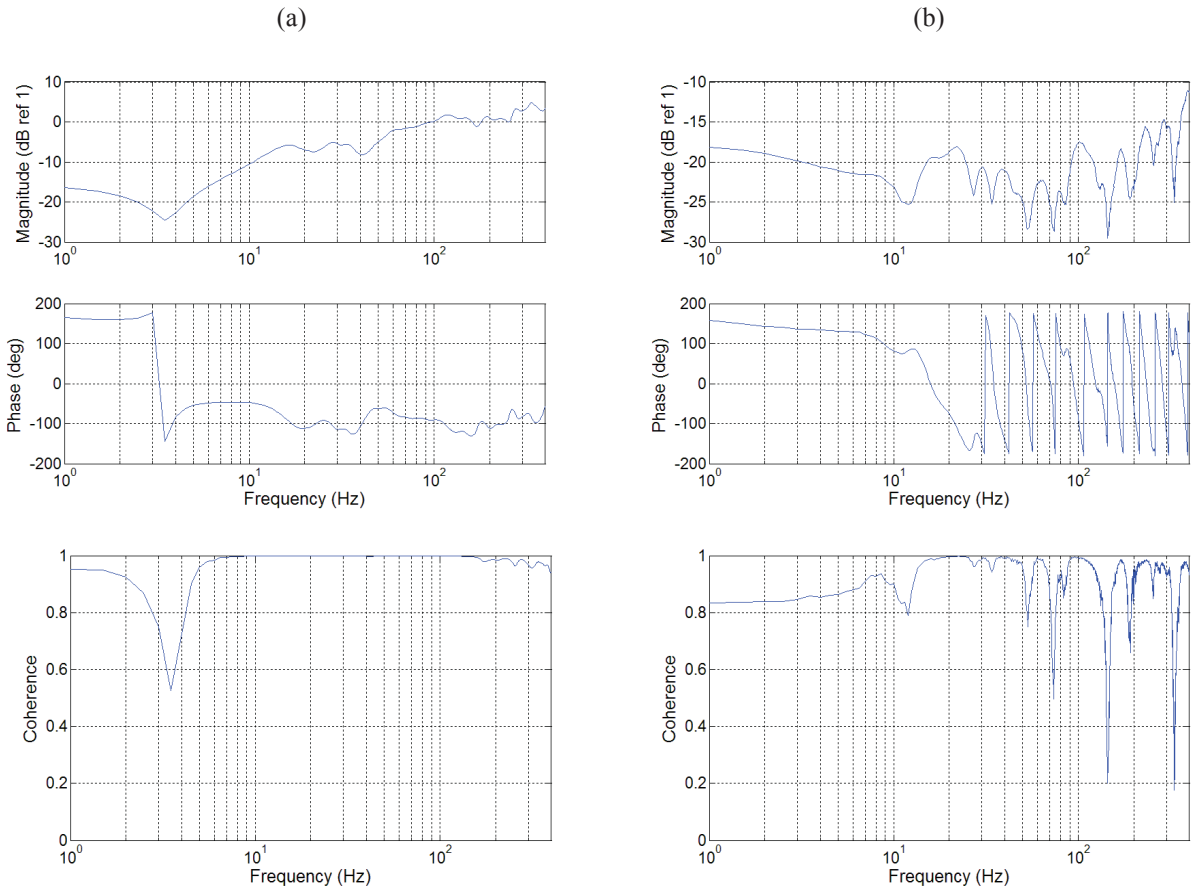

Figure 3.22: Typical FRF and coherence measured on (a) the long plain wall of the original structure due to an impulsive input close to the measurement point and (b) the long plain wall of the original structure due to an impulsive input on the window wall of the original structure.

3.2.2 NExT Modal Analysis

In this section, an output-only experimental modal analysis was pursued to extract structural eigenproperties using the two room structure's response to a simulated sonic boom using the data described by Haac et al. (2009). First, the instrumentation and experimental setup used to collect the structural response will be discussed. Next, the procedure used to extract eigenproperties from the structural response data will be discussed. Finally, the results of the analysis will be presented and discussed.

In these tests, there were 62 PCB 330A accelerometers placed around the two room structure on mainly the interior surfaces (Haac et al., 2009). In this set of tests, some higher-quality accelerometers, PCB model 333B32-F provided by NASA, were collocated with the PCB 330A sensors for comparison only. The data recorded by these accelerometers was not used in the calculation of structural modes. Again, a linear distribution of detonating cord was used to

simulate a sonic boom. The distribution used to excite the two room structure was identical to the distribution used when exciting the single room structure and it was ignited in the same place. A picture of the detonating cord being ignited to simulate a sonic boom to excite the two room structure is shown in Figure 3.23 (Haac et al., 2009). Several structure door configurations were tested; both doors were closed in the test from which eigenproperties were extracted.

Figure 3.23: Picture of linear charge being detonated to simulate a sonic boom to propagate towards and excite the two room structure.

The approach to determine modal properties from the acceleration response of the structure to a sonic boom is essentially the same as the approach used for the single room structure shown in Figure 3.12. First, the structural response data recorded in the test was downsampled to a frequency of 6400 Hz. Then, cross-correlations between each acceleration signal to a common, reference acceleration signal. Structural NExT IRFs were obtained by examining only the second half of these cross-correlations containing the exponential decay for positive time differences. The FFTs of these NExT IRFs were calculated to obtain NExT FRFs and summed to calculate a simple mode indicator function. This was repeated using many different references. Finally, a single reference sensor was chosen based on how continuous its mode indicator function curve was and how well-separated the peaks were. The reference sensor chosen was positioned near the center of the original window wall and its simple mode indicator function is plotted from 1 to 100 Hz in Figure 3.24.

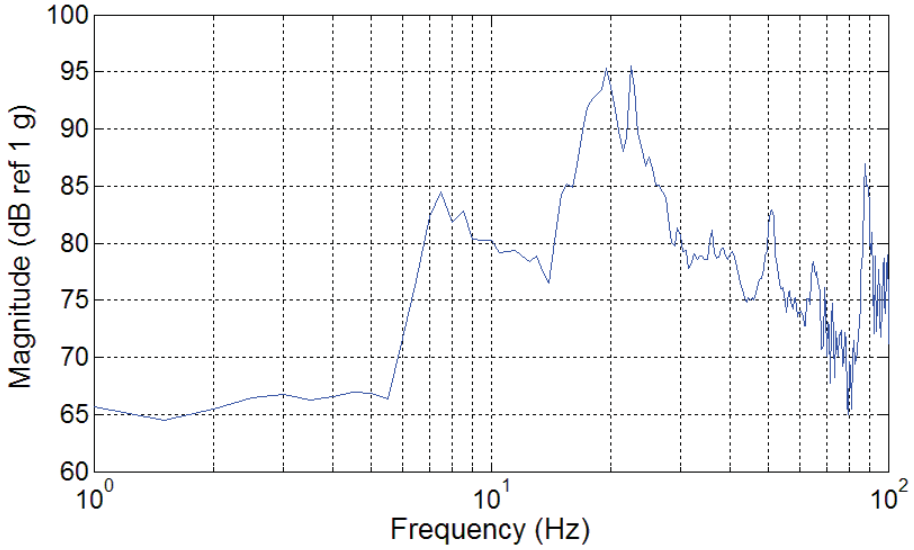

Figure 3.24: Simple mode indicator function for the two room structure obtained using only the structural response to a sonic boom with the accelerometer near the center of the original window wall as the reference.

Next, the accelerance NExT FRFs were integrated once to calculate a mobility FRF and then again to obtain the receptance FRFs. Again, the Global SVD method was applied to the set of NExT FRFs over the frequency range from 5 to 60 Hz. Based on the square error between real and imaginary parts of measured and regenerated NExT FRFs, 15 modes were assumed in the frequency range from 5 to 60 Hz (Corcoran et al., 2009). The analysis was repeated for this number of modes and the measured FRFs were regenerated. The regenerated simple mode indicator function is compared to the measured simple mode indicator function in Figure 3.25. It is evident from this plot that the curve-fitting procedure performed well in general over the frequency range. However, no modes were extracted after about 23 Hz as indicated by the smoothly decaying magnitude of the simple mode indicator function.

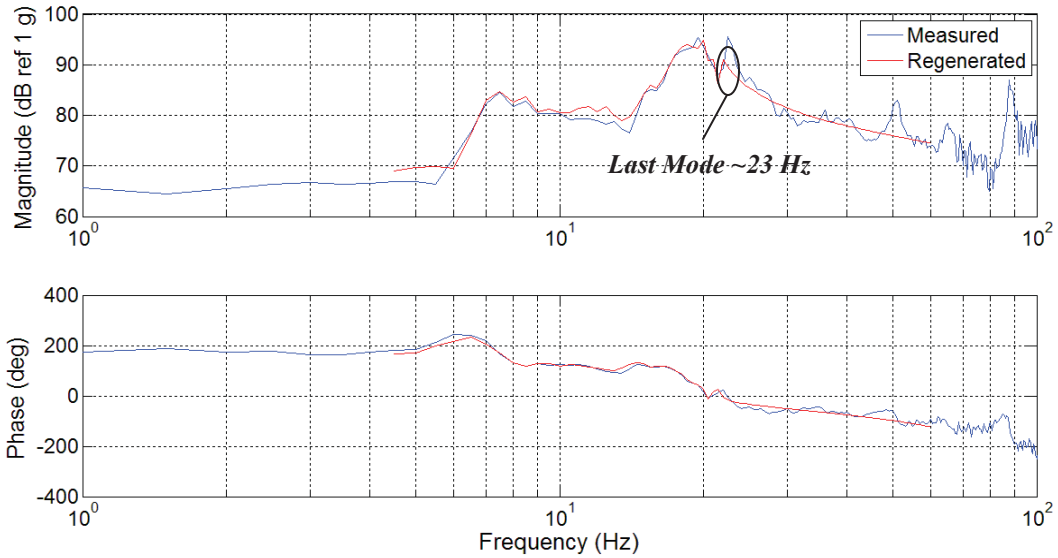

Figure 3.25: Comparison between magnitude and phase of measured and regenerated mode indicator functions of the two room structure.

It was clear from the extracted eigenproperties that some of the modes were fictional, computational modes extracted simply to provide a better curve fit so the procedure used previously to identify these modes was repeated (Corcoran et al., 2009). The eigenproperties of the physical modes left after the procedure was completed are listed in Table 3.3. The shapes of these physical modes are given in Figure 3.26 and Figure 3.27 with the undeformed structure plotted as a red box. The mode shapes are plotted in 3D in Figure 3.26 and three 2D views of the mode shapes are shown in Figure 3.27: (a) a front view facing the window walls, (b) a side view facing the exterior door, and (c) a top view looking down at the ceiling. In each 2D view, the front surfaces are removed to see the remaining walls of the structure.

Table 3.3: Modal properties of physical modes extracted using NExT and the Global SVD method on two room structural response data to a simulated sonic boom over the 5 to 60 Hz frequency range.

Mode	***Natural Frequency (Hz)***	***Damping Ratio (%)***
1	6.98	8.17
2	8.09	0.79
3	8.27	5.07
4	9.91	3.12
5	20.15	2.76
6	20.76	1.74
7	21.53	0.48

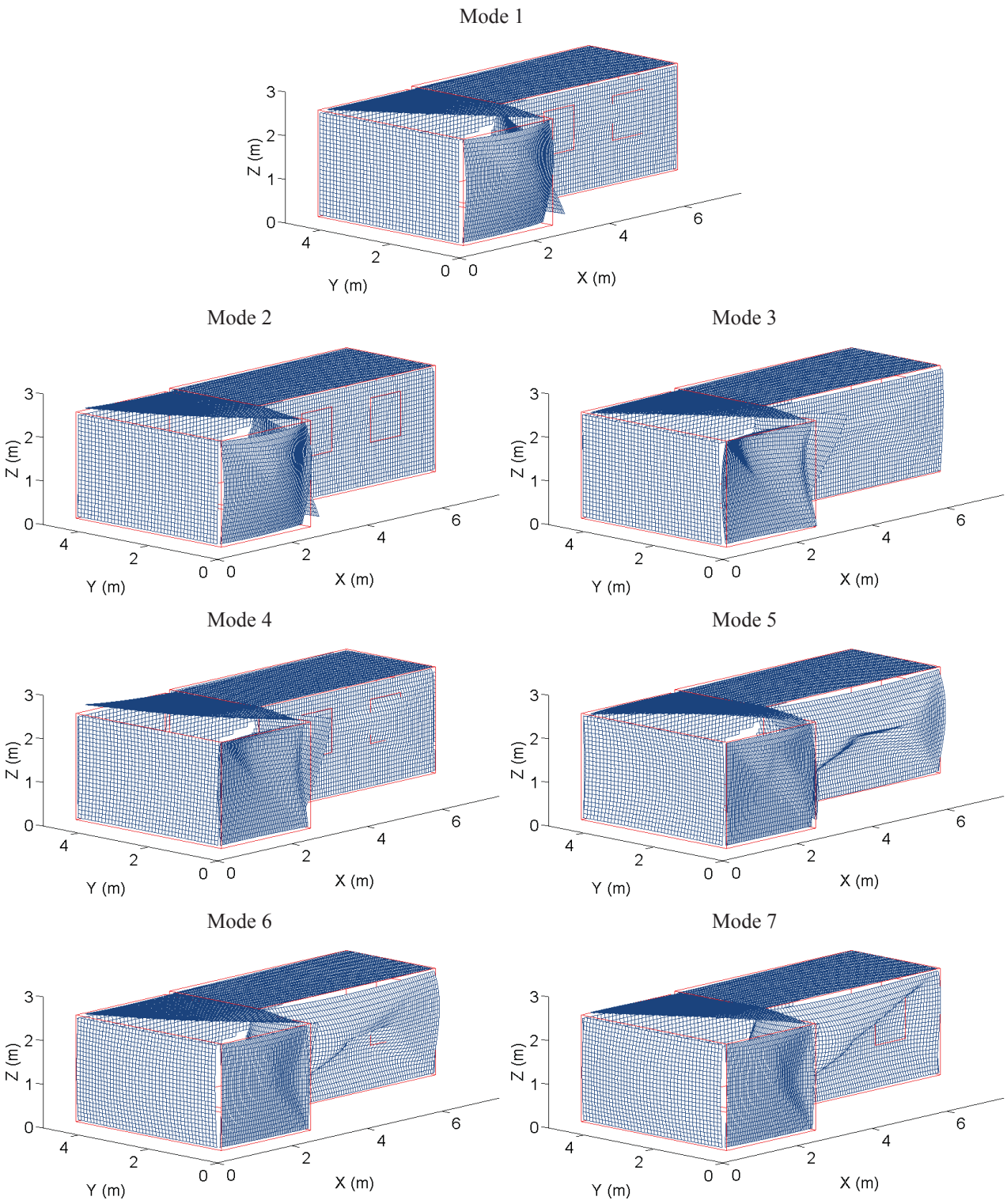

Figure 3.26: Three dimensional (3D) views of physical mode shapes of the two room structure extracted using NExT and the Global SVD method on the structural response to a simulated sonic boom.

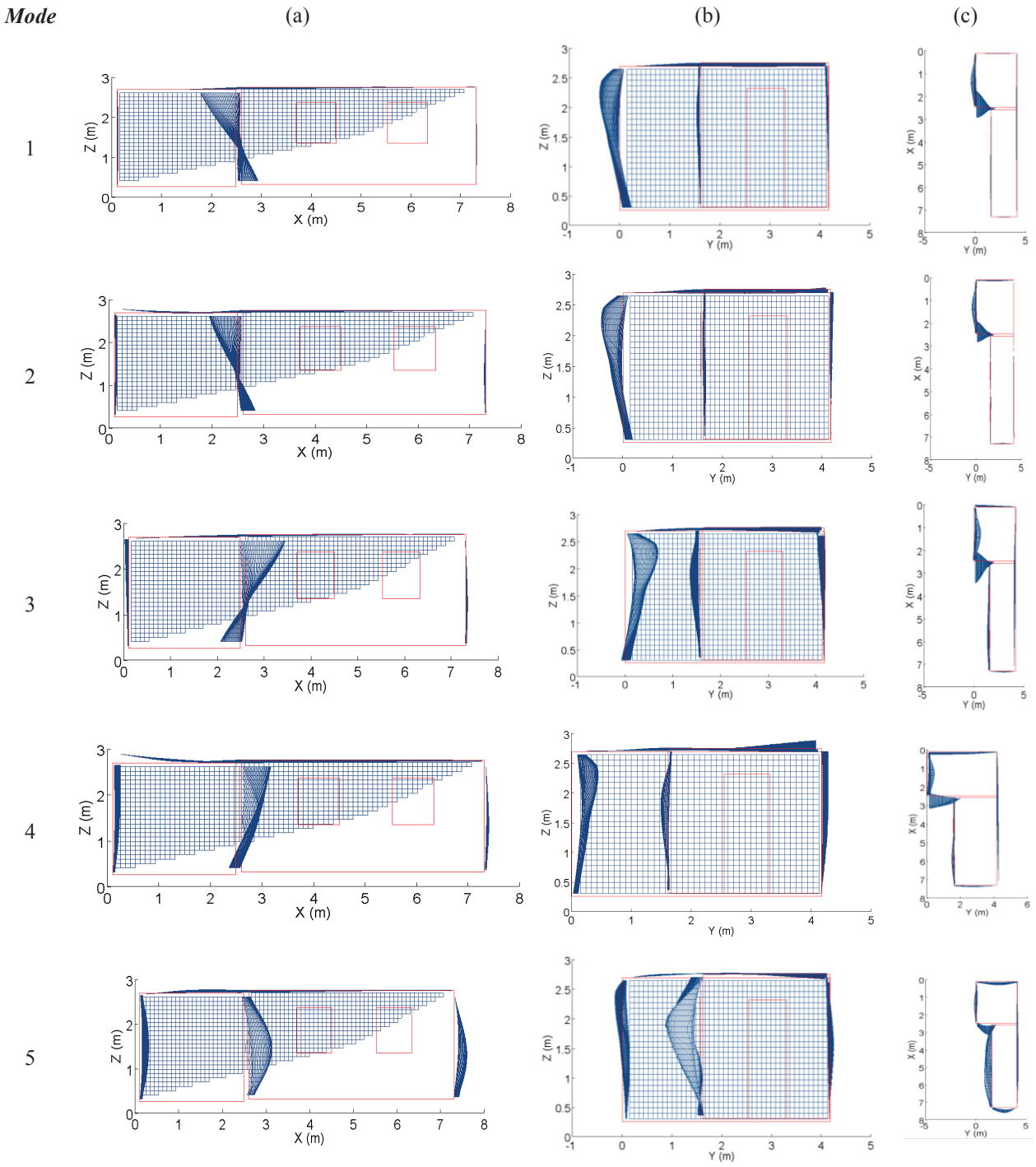

Figure 3.27: Physical mode shapes of the two room structure extracted using NExT and the Global SVD method on output-only structural response data to a simulated sonic boom plotted facing (a) the walls with windows, (b) the wall with the exterior door, and (c) looking down on the ceilings with these surfaces removed in each view.

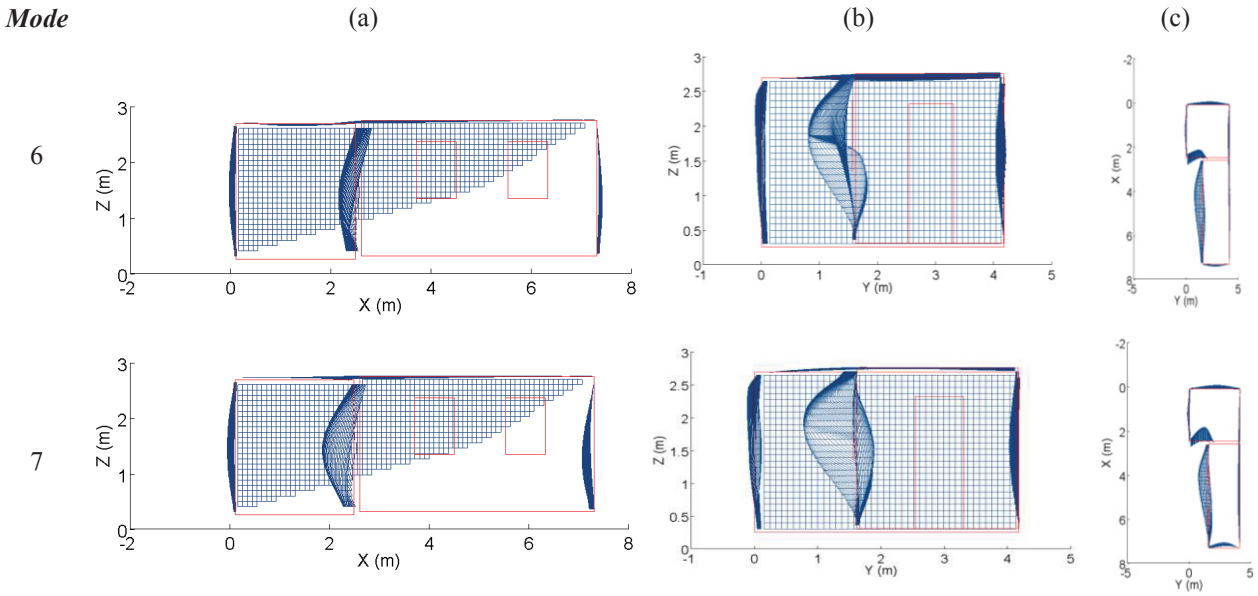

Figure 3.27: Physical mode shapes of the two room structure extracted using NExT and the Global SVD method on output-only structural response data to a simulated sonic boom plotted facing (a) the walls with windows, (b) the wall with the exterior door, and (c) looking down on the ceilings with these surfaces removed in each view, cont.

From Figure 3.26 and Figure 3.27, it can be seen that the entire walls of the structure could not be shown due to the limited number of accelerometers. However, some insight can still be gained from the mode shapes of the wall portions that were measured. The first two modes consist primarily of motion from the window wall of the addition structure and the wall which connects the window wall to the original structure. In fact, the motion of these two modes is nearly identical which indicates that the output-only analysis may again have extracted a primary component of the simulated sonic boom. Again, the natural frequency of 7 Hz is very close to the fundamental frequency of the sonic boom, related to the boom duration. Also, it can be seen that the damping ratio is abnormally high compared to the other structural modes which indicates that this is probably a component of the forced response to the impulsive input which is damped out fairly quickly leaving the structure to vibrate freely in its physical modes.

The third mode shape shows motion similar to the first two mode shapes. In addition, motion of the window wall and long plain wall of the original structure is introduced which exhibits leaning of the original structure similar to the fundamental mode shape of the single room structure extracted by the finite element model and the NExT analysis discussed previously. In the fourth mode, the long plain wall and the window wall of the original structure move out of phase with each other and the ceiling and the long plain wall of the addition structure begin to

move. The fifth mode demonstrates more complex motion from the window wall of the original structure indicating dynamics from the small windows and now each of the side walls bows out in phase. In the sixth mode, the complexity of the original structure window wall's motion increases as the two windows now move out of phase with each other and the exterior door wall now bows out of phase with the other two side walls. Finally, the seventh mode, very similar to the fifth mode, primarily consists of complex motion of the original structure window wall in which the small windows move out of phase with each other and each of the side walls bowing in phase. Damping ratios of the physical structural modes ranged from 0.5 to 8.2 % with an average of about 3.2 %, a median of about 2.8 %, and a decreasing trend as frequency increases.

In the previous section, it was shown that conventional modal testing was incapable of exciting the entire structure into vibration while maintaining good coherence between input force and output acceleration. In the tests where good coherence was maintained, structural modes were not well captured in the FRF. So, conventional modal testing with impact hammers was incapable of extracting global structural eigenproperties. However, performing a NExT analysis on the structural response to a simulated sonic boom in which global structural motion was attained was capable of extracting low frequency global modal properties.

3.2.3 Comparison of Modal Analysis Methods

Presented in this section is a comparison of the results obtained from the experimental modal testing of the two room structure with the modal results obtained from the finite element model of the two room structure used by the numerical model to predict sonic boom transmission into the building (Remillieux et al., 2009). This is done to examine the use of the sonic boom response to extract modal properties experimentally with NExT in a building more complex than the single room structure discussed previously. Again, the finite element model results are used to gain perspective and provide more insight into the experimental results. The experimental results were not used to tune the finite element model or as an input to the model in any way. Natural frequencies and mode shapes calculated from the finite element model are compared to the natural frequencies and mode shape extracted in the NExT experimental modal analysis of the two room structure in Figure 3.28 for the first few modes up to a frequency of about 21 Hz.

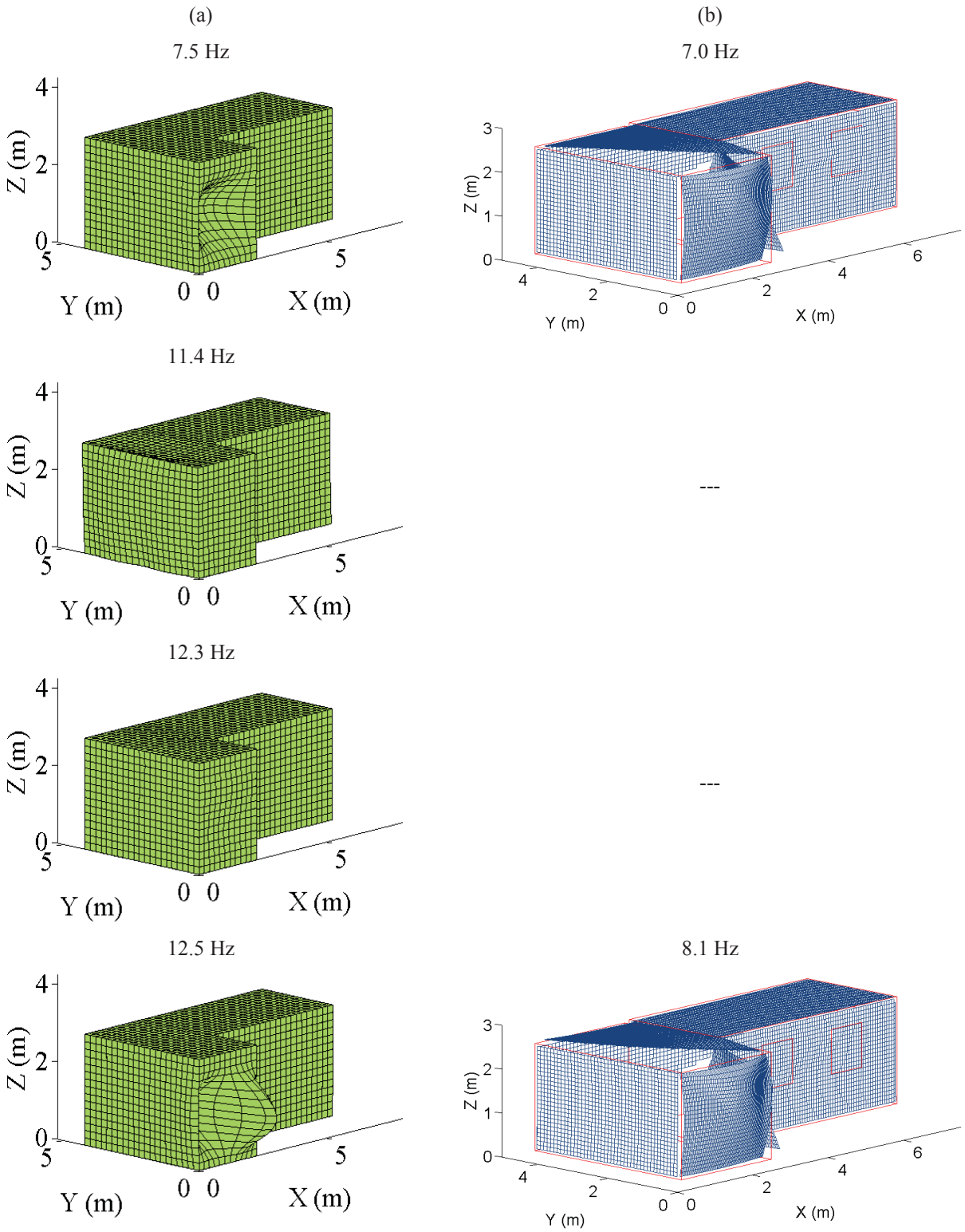

Figure 3.28: Comparison of natural frequencies and mode shapes of the two room structure calculated (a) from a finite element model (Remillieux et al., 2009) and (b) in the NExT experimental modal testing and analysis.

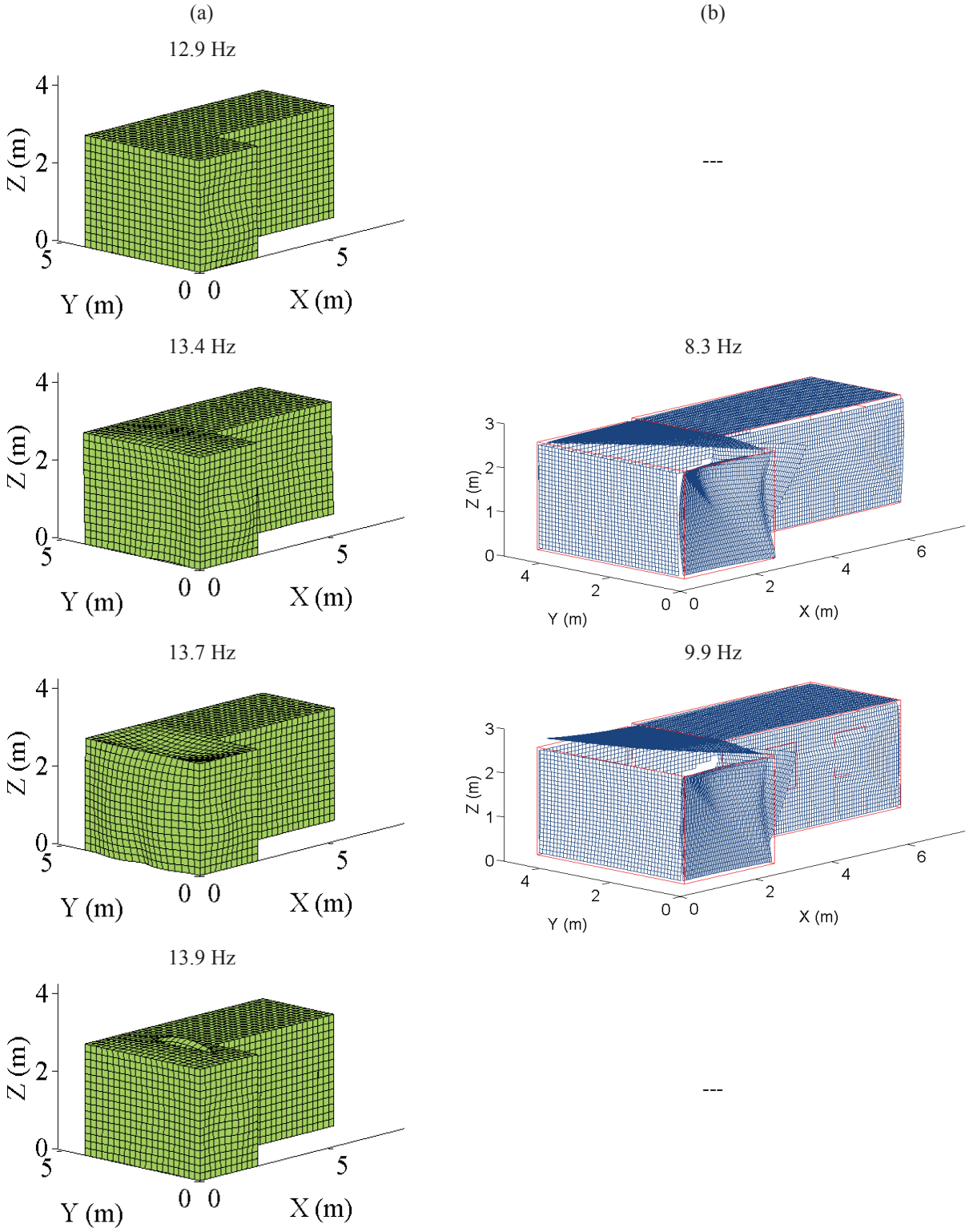

Figure 3.28: Comparison of natural frequencies and mode shapes of the two room structure calculated (a) from a finite element model (Remillieux et al., 2009) and (b) in the NExT experimental modal testing and analysis, cont.

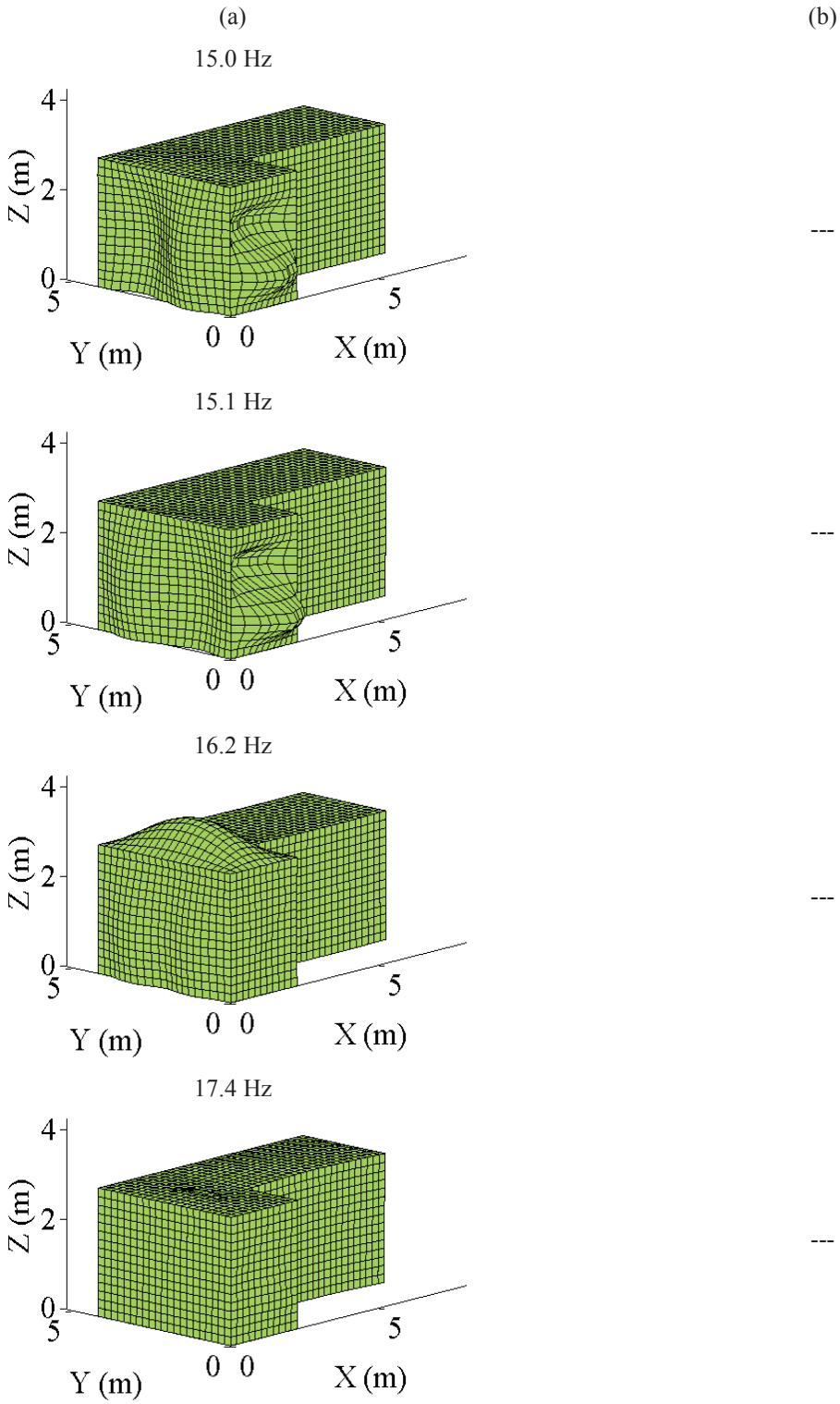

Figure 3.28: Comparison of natural frequencies and mode shapes of the two room structure calculated (a) from a finite element model (Remillieux et al., 2009) and (b) in the NExT experimental modal testing and analysis, cont.

(a) (b)

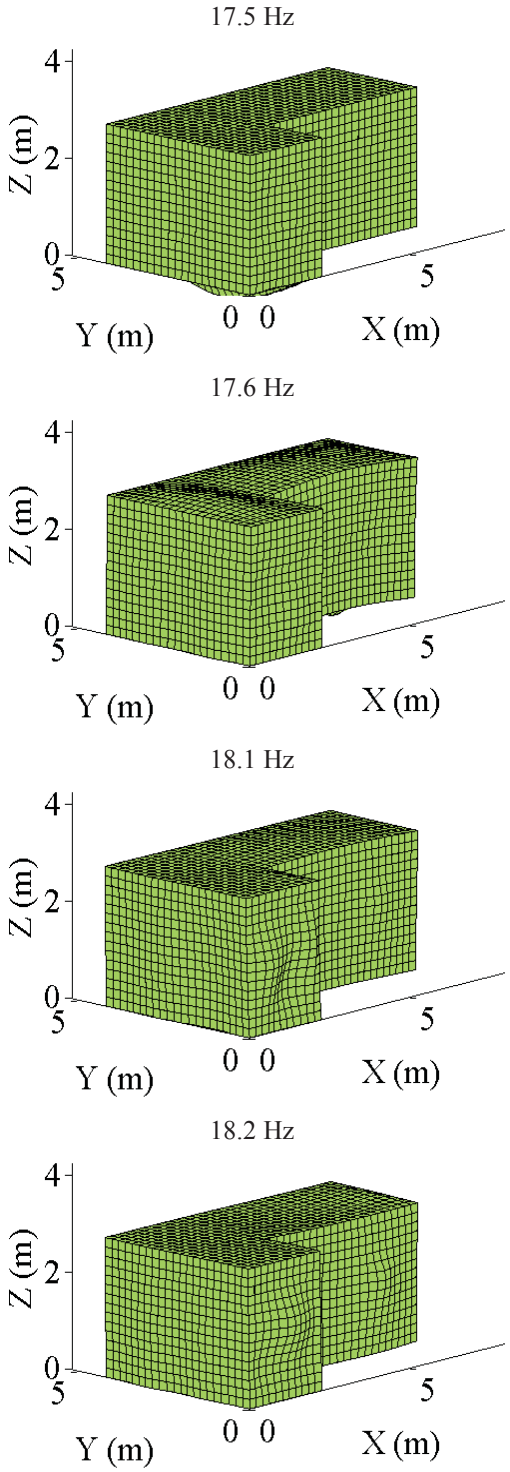

Figure 3.28: Comparison of natural frequencies and mode shapes of the two room structure calculated (a) from a finite element model (Remillieux et al., 2009) and (b) in the NExT experimental modal testing and analysis, cont.

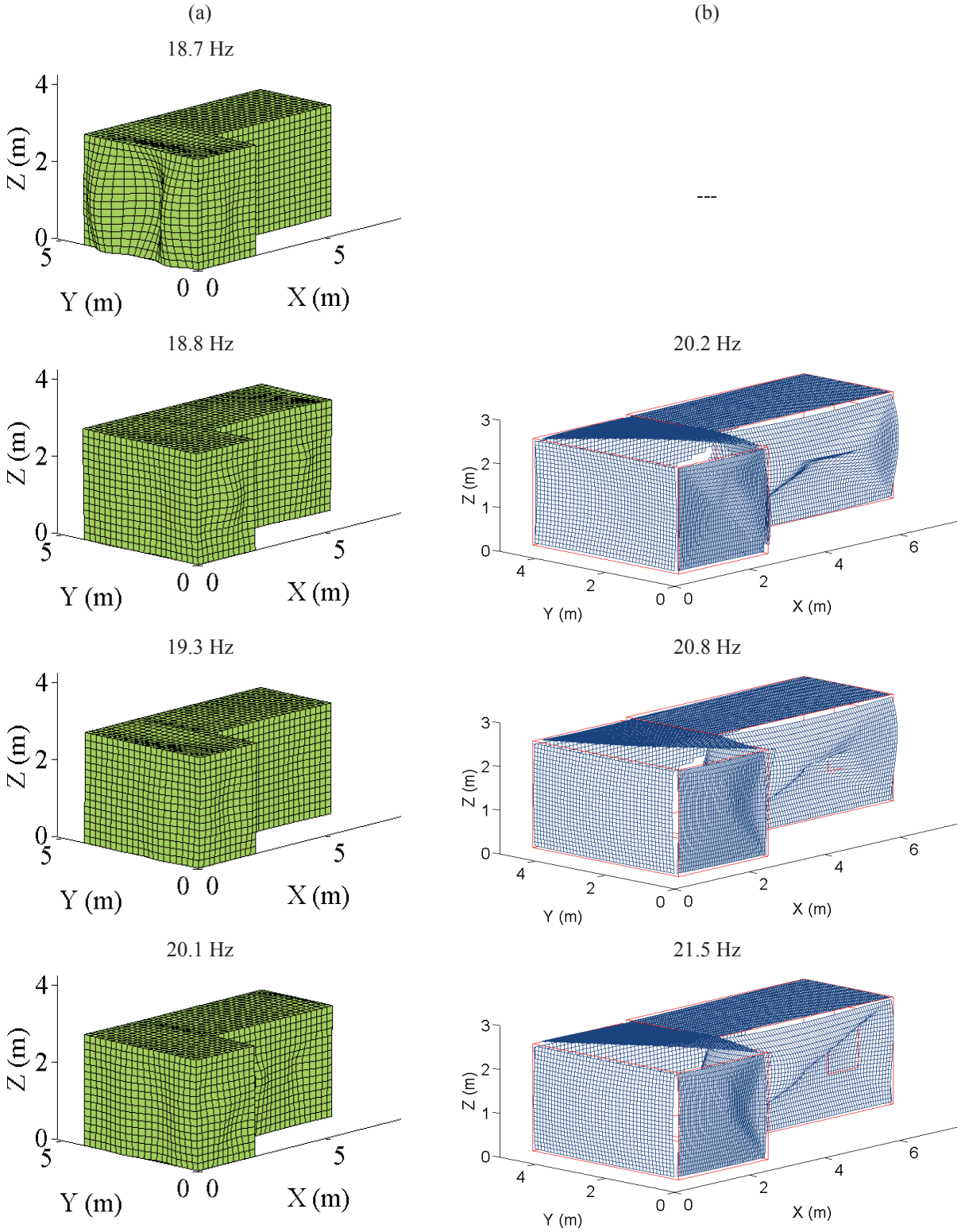

Figure 3.28: Comparison of natural frequencies and mode shapes of the two room structure calculated (a) from a finite element model (Remillieux et al., 2009) and (b) in the NExT experimental modal testing and analysis, cont.

Again, the main difference between the finite element analysis and the experimental modal analysis of the two room structure is the extraction of many more modes from the finite element model. This is probably because many more surfaces are modeled using finite elements such as the attic walls (not pictured) and the floors. The surfaces which were included in the experimental analysis had only a few sensors to describe their motion: one at the center and one at each corner for most walls. Therefore, more than one half-wavelength in each direction of each wall is not captured by the experimental modal test. Another reason why the experimental modal analysis could not extract this many modes is due to how close some are in frequency such as the finite element modes extracted with natural frequencies of 17.4, 17.5, and 17.6 Hz. Even though the Global SVD method is a multi-degree of freedom curve-fitting procedure, it clearly has some trouble extracting modes that are so close in frequency. Other than this difference, the results obtained from each analysis match very well.

The fundamental mode of the two room structure is the motion of the large window in the addition room which vibrates with a natural frequency of about 7 Hz. This is demonstrated quite clearly in both the finite element result as well as the result from the experimental modal analysis using NExT. The next two modes extracted in the finite element analysis with natural frequencies of about 11.4 and 12.3 Hz did not have a counterpart from the experimental modal analysis. They demonstrate perfectly one of the reasons mentioned previously. No displacement is shown in the plot which suggests that the motion of these modes comes from the attics or floors (not pictured), thus the experimental modal analysis does not capture these modes. Other modes which were not captured in the experimental modal test and analysis due to this reason include the finite element modes with natural frequencies of 12.9, 13.9, 17.4, 17.5, 17.6, and 18.2 Hz.

The mode extracted in the finite element analysis with a frequency of 12.5 Hz and in the experimental modal analysis with a frequency of 8.1 Hz demonstrates motion again from the large window. The mode shape from the finite element model shows two half-wavelengths in the horizontal direction while the shape from the experimental analysis shows only one. This is due to accelerometers placed only along the center and one side of the window which is shown in the plot as one side of the window displacing more than the other. While still exhibiting motion from the large window, the mode with a natural frequency of 13.4 Hz in the finite element results and of 8.3 Hz in the experimental results begins to demonstrate motion from the ceiling and the small

windows as well. The next mode with a finite element natural frequency of 13.7 Hz and an experimental natural frequency of 9.9 Hz shows even more motion from the ceiling with less from the small windows while the long plain wall of the addition structure begins to displace.

Modes extracted in the finite element analysis with frequencies around 15.0, 15.1, and 18.1 Hz were not captured in the experimental modal test due to most sensors being placed on nodes such as the horizontal center of the long plain wall of the addition structure and the vertical center of the large window. The next mode not accounted for in the experimental modal test is the finite element mode with a natural frequency of 16.2 Hz. This one was not extracted due to the lack of excitation of the ceiling by the sonic boom since most of the energy was absorbed by the exterior surfaces. The mode extracted in the finite element analysis with a natural frequency of 18.7 Hz was not found in the experimental analysis because of the lack of sensors needed to describe its motion which comes from the three horizontal half-wavelengths of the long plain wall of the addition.

The last three modes in the figure were matched well in each analysis. The mode extracted with a frequency of 18.8 Hz from the finite element model and 20.2 Hz from the experimental modal analysis exhibits motion from the large window and the two small windows, all in phase. The next mode with a natural frequency of 19.3 Hz in the finite element mode and 20.8 Hz in the experimental mode shows less motion from one of the small windows while retaining the motion from the others. The last mode demonstrates motion with the large window and small window closest to it in phase and the last small window out of phase with the other two. It was extracted with natural frequencies of 20.1 Hz from the finite element model and 21.5 Hz from the experimental modal analysis.

It has been shown that the modal results extracted experimentally using the structural response to a simulated sonic boom with NExT match the results obtained from the finite element model very well. The absence of modes not extracted in the experimental analysis but calculated from the finite element model is explained by reasons such as the lack of measurements from all surfaces, the lack of measurements from multiple points on each surface, the placement of measurements on nodes of modes, and the closely-spaced nature of the modes extracted in the finite element model. However, using NExT with the sonic boom response does provide accurate properties of the other modes. This suggests that an impulsive excitation can be used with NExT.

4 Acoustic Modal Analysis

In this chapter, acoustic modal analysis of the cavities enclosed by the single and two room structures will be discussed. Three configurations of the two room structure cavities will be considered in the chapter. Due to the inability to measure the input force using a speaker at very low frequencies, a conventional modal test and analysis is not attempted. Therefore, the analysis of each cavity begins with a theoretical approach to calculate acoustic natural frequencies for comparison with the NExT approaches. Then, experimental modal testing and analysis of the acoustic cavities using NExT and the interior pressure response to random, stationary input is discussed. For each cavity, this input is white noise played through a speaker. Then, each cavity is analyzed using NExT and its response to a sonic boom. The results from the theoretical and NExT analyses will then be compared for each cavity.

The approach to extract acoustic modal properties from pressure response data using NExT was the same for each type of cavity and input. A diagram of this approach is shown in Figure 4.1. The cross-correlations between responses were calculated first assuming a single reference response. The FFT of the cross-correlations was calculated and summed to form a mode indicator function. This was repeated for different references to form a decision as to which reference to use in the analysis. The LSCE method was then applied to the cross-correlations using the proper reference assuming some estimate of the number of modes in the frequency range of the data. NExT IRFs were regenerated from the extracted modal properties and error between the measured and regenerated curves was computed. The assumed number of modes was increased consecutively and the analysis and error calculation repeated. The percent difference in modal properties extracted in the current analysis to the previous analysis was also calculated to determine the stability of the properties. The correct number of modes to assume was determined from the error plot and the overall stability of the modal properties. Physical modes were separated from computational modes by examining the feasibility of the modal properties and their stability.

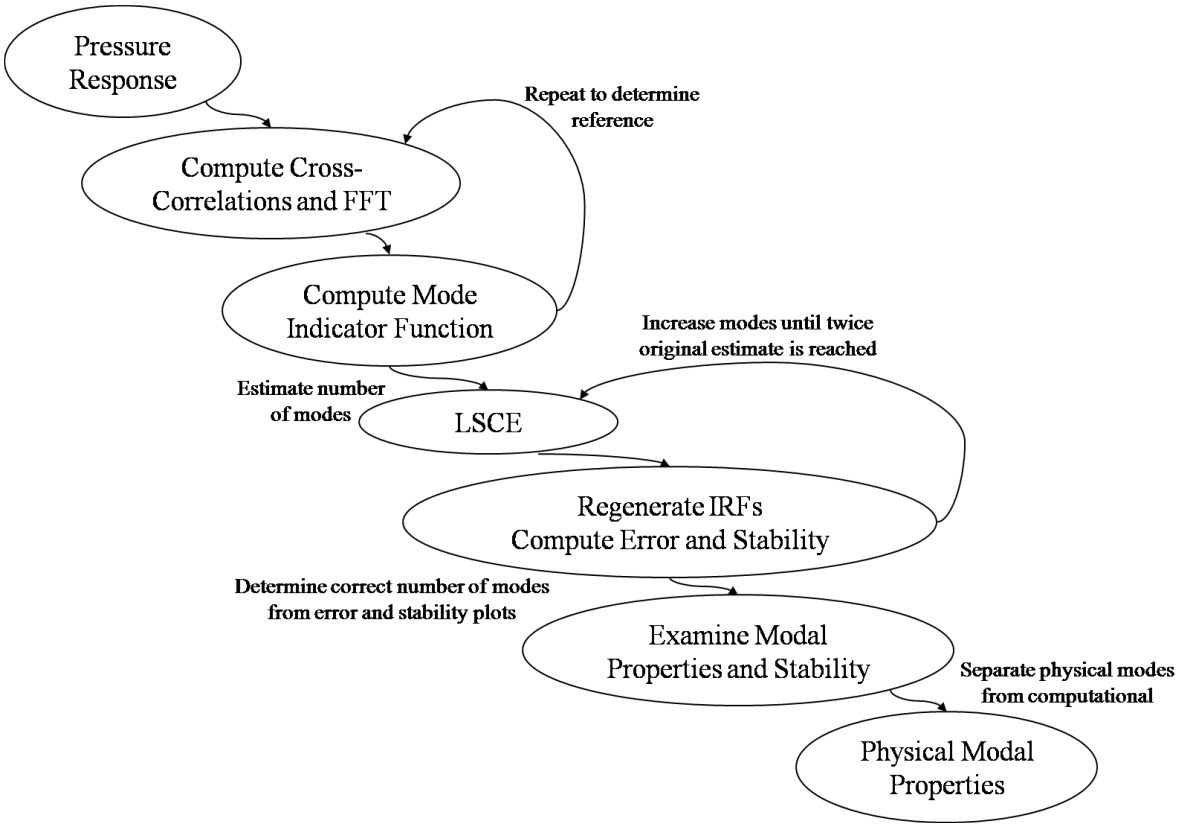

Figure 4.1: Diagram of approach used to obtain acoustic modal properties from pressure response data using NExT for each structure cavity and type of input.

4.1 Single Room Cavity Modal Analysis

Presented in this section is the acoustic modal analysis of the cavity enclosed by the single room structure. First, natural frequencies of the room will be predicted analytically. Then, modal testing and analysis of the room using a speaker playing white noise will be discussed. Next, modal testing and analysis of the room using the interior pressure response to a simulated sonic boom will be given. Finally, a comparison of the analyses will be given.

4.1.1 Predicted Modal Properties

In this section, acoustic natural frequencies of the rectangular, rigid single room structure cavity will be predicted analytically. This technique was used and validated by the numerical model to determine acoustic modal properties of the interior cavity which contribute to the interior pressure response to sonic boom transmission (Remillieux et al., 2009). The natural frequencies of the rectangular room were calculated analytically under the assumption that the walls are rigid boundaries using

$$f_n = \frac{c}{2}\sqrt{\left(\frac{n_x}{L_x}\right)^2 + \left(\frac{n_y}{L_y}\right)^2 + \left(\frac{n_z}{L_z}\right)^2} \tag{4.1}$$

where c is the speed of sound, n_x, n_y, and n_z are the mode indices in the three orthogonal directions, and $L_x = 2.58$ m (101.75 in), $L_y = 4.60$ m (181.25 in), and $L_z = 2.54$ m (100 in) are the corresponding internal room dimensions. The rigid boundary assumption is reasonable since the acoustic impedance of the hard wall surface is much higher than the acoustic impedance of air, so the analytical results are expected to be in good agreement with the experimental results. The analytical frequencies of the first ten modes are presented in Table 4.1.

Table 4.1: First ten predicted acoustic natural frequencies of single room structure cavity assuming rigid walls.

Mode	***Natural Frequency (Hz)***
1	37.25
2	66.36
3	67.52
4	74.50
5	76.10
6	77.11
7	94.67
8	99.77
9	100.55
10	101.74

4.1.2 Noise Response Modal Analysis

In this section, the acoustic modal testing and analysis using the interior pressure response to white noise will be discussed. First, the instrumentation and experimental setup used in testing will be presented. This will be followed by a description of the tests. Then, the procedure for analysis of the data collected in these tests will be given including spectrum calculations and modal parameter extraction using NExT. Finally, the results of the acoustic modal analysis of the will be given.

Since the essential problem is to predict interior acoustic response to a sonic boom, microphones are necessary to measure the pressure response inside the room as part of

determining eigenproperties of the room itself. Fourteen Panasonic Electret Condenser Microphones (model WM-61A), shown in Figure 4.2, were mounted to four wooden poles placed vertically in different positions inside the structure (Corcoran et al., 2009).

(a) (b)

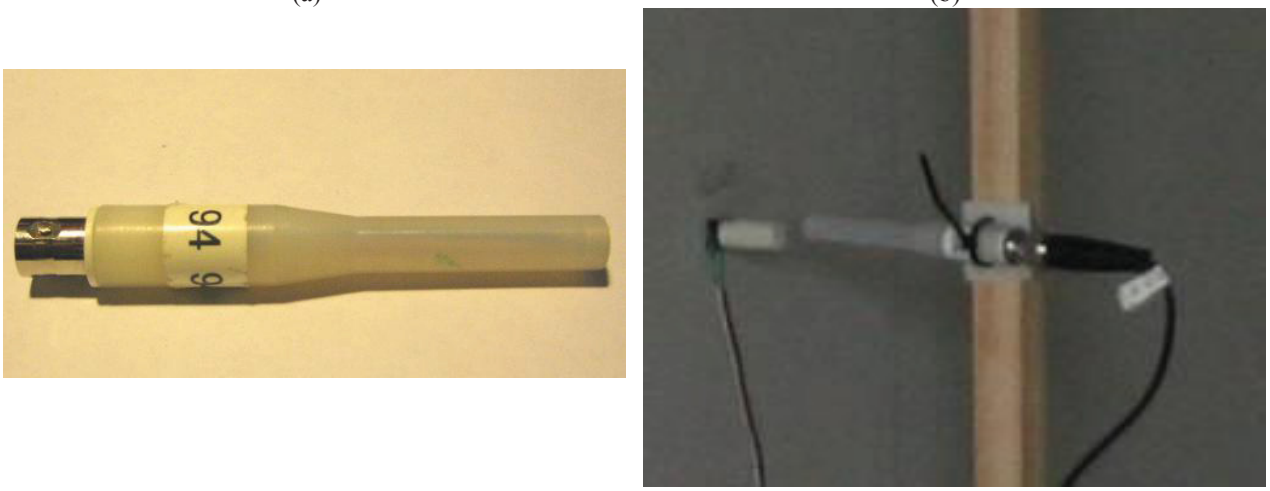

Figure 4.2: Pictures of (a) microphone used to measure structure's interior acoustic response and (b) microphone installed on wooden pole inside the single room cavity.

Acoustic tests were performed using the Alesis M1 Active Mk2 speaker, placed in a corner of the room on the floor as shown in Figure 4.3, as the acoustic input. Data was recorded with the inside microphones for 32 seconds at a sampling frequency of 12.8 kHz using a 5 V peak white noise input low-pass filtered at 400 Hz. The input signal was then halved to a level of 2.5 V peak and data was recorded again with the same parameters. The tests were performed with and without three or four 2 ft strips of R14 insulation placed in each corner of the room on the floor to add damping, shown in Figure 4.3 (Corcoran et al., 2009).

(a) (b)

Figure 4.3: Speaker, microphone pole, and insulation damping setup used in acoustic modal testing.

First, spectrums of the microphone signals obtained while playing white noise through the Alesis speaker were calculated. Each microphone signal was downsampled from about 12.8 kHz to 210 Hz. This resampling was done in anticipation of using a time domain experimental modal analysis technique. Since a frequency range cannot be specified using this type of technique, an upper limit was placed on the frequency range of analysis using a Nyquist frequency of 105 Hz. Sensitivities were then applied to convert the voltage signals into units of pressure (Pa). Then, spectrums were calculated in 256-point blocks without overlap between blocks for a total of 25 blocks. The separate blocks were then averaged to calculate an overall spectrum for each microphone signal.

Next, the idea of the simple mode indicator function discussed previously was applied to gain an overall view of the spectrums obtained in each test. The simple mode indicator functions were obtained by summing the individual microphone spectrums in each speaker test. Figure 4.4 shows the simple mode indicator functions for the high-level input speaker tests with and without damping added to the room. For comparison, the natural frequencies obtained analytically are plotted as vertical black lines. From these functions, it can be seen that there exists a high modal density even at low frequencies. This renders simple modal parameter extraction techniques, such as the peak-picking method which can be applied to spectra in a conventional analysis, inaccurate. It can also be seen from this plot that the analytical natural frequencies are closely aligned with peaks in each of the mode indicator functions. However, there appear to be many more maxima than are predicted by the analytical expression for acoustic modes. Looking back at the structural modal results, it can be seen that many of these peaks are associated with structural modes which were excited in the speaker tests such as the peaks around 15, 17, 20, 43, and 50 Hz. Also, it can be seen that the addition of damping has very little effect on the response of the room.

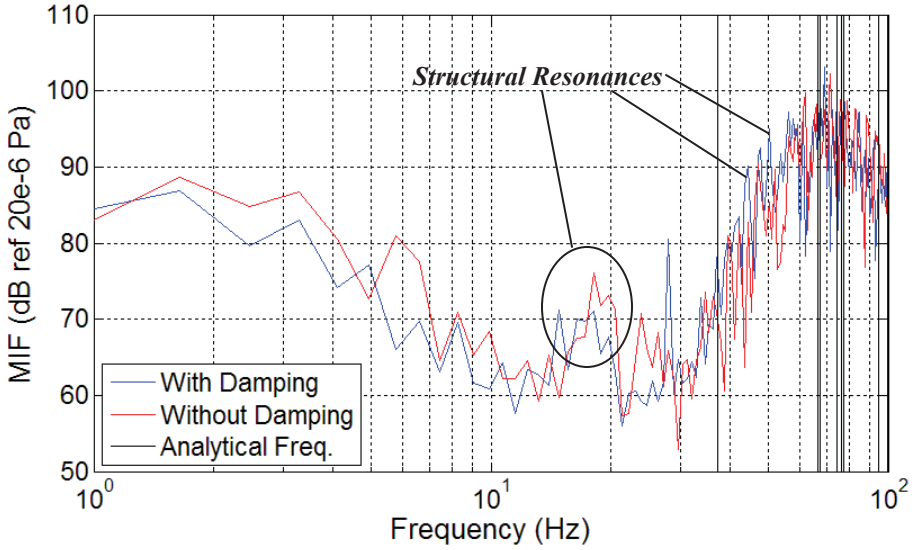

Figure 4.4: Mode indicator functions obtained from the high-level input speaker tests plotted with and without damping compared to natural frequencies obtained analytically plotted as vertical black lines.

Since the application of experimental modal analysis techniques to extract modal properties requires measurement of an input force to form a frequency response function which is difficult to perform accurately using a speaker as the input to the system, NExT was then pursued to extract eigenproperties of the room since there is no need to measure the force input to the system. The pressure signals measured without acoustic damping added to the room while the speaker played high level white noise which were downsampled to a rate of 210 Hz were used in this analysis. Cross-correlations were calculated between each microphone signal to a reference microphone's signal. In this case, the reference was taken to be the microphone closest to the speaker positioned in a corner of the structure. This microphone was used as a reference because the least number of modes were expected to have a node in the corner of a rectangular cavity.

The second halves of all the cross-correlations for positive time differences, or NExT IRFs, were then examined using the single reference LSCE method (Mohanty and Rixen, 2004a) for experimental modal analysis. This method is a multiple degree of freedom time domain curve-fitting procedure which fits a sum of decaying exponentials or modes to a set of IRFs simultaneously. In this method, an initial estimate of the number of modes is assumed and a curve is fit to the exponentially decaying sinusoids using that number of modes. A convenient initial estimate came from the number of predicted modes in the frequency range. The measured NExT IRFs are then regenerated using the extracted eigenproperties and the square error

between the measured and regenerated curves is calculated and averaged for all NExT IRFs. The number of modes assumed is then increased consecutively and the LSCE algorithm is repeated. The extracted eigenproperties from the current analysis are compared with the eigenproperties from the previous analysis by calculation of the percent difference to examine the stability of the modes. This is repeated until two and a half times the initial estimate of modes is reached.

Based on the square error and stability of the eigenproperties, 25 assumed modes was selected as the correct number (Corcoran et al., 2009) with the hope that some of the closely spaced modes predicted by the analytical analysis could be better resolved with a higher number of extracted modes. By inspection of the modal properties and their stability, obviously some of these modes exist purely as computational artifacts of a numerical curve-fitting procedure, not as genuine physical modes of the system. These are identified by abnormally high damping ratios or negative damping ratios and modes with unstable modal properties (Corcoran et al., 2009).

After removing obvious computational modes and all modes with unstable eigenproperties, the extracted eigenproperties of the physical modes of the system are given in Table 4.2. Also included in this table is the origin of the particular mode, i.e. structural or acoustic, which is obtained by inspection of these frequencies and comparison with natural frequencies extracted in the structural experimental modal analysis and predicted in the analytical acoustic analysis.

Comparing these modes with the predicted modes given in Table 4.1, it can be seen that there were many more modes extracted than expected. Some of these can be explained as structural modes excited by the speaker which radiated sound that was sensed up by the microphones. These are indicated as such in the last column of Table 4.2. Comparing the first two modes of Table 4.2 which are well below the first expected acoustic natural frequency to the structural modal natural frequencies extracted in both conventional and NExT analyses, in Table 3.1 and Table 3.2 respectively, it can be seen that these are structural modes. Modes 4, 5, 6, and 9, also not predicted, can also be found in Table 3.1 indicating that they are structural modes, too. All modes which could not be explained as structural modes extracted in the structural experimental modal analysis were labeled as acoustic modes in the last column of Table 4.2.

Table 4.2: List of eigenproperties of all physical modes extracted using NExT with the LSCE method assuming 25 modes in the frequency range 0 to 105 Hz.

Mode	*Natural Frequency (Hz)*	*Damping Ratio (%)*	*Mode Origin*
1	15.08	3.78	Structural
2	22.35	0.10	Structural
3	37.62	2.74	Acoustic
4	42.05	3.27	Structural
5	45.22	5.80	Structural
6	50.52	4.25	Structural
7	55.06	4.95	Acoustic
8	59.18	6.16	Acoustic
9	62.93	6.55	Structural
10	66.51	6.51	Acoustic
11	70.00	5.76	Acoustic
12	73.97	4.94	Acoustic
13	78.22	4.30	Acoustic
14	82.44	3.74	Acoustic
15	86.89	3.20	Acoustic
16	91.91	2.73	Acoustic
17	97.14	2.48	Acoustic
18	99.08	8.59	Acoustic
19	102.45	3.20	Acoustic

4.1.3 Sonic Boom Response Modal Analysis

In this section, acoustic modal properties of the single room structure will be extracted using the interior acoustic response to a simulated sonic boom with NExT and the LSCE method. The microphones used and their positions were identical to that of the experimental modal analysis using white noise. The procedure used to extract the modal properties was also nearly identical to the process used in the noise response analysis.

First, NExT IRFs were computed by calculating the cross-correlations between each pressure response signal and the reference signal recorded by the same microphone as in the previous analysis downsampled to 210 Hz. The FFTs of the NExT IRFs, or NExT FRFs, were computed

and summed linearly to obtain a mode indicator function as shown in Figure 4.5. Resonances in the function occur at frequencies of about 9, 18, 22, 25, 26, 32, and 36 Hz.

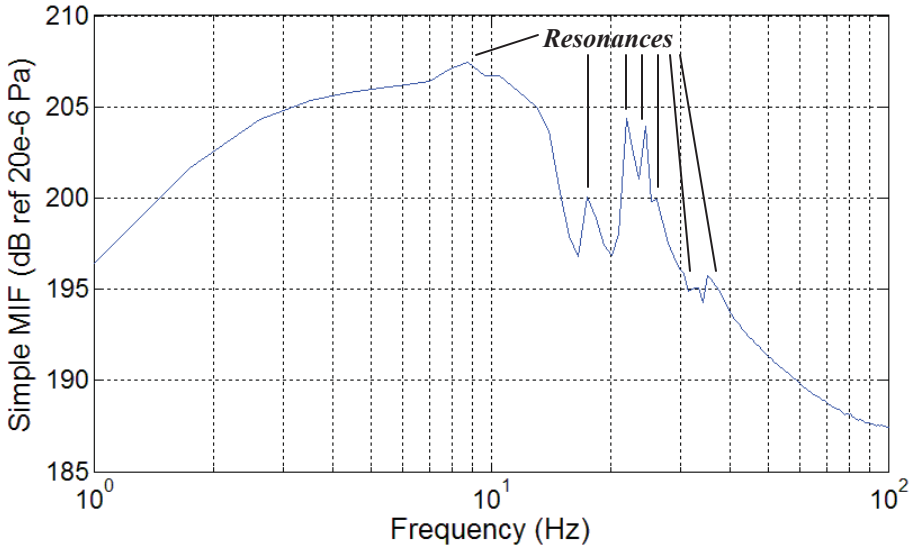

Figure 4.5: Simple mode indicator function of single room structure cavity obtained by summing NExT FRFs with the reference signal recorded by a microphone in the corner of the single room cavity.

The LSCE method was then applied to extract modal properties from the NExT IRFs which were then regenerated and square error was computed between measured and regenerated curves and averaged for all IRFs. The number of assumed modes began at one mode and was increased consecutively up to 20 assumed modes. Based on the low square error between measured and regenerated NExT IRFs and the stability of modal properties, 20 modes was selected as the correct number of modes in the frequency range (Corcoran et al., 2009).

Again, many fictitious, computational modes were extracted (Corcoran et al., 2009). All modes with at least a stable natural frequency were retained as genuine, physical modes of the system while unstable modes were disregarded as fictitious, computational modes. The list of all genuine, physical modal properties is given in Table 4.3. Again, the genuine, physical modes are labeled with their origin, i.e. structural or acoustic, in the last column of the table. The origin is determined by inspection of and comparison with the natural frequencies obtained from the structural experimental modal analysis. It can be seen from the natural frequencies of the previous structural analyses that modes 1, 5, 6 and 9 were extracted as physical modes of the structure. Although modes 2 and 7 were not extracted in the structural modal analyses, they did appear as resonances in the mode indicator functions and are probably structural modes missed

by the modal analyses. This observation is reinforced by the fact that these modes have high damping ratios uncharacteristic of the other acoustic modes.

Table 4.3: Modal properties of genuine, physical modes extracted using NExT and the LSCE method on the interior acoustic response to a simulated sonic boom.

Mode	*Natural Frequency (Hz)*	*Damping Ratio (%)*	*Mode Origin*
1	19.94	16.95	Structural
2	24.87	12.08	Structural
3	31.51	9.26	Acoustic
4	35.73	8.78	Acoustic
5	39.79	5.28	Structural
6	50.91	6.79	Structural
7	51.34	24.62	Structural
8	57.19	4.22	Acoustic
9	62.17	3.85	Structural
10	67.82	2.42	Acoustic
11	72.32	4.41	Acoustic
12	79.03	1.56	Acoustic
13	84.33	7.88	Acoustic
14	84.75	4.10	Acoustic
15	95.54	1.86	Acoustic
16	101.78	1.02	Acoustic

4.1.4 Comparison of Modal Analysis Methods

In this section, a detailed comparison of the results of the analytical modal analysis and experimental modal analyses for the single room cavity will be given. Since the numerical model to predict sonic boom transmission into buildings validated the use of the analytical method for determining acoustic modal properties (Remillieux et al., 2009), the predicted results can be used to examine the use of NExT to extract modal properties of the acoustic modes of the cavity. Also, using NExT with the pressure response to white noise adheres to the random, stationary assumption in the original derivation of the technique. However, applying the technique to the interior pressure response to a sonic boom violates this assumption and is more in line with the impulsive input derivation. The comparison of the results of these different NExT analyses will be useful to determine the differences inherent in these assumptions. The predicted natural

frequencies of the room are compared with the measured modal properties extracted in the NExT analyses visually in Figure 4.6 and numerically in Table 4.4. Again, the origins of the modes are included in the table.

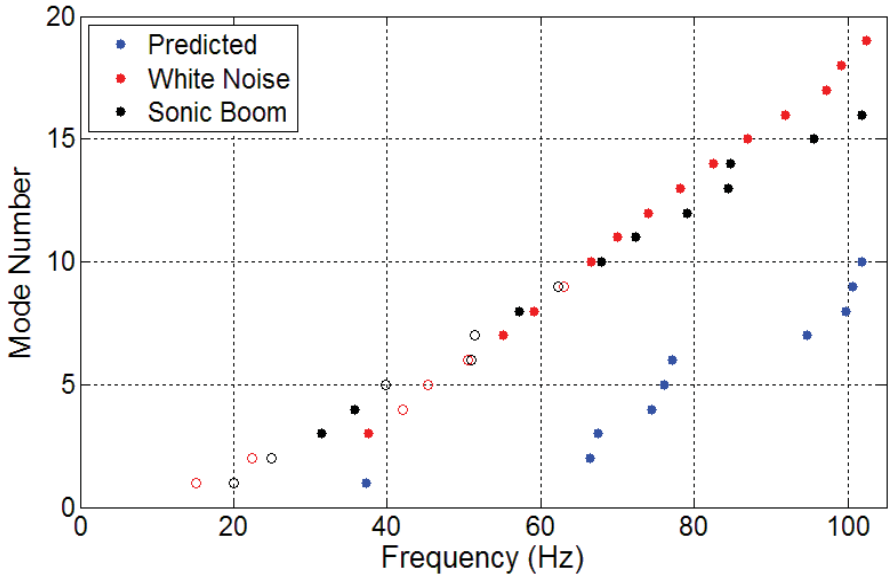

Figure 4.6: Comparison between natural frequencies of the single room cavity obtained analytically and experimentally using NExT with both white noise and sonic boom response. Closed circles (●, ●, and ●) indicate acoustic modes and open circles (○ and ○) structural modes extracted in the acoustic analysis.

Aside from the modes labeled structural, it can be seen that the predicted natural frequencies match the natural frequencies measured experimentally very well. The natural frequencies which did not match very well were very closely spaced in frequency, e.g. the modes with natural frequencies of around 66 and 67 Hz and around 74.5 to 77 Hz, which indicates that the curve-fitting procedure used most likely had difficulty resolving these modes. Other than that, there were a few modes extracted that were not predicted analytically which all seem to occur in the large frequency ranges where no modes were predicted analytically, e.g. from about 40 Hz to 65 Hz and 80 to 95 Hz. These modes could be stable computational modes which are there to preserve the curve-fit in these frequency ranges, or they could exist due to large modifications of the assumed rectangular geometry of the room such as the large instrumentation racks in the center of the room.

Also, it can be seen from the table that the two different experimental modal analyses produced very consistent results. Both analyses extracted very similar natural frequencies including those of structural modes. The main difference between the two NExT analyses was in the estimation of the modal damping ratios. At low frequencies, i.e. 15 to 50 Hz, the analysis

using the response to a sonic boom extracted much higher damping ratios than the analysis using the response to white noise. Then, at higher frequencies from about 60 to 100 Hz, the damping ratios from the analysis using the response to a sonic boom dropped lower than their counterparts from the analysis using the response to white noise.

Table 4.4: Comparison between predicted natural frequencies and experimentally measured modal properties extracted in the NExT modal analyses.

Predicted	***NExT, White Noise***		***NExT, Sonic Boom***		
Natural Frequency (Hz)	***Natural Frequency (Hz)***	***Damping Ratio (%)***	***Natural Frequency (Hz)***	***Damping Ratio (%)***	***Mode Origin***
---	15.08	3.78	19.94	16.95	Structural
---	22.35	0.10	24.87	12.08	Structural
---	---	---	31.51	9.26	Acoustic
37.25	37.62	2.74	35.73	8.78	Acoustic
---	42.05	3.27	39.79	5.28	Structural
---	45.22	5.80	---	---	Structural
---	50.52	4.25	50.91	6.79	Structural
---	---	---	51.34	24.62	Structural
---	55.06	4.95	---	---	Acoustic
---	59.18	6.16	57.19	4.22	Acoustic
---	62.93	6.55	62.17	3.85	Structural
66.36	66.51	6.51	---	---	Acoustic
67.52	70.00	5.76	67.82	2.42	Acoustic
74.50	73.97	4.94	72.32	4.41	Acoustic
76.10	---	---	---	---	Acoustic
77.11	78.22	4.30	79.03	1.56	Acoustic
---	82.44	3.74	84.33	7.88	Acoustic
---	86.89	3.20	84.75	4.10	Acoustic
---	91.91	2.73	---	---	Acoustic
94.67	97.14	2.48	95.54	1.86	Acoustic
99.77	99.08	8.59	---	---	Acoustic
100.55	---	---	---	---	Acoustic
101.74	102.45	3.20	101.78	1.02	Acoustic

Modal damping ratios of the acoustic modes extracted in the NExT experimental modal analysis using the interior pressure response to white noise ranged from about 2.5 % to 8.6 % and exhibit a fairly constant trend. The average modal damping ratio is about 4.6 % and the

median value is 4.3 %. The damping ratios of acoustic modes extracted in the NExT analysis using sonic boom response ranged from about 1.0 % to 9.3 % with a more decreasing trend. The average ratio for this analysis is about 4.6 % and the median is 4.2 %.

Based on this comparison, using NExT to extract acoustic modal properties from the interior pressure response will provide accurate results for the single room structure cavity. More specifically, using NExT with the response to white noise and with the response to a sonic boom provide very similar results indicating that either random, stationary or impulsive inputs can be used with NExT. Also, the advantage of the experimental modal analysis procedures being able to determine damping ratios for the acoustic modes, since the walls of the structure are not perfectly reflective, has been demonstrated.

4.2 Two Room Cavity Modal Analysis

Presented in this section will be the acoustic modal analysis of the two room structure's cavities. A more interesting physical analysis is presented by these cavities due to the increased complexity of the acoustic system with two interconnected cavities. Physical phenomena like Helmholtz resonators are encountered and studied by varying the configuration of the cavities in the two room structure. First, an analytical analysis will be performed to predict acoustic natural frequencies, followed by a conventional spectrum measurement with a microphone while exciting the cavities with a speaker. Then, an output-only modal analysis with NExT will be performed to extract modal properties of the cavities with interior pressure response to a simulated sonic boom. These analyses will be completed for three configurations of the two room structure's doors. The configuration in which both exterior and interior doors are closed will be referred to as the closed-closed configuration while the configuration with the exterior door closed and interior door open will be called the open-closed configuration. The last configuration in which both doors are open will be referred to as the open-open configuration. Finally, the analyses will be reviewed and compared to determine the validity of using NExT with the interior pressure response to a sonic boom to measure acoustic modal properties.

4.2.1 Predicted Modal Properties

In this section, an analytical analysis of the two rooms' modes will be performed to provide a general understanding of where the modes may lie in the frequency spectrum. First, the rectangular room modes will be calculated assuming rigid boundaries at the structure walls,

windows, and doors. Then, a Helmholtz resonator analysis will be performed since these resonances may play a role in the acoustic dynamics in the open-open and open-closed configurations due to the small mass of air in the doorways compressing the large volumes of air contained in the rooms.

The analytical natural frequencies were calculated for the rectangular original structure room and addition structure room assuming rigid boundaries, again with the use of eq. (4.1). The room dimensions for each of the two rooms are given in Table 4.5. The first ten natural frequencies calculated analytically for both rooms are given in Table 4.6.

Table 4.5: Two room structure room dimensions used in analytical acoustic analysis.

Dimension	***Original Structure Room***	***Addition Structure Room***
L_x	4.72 m (186 in)	2.26 m (89 in)
L_y	2.58 m (101 ¾ in)	4.14 m (163 in)
L_z	2.54 m (100 in)	2.48 m (97 ½ in)

Table 4.6: Predicted natural frequencies calculated for the two room structure cavities assuming rectangular geometry and rigid walls.

Mode	***Original Structure Room Natural Frequency (Hz)***	***Addition Structure Room Natural Frequency (Hz)***
1	36.30	41.42
2	66.36	69.25
3	67.52	75.86
4	72.60	80.69
5	75.64	82.85
6	76.66	86.44
7	94.67	102.72
8	98.36	107.98
9	99.15	110.76
10	101.39	112.33

From Table 4.6, it can be seen that the first acoustic mode is in the original structure room with a natural frequency of about 36 Hz while the second acoustic mode exists in the addition structure room with a slightly higher natural frequency of about 41 Hz due to this particular cavity being slightly smaller than the other. Acoustic modal density becomes very high around 70 Hz. In the open-open configuration, it was believed that the rooms may act as coupled

Helmholtz resonators. The two rooms may act as large compressible volumes of air being compressed by the mass of the air in each doorway resulting in a two degree of freedom mechanical system, as depicted in the schematic in Figure 4.7.

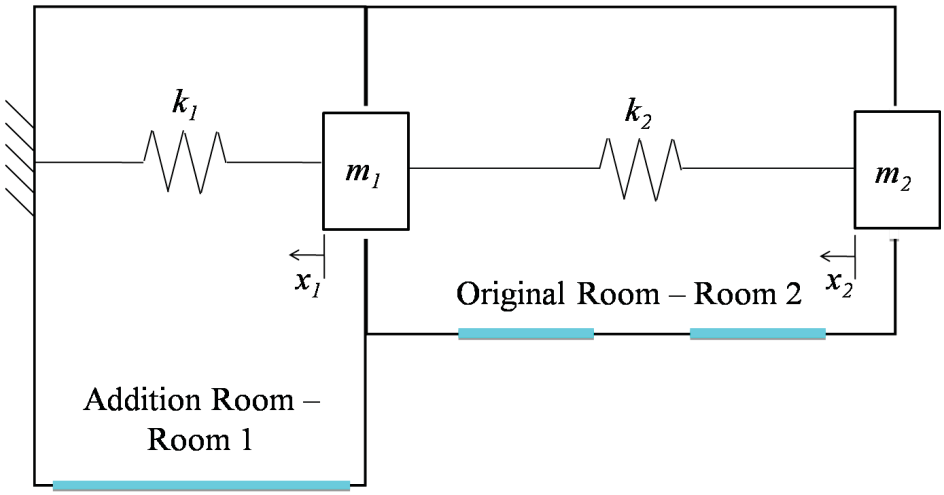

Figure 4.7: Schematic of two room structure in open-open configuration as coupled Helmholtz resonator.

The equations of motion for the two degree of freedom, homogeneous system depicted are

$$\begin{cases} m_1\ddot{x}_1 + (k_1 + k_2)x_1 - k_2x_2 = 0 \\ m_2\ddot{x}_2 - k_2x_1 + k_2x_2 = 0 \end{cases} \tag{4.2}$$

where m_1 and m_2 are the masses of the air contained in the doorways, k_1 and k_2 are the stiffnesses associated with the bulk compressibility of the air contained in the rooms, and x_1 and x_2 are the displacements associated with the mass of air in the doorways. Equation (4.2) can be rewritten in matrix form as

$$\begin{bmatrix} m_1 & 0 \\ 0 & m_2 \end{bmatrix} \begin{Bmatrix} \ddot{x}_1 \\ \ddot{x}_2 \end{Bmatrix} + \begin{bmatrix} k_1 + k_2 & -k_2 \\ -k_2 & k_2 \end{bmatrix} \begin{Bmatrix} x_1 \\ x_2 \end{Bmatrix} = \begin{Bmatrix} 0 \\ 0 \end{Bmatrix}. \tag{4.3}$$

Since the doors used in the construction of the two room structure were identical in size, the masses of the air in each doorway were equal and could be calculated using a technique discussed by Kinsler et al. (2000) where

$$m_1 = m_2 = \rho S L_e \tag{4.4}$$

where ρ is the density of air, about 1.29 kg/m^3 (0.075 lb$_m$/ft^3), S is the area of the doorway, about 0.70 x 2.16 m (27 ¾ x 85 in), and L_e is the length of the doorway with a correction applied

to account for air outside of the doorway which acts with the mass. Uncorrected, the length of the doorway, l, is about 11 cm (4 ½ in). To apply the correction to the length, the expression

$$L_e = l + 2\delta, \tag{4.5}$$

was used where δ is the end correction of the doorway, calculated by

$$\delta = \frac{2S}{\pi L}\left\{\left(1+\frac{1}{\alpha}\right)\ln\left[\left(1+\alpha^2\right)^{1/2}+\alpha\right]+\left(1+\alpha\right)\ln\left[\left(1+\frac{1}{\alpha^2}\right)^{1/2}+\frac{1}{\alpha}\right]+ \right.$$
$$\left. \frac{1}{3}\alpha\left(1+\alpha\right)\left[1+\frac{1}{\alpha^3}-\left(1+\frac{1}{\alpha^2}\right)^{3/2}\right]\right\} \tag{4.6}$$

where L is the perimeter of the doorway and α is the aspect ratio of the largest doorway dimension to the smallest (Morfey, 1969). Substituting the values obtained into eq. (4.4) gives the mass of the air in each doorway to be about 2.17 kg (4.8 lb_m).

The stiffness constants were calculated using the expressions

$$k_1 = \rho c^2 \frac{S^2}{V_1}$$
$$k_2 = \rho c^2 \frac{S^2}{V_2} \tag{4.7}$$

where c is the speed of sound in air, 343 m/s (1,125 ft/s), and V_1 and V_2 are the volumes of the addition structure room and the original structure room, respectively (Kinsler et al., 2000). The dimensions of the addition structure room were measured to be about 2.26 x 4.14 x 2.48 m (89 x 163 x 97 ½ in) and of the original structure room were about 4.72 x 2.58 x 2.54 m (186 x 101 ¾ x 100 in) yielding volumes of about 23.2 m^3 (819 ft^3) and 31.0 m^3 (1,095 ft^3), respectively. Substituting all known values into eq. (4.7) gives stiffness constants of about 13.4 kN/m for the addition structure room volume and about 10.0 kN/m for the original structure room volume.

Substituting the known mass and stiffness constants into eq. (4.3) and solving the eigenvalue problem gives the natural frequencies and mode shapes of the two Helmholtz resonances. The natural frequencies calculated are given in Table 4.7.

A similar Helmholtz effect occurs when the structure is open-closed in which the rooms on either side act as springs attached to the mass of air in the doorway between them as shown in Figure 4.8. In this case, the resulting mechanical system is a single degree of freedom system

with an equivalent stiffness equal to the sum of the stiffnesses of the individual rooms with the equation of motion

$$m_1\ddot{x}_1 + \left(k_1 + k_2\right)x_1 = 0\,. \tag{4.8}$$

Using the values calculated in the previous Helmholtz analysis, the resulting natural frequency for this system is about 16.55 Hz shown in Table 4.7.

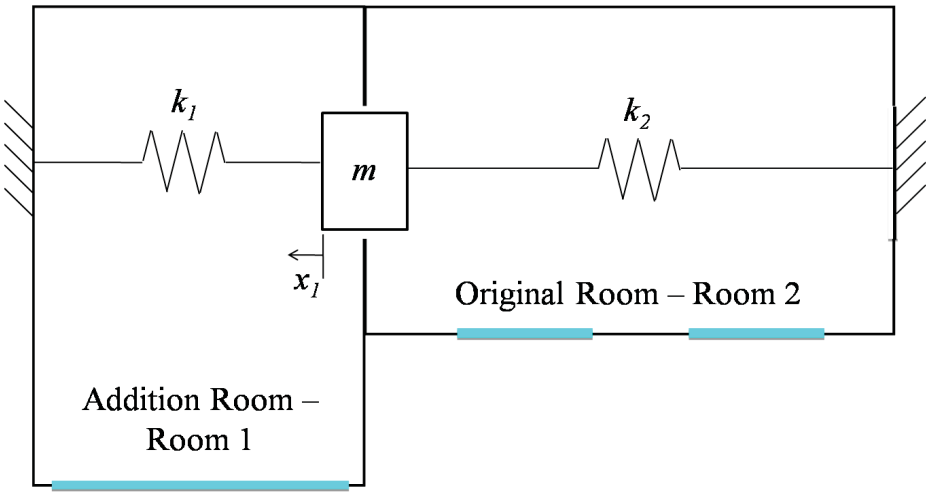

Figure 4.8: Schematic of two room structure in open-closed configuration as Helmholtz resonator.

Table 4.7: Predicted Helmholtz natural frequencies calculated for two room structure in its open-open and open-closed configurations in which the two rooms are the large volumes being compressed by the mass of the air in the open doorways.

Open-Open Configuration Natural Frequency (Hz)	***Open-Closed Configuration Natural Frequency (Hz)***
7.39	16.55
18.35	

4.2.2 Room Spectra Measurements

In this section, a conventional spectrum measurement of the room acoustics will be discussed. First, the instrumentation and experimental setup for the acoustic tests will be given. Then, a description of the tests will be discussed followed by the procedure used to analyze the data collected. Finally, the results of the analysis will be given.

The conventional acoustic tests were small scale tests consisting of two microphones and a speaker. The microphones used were the same Panasonic Electret Condenser Microphones

(model WM-61A) and the speaker was the Alesis M1 Active Mk2 self-powered speaker, discussed previously. The microphones were placed in the structure rooms, one in a corner of each room (Corcoran et al., 2009). The microphone output was recorded by the HP Agilent Dynamic Signal Analyzer (35665A), kept on the instrumentation racks, for acquisition and spectrum analysis. The HP signal analyzer was also used to provide an input signal to the speaker (Corcoran et al., 2009).

First, the speaker was positioned on the floor of the original structure room in a corner angled upwards at about a 25 degree angle, as shown in Figure 4.9. Acoustic foam was placed in all corners of the two room structure to provide additional damping for the interior acoustic modes, simulating a more realistic residential room (Corcoran et al., 2009).

(a) (b)

Figure 4.9: Picture of (a) original structure room speaker setup and (b) addition structure room speaker setup used in acoustic modal testing.

Pink noise with a 1 V_{pk} level was supplied from the HP signal analyzer to the speaker. Mean square pressure spectrums were measured from both microphones using the HP signal analyzer from 0 to 400 Hz using 800 spectral lines for all three door configurations. The speaker was then moved to the addition structure room. Again, the speaker was placed on the floor in a corner of addition structure room and angled at about 25 degrees, as shown in Figure 4.9.

Using the same input, mean square pressure spectrums were measured with both microphones over the same frequency range with the same number of spectral lines. This was repeated for all door configurations discussed in the previous set of tests. The spectrums measured by the microphone in the original structure room while the speaker was in the same room for the three different door configurations are plotted in Figure 4.10(a) and the pressure spectrums measured in the addition structure room while the speaker was in that room is plotted in Figure 4.10(b) for the three door configurations.

First examining Figure 4.10(a) corresponding to the original structure room, the most obvious difference in door configurations occurs at low frequencies. From 1 to 30 Hz, the spectrum measured when both doors are opened demonstrates strong resonance from 5 to 7 Hz and again around 22 Hz. From the calculations performed previously, it can be seen that these resonances are close to the natural frequencies of the two rooms when treated as Helmholtz resonators indicating that this effect plays quite a role in the low-frequency spectrum when the doors are opened. Another major difference occurs between the blue and the red curves around 6 Hz; when the interior door is opened, the spectrum jumps up about 6 dB. This can be explained by the fundamental structural mode found previously in the structural modal analysis. It was shown that this mode consists primarily from motion of the large window wall of the addition structure and when the door is closed, the microphone in the original structure room does not sense the sound radiated from the vibration of this mode well. Other than those key differences at low frequencies, the spectrums match each other very well past about 40 Hz indicating little change in the acoustic nature of the rooms when doors are opened or closed. This suggests that the mass of the air in the doorways only couples the acoustics of the separate rooms when wavelengths are greater than the effective radius of the door (about 1.1 m). This corresponds to frequencies of less than about 49 Hz.

(a)

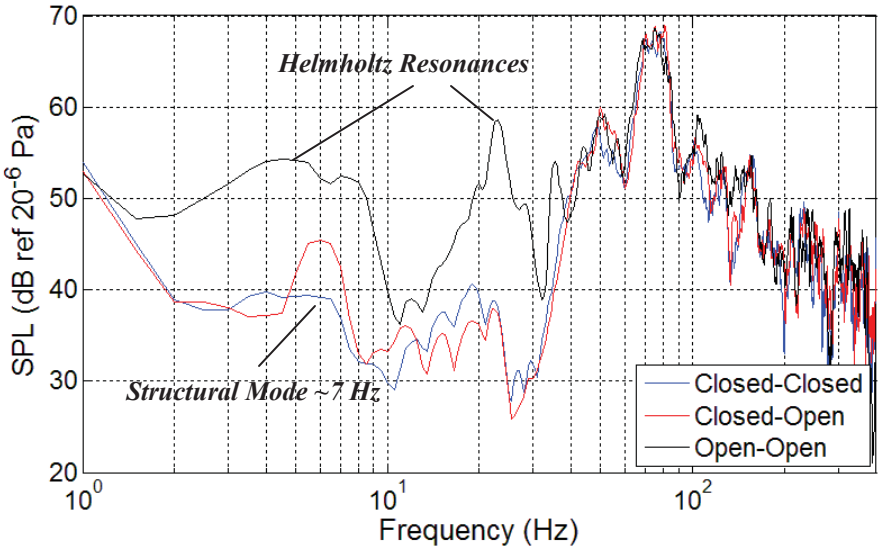

(b)

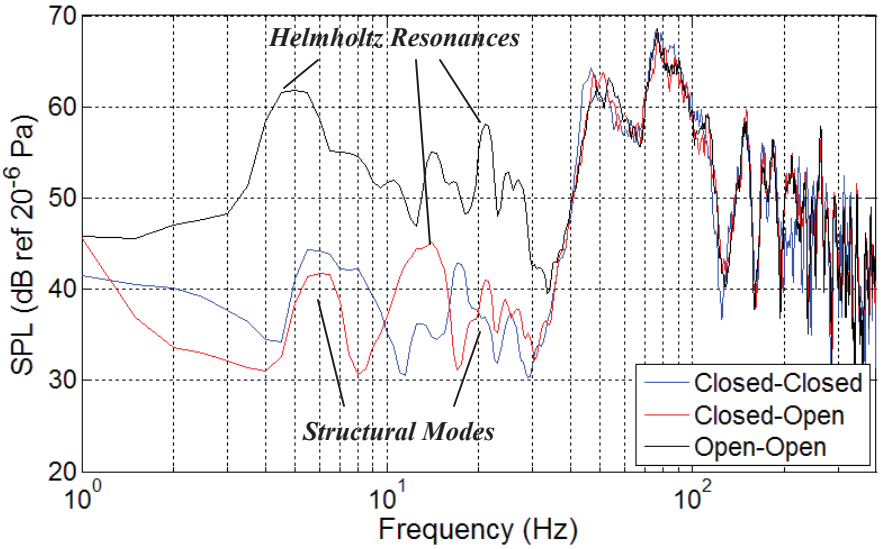

Figure 4.10: Pressure spectrum measured in a corner of the (a) original structure room and (b) addition structure room due to pink noise being played through a speaker in an opposite corner of the same room for three different door configurations.

Looking at Figure 4.10(b) for the addition structure room, again the large jump in magnitude due to the Helmholtz resonator effect is demonstrated by the black curve. However, now the difference in magnitude between the blue and red curves around 6 Hz is not nearly as great as measured in the original structure room. In fact, the level is higher when the interior door is closed now due to the pressure buildup from the window wall vibrating in its fundamental mode

in the addition room. Additional differences in magnitude in the 10 to 30 Hz frequency range can be explained by structural modes, such as the peak which occurs in the red curve at about 20 Hz which corresponds to a structural mode which consists of motion mainly from the window wall of the original structure. Again, the curves come into close agreement past about 40 Hz reinforcing the lack of coupling of room acoustics at wavelengths smaller than the effective radius of the doorway.

4.2.3 Sonic Boom Response Modal Analysis

In this section, the NExT analysis used to obtain acoustic modal properties of the cavities of the two room structure for the three different door configurations will be discussed. It was shown for the case of the single room cavity that probably the simplest experimental method of determining acoustic modal properties at low frequencies is to excite the cavity with random noise from a speaker and measure the pressure spectrum. Resonant frequencies can be determined directly from the pressure spectrum or if natural frequencies and damping ratios are needed, the same data can be used with NExT to extract these modal properties. For completeness and to examine NExT further with more complicated acoustic cavities, the technique will be used to extract modal properties from sonic boom excitation of the two room cavity. First, the instrumentation and experimental setup used to gather the interior pressure response data will be discussed, followed by the procedure used to extract modal properties from this data. Finally, the results of the analysis will be presented for all door configurations.

Nine microphones, again Panasonic Electret Condenser Microphones (model WM-61A), were positioned in the two room structure are to record interior pressure response (Haac et al., 2009). The data streams were downsampled from 51.2 kHz to a sampling frequency of about 210 Hz to limit the frequency range of analysis to the Nyquist frequency of 105 Hz. Each pressure response signal was cross-correlated to a reference response signal to obtain NExT IRFs. The reference microphone, selected based on its position in the structure, was the microphone in the corner of the original structure room. The FFTs of these NExT IRFs were calculated to determine NExT FRFs of the acoustic system. To gain perspective on where the acoustic modes may lie in the frequency domain, the NExT FRFs were summed linearly to form simple mode indicator functions, plotted in Figure 4.11 by door configuration.

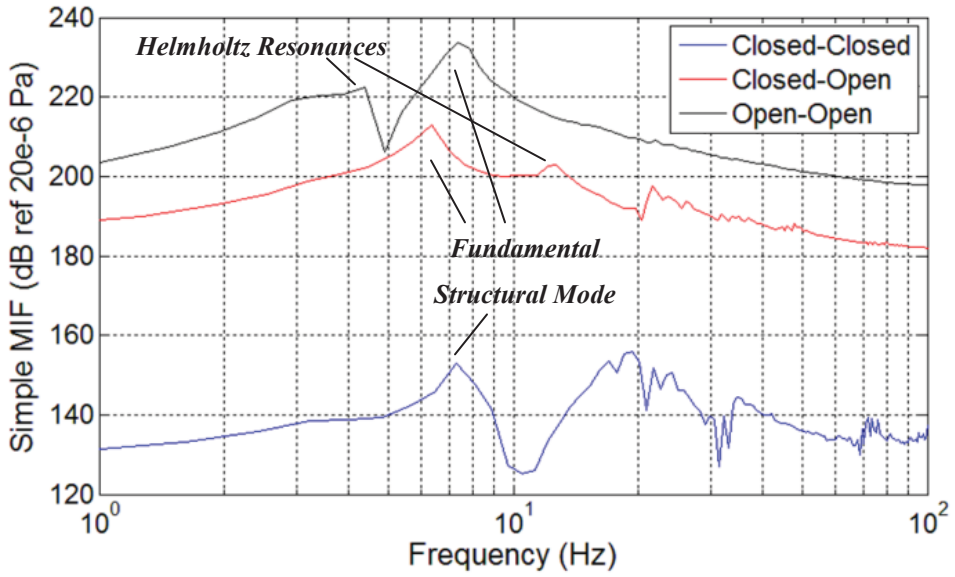

Figure 4.11: Simple mode indicator function for the two room structure calculated using the interior pressure response to sonic boom excitation and the microphone in the corner of the original structure room as reference plotted for each door configuration.

From Figure 4.11, it can be seen that the NExT FRFs capture resonances in the sonic boom pressure signals and that the cavities respond quite differently depending on their configuration. In the open-open configuration, the cavity responds almost as a two degree of freedom system demonstrating only two major areas of resonance. These resonances correspond to the first Helmholtz resonance around 4.5 Hz and the fundamental structural mode around 7 Hz. The fundamental structural mode is captured again in the open-closed configuration along with a Helmholtz resonance around 12 Hz. Lesser resonances in this configuration are captured beyond 20 Hz. The most complex response is in the closed-closed configuration. Again, the fundamental structural mode is captured around 7 Hz. However, there are now many more significant areas of resonance from 20 to 40 Hz.

Again, the single reference LSCE method was employed to extract acoustic eigenproperties (Corcoran et al., 2009). The number of assumed modes began at one and was increased consecutively applying the method, regenerating IRFs, calculating square error, and examining the stability of the eigenproperties at each assumed number of modes. The process came to conclusion when about twice the number of resonances captured by the simple mode indicator function was reached for each door configuration. Basically, the same method was employed as in the single room structure NExT acoustic analyses.

From the square error plots the stability diagrams, a decision was made as to the correct number of assumed modes. Based on the square error and stability in properties of the modes which clearly appear in the mode indicator functions, 30 modes were assumed in the frequency range for the closed-closed configuration, 26 modes for the open-closed configuration, and 21 modes for the open-open configuration (Corcoran et al., 2009).

Examining the full list of modal properties for all extracted modes, there were obviously some computational modes extracted only to preserve the curve fit, rather than being actual physical modes of the system being tested. These modes are indicated by unstable eigenproperties and either negative or very high damping ratios and were removed by inspection to achieve the final list of physical modes (Corcoran et al., 2009). The eigenproperties of all physical modes extracted over the frequency range from 0 to 105 Hz for the closed-closed door configuration are shown in Table 4.8. Also included in this table are origins of the modes, structural or acoustic. The origin is obtained by inspection of the extracted natural frequencies and comparison with the natural frequencies extracted in the structural experimental modal analysis.

In the NExT sonic boom analysis of the closed-closed configuration cavities, 21 physical acoustic modes were extracted, the fundamental having a natural frequency of about 16.8 Hz. Along with the physical acoustic modes, four structural modes found in the structural experimental modal analysis were extracted due to their excitation by the sonic boom and radiation of sound sensed by the microphones inside the structure. Modal damping ratios of the acoustic modes ranged from about 0.1 % to 12.4 % with an average ratio 3.6 % and a median value of 2.0 %. The damping ratios display a small decreasing trend as frequency is increased. Some physical modes were extracted with very high damping ratios. While it is not believed that these damping ratios are correct, the modes were decided to be genuine based on the stability of other modal properties and the presence of resonances at the extracted natural frequencies.

Table 4.8: All extracted modal properties of physical modes of the two room structure in the closed-closed configuration and their origin using NExT and the LSCE method with the sonic boom pressure response.

Mode	*Natural Frequency (Hz)*	*Damping Ratio (%)*	*Mode Origin*
1	8.17	12.10	Structural
2	10.16	3.68	Structural
3	16.75	10.14	Acoustic
4	19.94	14.21	Structural
5	23.03	26.45	Structural
6	23.12	12.35	Acoustic
7	28.72	1.38	Acoustic
8	32.24	9.79	Acoustic
9	35.40	5.21	Acoustic
10	41.30	1.98	Acoustic
11	46.31	1.41	Acoustic
12	50.24	0.60	Acoustic
13	54.61	2.92	Acoustic
14	59.76	1.95	Acoustic
15	62.62	0.08	Acoustic
16	66.33	4.08	Acoustic
17	70.11	3.18	Acoustic
18	74.17	2.35	Acoustic
19	74.98	5.13	Acoustic
20	80.20	1.34	Acoustic
21	83.78	0.99	Acoustic
22	90.64	0.93	Acoustic
23	93.96	6.97	Acoustic
24	95.47	0.25	Acoustic
25	102.65	1.92	Acoustic

The modal properties of all physical modes extracted over the frequency range 0 to 105 Hz for the two room structure in the open-closed configuration are listed in Table 4.9. Again, the origin of the modes is included in the table. In the open-closed configuration, 18 physical acoustic modes were extracted with two structural modes in the analysis. The fundamental acoustic mode was extracted with a natural frequency of about 17.3 Hz which corresponds to the predicted Helmholtz resonance. Modal damping ratios of the acoustic modes ranged from about

0.2 % to 10.4 % with an average of 3.8 % and a median value of 2.7 %. The damping ratios display a downward trend stronger than the trend in the closed-closed configuration as frequency is increased. Low frequency modes were extracted from the closed-closed configuration and the open-closed configuration in this analysis. This is because of the suppression effect of the modes beyond about 10 Hz by the autospectrum of the sonic boom input. In fact, the modal properties extracted in the sonic boom analysis were very similar for both door configurations over the entire frequency range.

Table 4.9: All extracted modal properties of physical modes of the two room structure in the open-closed configuration and their origin using NExT and the LSCE method with the sonic boom pressure response.

Mode	***Natural Frequency (Hz)***	***Damping Ratio (%)***	***Mode Origin***
1	10.43	29.83	Structural
2	17.26	10.39	Acoustic
3	21.54	14.48	Structural
4	25.25	9.61	Acoustic
5	30.68	6.94	Acoustic
6	35.95	7.01	Acoustic
7	42.80	3.59	Acoustic
8	45.83	5.64	Acoustic
9	48.80	5.23	Acoustic
10	52.31	3.17	Acoustic
11	57.77	2.78	Acoustic
12	69.92	0.23	Acoustic
13	71.60	2.19	Acoustic
14	74.98	2.64	Acoustic
15	78.52	1.65	Acoustic
16	83.59	1.53	Acoustic
17	86.35	0.95	Acoustic
18	91.12	1.65	Acoustic
19	96.12	1.72	Acoustic
20	102.84	1.50	Acoustic

The modal properties of the physical modes extracted over the frequency range 0 to 105 Hz for the open-open configuration are listed in Table 4.10. In the open-open configuration, 15 physical acoustic modes and two structural modes were extracted in the sonic boom analysis.

The fundamental acoustic mode has a natural frequency of about 6.6 Hz. This mode and the mode with a natural frequency of about 14.2 Hz correspond to the two Helmholtz resonances predicted analytically. Modal damping ratios ranged from 0.8 % to 65.4 % with an average ratio of 9.0 % and a median ratio of 3.9 %. The modal damping ratios display a very strong decreasing trend as frequency is increased, more so than the other door configurations.

Table 4.10: All extracted modal properties of physical modes of the two room structure in the open-open configuration and their origin using NExT and the LSCE method with the sonic boom pressure response.

Mode	*Natural Frequency (Hz)*	*Damping Ratio (%)*	*Mode Origin*
1	6.57	65.40	Acoustic
2	9.48	41.52	Structural
3	14.18	20.70	Acoustic
4	19.88	13.64	Structural
5	24.41	11.09	Acoustic
6	32.19	7.11	Acoustic
7	44.38	3.85	Acoustic
8	48.35	6.51	Acoustic
9	52.83	4.14	Acoustic
10	64.02	4.12	Acoustic
11	68.97	1.93	Acoustic
12	74.43	2.03	Acoustic
13	79.32	1.98	Acoustic
14	84.41	2.19	Acoustic
15	88.97	1.80	Acoustic
16	94.88	0.78	Acoustic
17	103.38	1.43	Acoustic

4.2.4 Comparison of Modal Analysis Methods

In this section, a detailed comparison of the results of the analytical modal analysis and experimental modal analysis of the acoustic cavities of the two room structure will be given. The analytical method for determining acoustic modal properties of the two room structure cavities used by the numerical model to predict sonic boom transmission into buildings has been validated by comparison of predicted to measured interior acoustic response (Remillieux et al., 2009). Because of this, the analytical method will provide a useful comparison with the use of

NExT with interior pressure response to measure acoustic modal properties. The predicted natural frequencies of the room are compared with the measured modal properties extracted in the NExT analyses in Figure 4.12 for the closed-closed configuration.

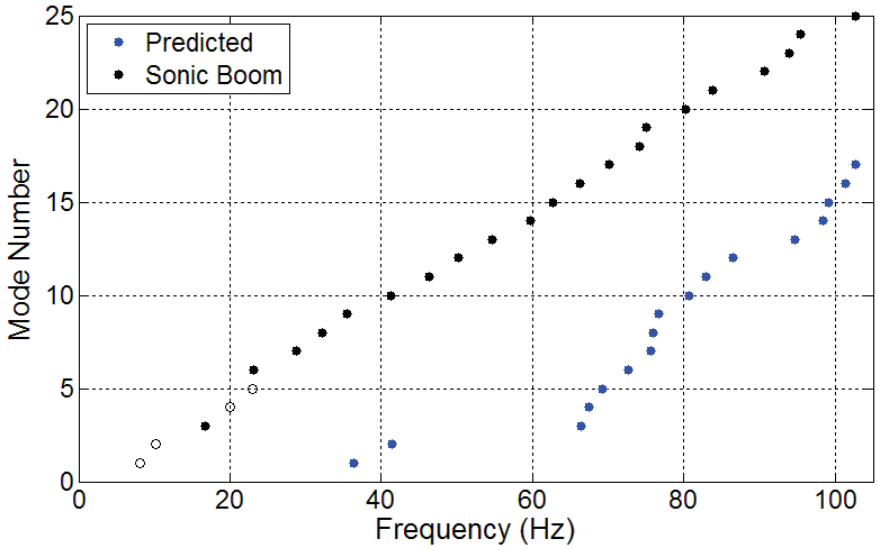

Figure 4.12: Comparison between natural frequencies of the two room structure in the closed-closed configuration obtained analytically and experimentally using NExT with the sonic boom response. Closed circles (● and ●) indicate acoustic modes and open circles (○) structural modes extracted in the acoustic analysis.

Several frequency ranges exist where there are differences between predicted and measured natural frequencies. First, at frequencies below the first predicted acoustic natural frequency, there are structural modes extracted from acoustic pressure measurements. This occurs in the NExT analysis using the sonic boom response because there is much low frequency excitation of the structural modes from the boom and suppression of the higher frequency modes due to the multiplication of the autospectrum of the sonic boom input. A few modes were extracted in the low frequency range were not extracted in the structural analysis. These could still be structural modes missed in the analysis due to insufficient excitation from the sonic boom or being closely spaced to other more dominant structural modes. Also, these modes could exist due to imperfections in the assumptions behind the analytical calculations such as not perfectly rigid walls, rectangular geometry, leakage to the exterior, or the large instrumentation racks in the center of the room.

Next, many modes were extracted in the experimental analyses which were not predicted in the mid 40 to mid 60 Hz range and the mid 80 to mid 90 Hz range. Since the structural experimental modal analysis was only capable of extracting modes out to about 23 Hz, many of

these modes are likely structural in nature. Again, they could also be due to violation of assumptions in the analytical calculations for the reasons mentioned previously or due to the numerical curve-fitting procedure preserving the fit of the curve in this range without the presence of modes. Other than these differences, the predicted acoustic modes were reasonably well-matched by extracted modes in natural frequency including the fundamental modes of each cavity around 36 and 40 Hz.

A visual comparison of the predicted natural frequencies with the experimentally measured modal properties from the sonic boom analysis of the two room structure in the open-closed configuration is given in Figure 4.13. Again, low frequency structural modes were extracted in the acoustic analysis along with a couple modes which were not extracted in the structural analysis. Some of these are likely structural modes missed in the structural analysis due to frequency limitations or acoustic modes associated with the approximate doubling of the volume of air by opening the interior door. Also, many modes were extracted again in the mid 40 to mid 60 Hz range which are probably either structural modes or unpredicted acoustic modes due to the reasons mentioned previously for the closed-closed configuration. The rest of the predicted acoustic natural frequencies match the experimental natural frequencies well including the Helmholtz resonance around 17 Hz.

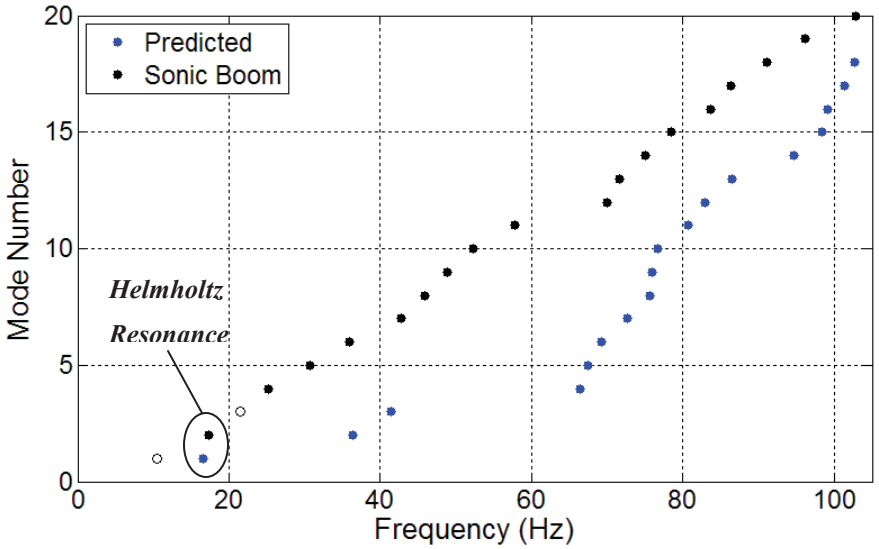

Figure 4.13: Comparison between natural frequencies of the two room structure in the open-closed configuration obtained analytically and experimentally with the sonic boom response. Closed circles (● and ●) indicate acoustic modes and open circles (○) structural modes extracted in the acoustic analysis.

The modal properties of the two room structure in the open-open configuration predicted analytically are compared to the properties extracted from the experimental acoustic analyses using NExT and the response to a sonic boom in Figure 4.14. Again, more modes were extracted in the experimental analysis in the low frequency range than were predicted. However, all except a couple of these are now quite clearly structural modes. The Helmholtz resonances predicted around 7 and 18 Hz were quite clearly extracted in each experimental analysis. Only a few modes were extracted in the mid 40 to mid 60 Hz range which were not predicted analytically. At higher frequencies, the predicted natural frequencies match the experimentally measured natural frequencies very well.

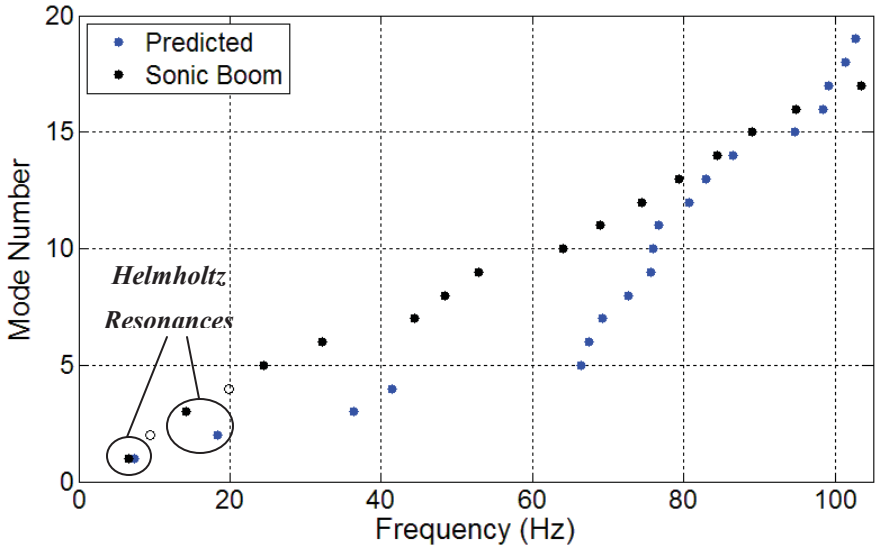

Figure 4.14: Comparison between natural frequencies of the two room structure in the open-open configuration obtained analytically and experimentally with the sonic boom response. Closed circles (● and ●) indicate acoustic modes and open circles (○) structural modes extracted in the acoustic analysis.

It has been shown that the use of sonic boom response with NExT while violating the random, stationary input assumption and not completely satisfying the extension to a perfect impulse excitation will accurately extract modal properties as the modal properties were compared to a very reasonable degree of accuracy with the analytically calculated acoustic modal properties.

5 Conclusions

This thesis demonstrates the use of the output-only experimental modal analysis technique NExT, in conjunction with impulsive structural and acoustic responses to extract modal properties of large residential structures and the acoustic cavities enclosed. Experimental modal testing of the residential structures discussed by Corcoran et al. (2009) was performed as part of an effort to validate a numerical model to predict sonic boom transmission into buildings (Remillieux et al., 2009). It was shown that conventional modal testing of such large structures in which the input force can be measured failed to excite the low frequency global modes of the structure which are of utmost importance in low frequency sonic boom applications. Also, measurement of the input force provided by a speaker to excite the acoustic cavities would have been inaccurate due to the small low frequency output by the speaker. For these reasons, output-only experimental modal analysis was applied, specifically NExT to the structural and acoustic response to simulated sonic booms obtained by Haac et al. (2009) in which sufficient low frequency excitation is attained.

One of the assumptions behind the original derivation of NExT is that the input force is random and stationary, shown in Chapter 2 (James et al., 1993). This assumption was extended for the work presented in this thesis in the following section to include an impulsive excitation which is closer to a sonic boom input than random noise. To examine this extension, experimental modal testing and analysis is discussed in detail for a single and two room structure and their interior acoustic cavities. First, it was shown in Chapter 3 that the experimental modal properties extracted using NExT and the single room structure's sonic boom response correspond closely with the modal properties extracted using conventional experimental modal testing and analysis techniques and with the modal properties calculated from a finite element model provided by Remillieux et al. (2009). In fact, the NExT results often coincided with the finite element results more closely than the conventional modal test results due to insufficient global excitation of the single room structure by an impact hammer.

NExT was then applied to the two room structure to examine its use with a more complex structure. While conventional impact hammer modal testing provided insufficient data to extract modal properties of the two room structure, the modal properties extracted experimentally using NExT with the structural response to a sonic boom (Haac et al., 2009) corresponded well to the

modal properties calculated from the finite element model of the structure discussed by Remillieux et al. (2009).

NExT was shown to be valid for acoustic systems as well in Chapter 4. In this chapter, three analyses were performed on the single room cavity and three configurations of the two room cavities. First, an analytical modal analysis of the rectangular single room cavity assuming rigid boundaries at the structure walls was performed to obtain acoustic natural frequencies. Then, an experimental modal test and analysis of this cavity was undertaken using NExT and the interior pressure response to white noise which does not violate the original random, stationary input of NExT. Finally, the experimental modal analysis of the cavity using NExT and the interior acoustic response to a sonic boom (Haac et al., 2009) was discussed. The modal properties extracted in the three analyses were compared to examine the use of NExT with pressure response data. Good agreement was demonstrated between all analyses and both NExT analyses were shown to have the additional advantage of extracting damping ratios of acoustic modes without measurement of the input force.

Then, the robustness of using NExT in experimental modal analysis of acoustic cavities was demonstrated for the more complex two room cavity. Acoustic modal properties were acquired with two different methods: analytical predictions and NExT with sonic boom response. The results were examined and compared with good agreement. Once again, robustness was demonstrated by varying the configuration of the cavity by closing and opening doors of the structure and obtaining accurate results for three different configurations.

In conclusion, the useful output-only experimental modal analysis technique, NExT, has been extended to include the assumption of an impulsive excitation rather than assuming a random, stationary input in this thesis. It has been demonstrated that this technique can be applied to large residential structures by comparing the results obtained using NExT with sonic boom response data with conventional modal test results and the results from a finite element model for a single and two room residential structure. Then, NExT was applied to acoustic cavities for the first time. It was applied to the response to random, stationary inputs adhering to the assumptions in the original derivation of the technique. Then, NExT was applied to the response to a sonic boom, an impulsive input. Since measuring the input force from a speaker at such low frequencies would be near impossible, the results of the NExT analyses were compared to

analytical predictions to provide perspective. The results of all analyses compared reasonably well and advantages to using NExT were demonstrated for both acoustic and structural systems.

References

Brincker, R., Zhang L., and P. Andersen. 2001. Modal identification of output-only systems using frequency domain decomposition. *Smart Materials and Structures* **10**: 441-445.

Corcoran, J.M., Haac, T.R., Remillieux, M., Burdisso, R.A., and G. Reichard. 2009. Development of a model for predicting the transmission of sonic booms into buildings. Part III: experimental modal testing and structural/acoustic properties. Virginia Tech Final Report submitted to NASA Langley Research Center (Award Number: NNX07AT36A).

Dickinson, S.M. and G.B. Warburton. 1967. Vibration of box-type structures. *Journal of Mechanical Engineering Science* **9**(4): 325-38.

Ewins, D.J. 2000. *Modal testing: theory, practice and application*. 2nd ed. Philadelphia: Research Studies Press Ltd.

Haac, T.R., Corcoran, J.M., Remillieux, M., Burdisso, R.A., and G. Reichard. 2009. Development of a model for predicting the transmission of sonic booms into buildings. Part II: experimental characterization of the vibro-acoustic response of simple structures to simulated sonic booms. Virginia Tech Final Report submitted to NASA Langley Research Center (Award Number: NNX07AT36A).

Hagerman, E. 2007. All sonic, no boom. <http://www.popsci.com/>. 1 March 2007. Accessed 16 February 2010.

Harris, F.J. 1978. On the use of windows for harmonic analysis with the discrete Fourier transform. *Proceedings of the IEEE* **66**(1): 51-83.

Hawkins, S.J. and J.A. Hicks. 1966. Sonic bang simulation by a new explosive technique. *Nature* **211**: 1244-1245.

James, G.H. III, Carne, T.G., and J.P. Lauffer. 1993. The natural excitation technique (NExT) for modal parameter extraction from operating wind turbines. Albuquerque, NM: Sandia National Laboratories. SAND92.

Kinsler, L.E., Frey A.R., Coppens, A.B., and J.V. Sanders. 2000. *Fundamentals of acoustics*. 4th ed. New York: John Wiley & Sons, Inc.

Klos, J. and R.D. Buehrle. 2007. Vibro-acoustic response of buildings due to sonic boom exposure: June 2006 field test. Hampton, VA: NASA Langley Research Center. NASA/TM-2007-214900.

Klos, J. 2008. Vibro-acoustic response of buildings due to sonic boom exposure: July 2007 field test. Hampton, VA: NASA Langley Research Center. NASA/TM-2008-215349.

Mohanty, P. and D.J. Rixen. 2002. Operational modal analysis in the presence of harmonic excitation. *Journal of Sound and Vibration* **270**: 93-109.

Mohanty, P. and D.J. Rixen. 2004. A modified Ibrahim time domain algorithm for operational modal analysis including harmonic excitation. *Journal of Sound and Vibration* **275**: 375-390.

Mohanty, P. and D.J. Rixen. 2006. Modified ERA method for operational modal analysis in the presence of harmonic excitations. *Mechanical Systems and Signal Processing* **20**: 114-130.

Morfey, L. 1969. Acoustic properties of openings at low frequencies. *Journal of Sound and Vibration* **9**(3).

Pawlowski, A. 2009. Supersonic travel may return, minus boom. <www.CNN.com/travel>. 19 June 2009. Accessed 22 June 2009.

Peeters, B. and G. de Roeck. 1999. Reference-based stochastic subspace identification for output-only modal analysis. *Mechanical Systems and Signal Processing* **13**(6): 855-878.

Peeters, B. and G. de Roeck. 2001. Stochastic system identification for operational modal analysis: a review. *Journal of Dynamic Systems, Measurement, and Control* **123**: 659-667.

Pierce, A.D. 1989. *Acoustics: an introduction to its physical principles and applications*. Woodbury, NY: Acoustical Society of America.

Popplewell, N. 1971. The vibration of a box-type structure I: natural frequencies and normal modes. *Journal of Sound and Vibration* **14**(3): 357-65.

Ravetta, P., Macko, N., and R. Burdisso. 2009. Sonic boom vibro-acoustic simulations using multiple point sources. AVEC, Inc. Final Report submitted to NASA Langley Research Center (NSB-8712-FR).

Remillieux, M.C., Corcoran, J.M., Haac, T.R., Burdisso, R. A., and G. Reichard. 2009. Development of a model for predicting the transmission of sonic booms into buildings. Part I: theory and validation of the vibro-acoustic modeling of structures to sonic booms. Virginia Tech Final Report submitted to NASA Langley Research Center (Award Number: NNX07AT36A).

Remillieux, M.C., Reichard, G., and R.A. Burdisso. 2010a. Vibro-acoustic response of simplified residential structures exposed to sonic booms. Part I: numerical model. Noise-Con 2010, Baltimore, MD, April 19-21.

Remillieux, M.C., Corcoran, J.M., Haac, T.R., Reichard, G., and R.A. Burdisso. 2010b. Vibro-acoustic response of simplified residential structures exposed to sonic booms. Part II: experimental validation. Noise-Con 2010, Baltimore, MD, April 19-21.

Shen, F., Zheng, M., Feng Shi, D., and F. Xu. 2003. Using the cross-correlation technique to extract modal parameters on response-only data. *Journal of Sound and Vibration* **259**(5): 1163-1179.

Taber, R.C., Vold, H., Brown, D.L., and G.T. Rocklin. 1985. Exponential window for burst random excitation. 3rd International Modal Analysis Conference (IMAC III), Orlando, Florida, 989-995.

Wahba, N.N. 1990a. Analysis of a plaster-wood wall using a series solution. *Computers & Structures* **35**(2): 121-40.

Wahba, N.N. 1990b. Analysis of a plaster-wood wall using finite-element method. *Computers & Structures* **36**(4): 743-53.

Xin, F.X., Lue, T.J. and C.Q. Chen. 2008. Vibroacoustic behavior of clamp mounted double-panel partition with enclosure air cavity. *Journal of the Acoustical Society of America* **124**(6): 3604-12.